EURAMET TC Project
Final Report

Project Title

Experimental study of blockage effect in wind tunnels for calibrations of anemometers

Coordinator, Institute, Country

Jan Geršl (CMI)

EURAMET Registration No.

1431

Subject Field

Flow

KCDB Identifier

Klicken oder tippen Sie hier, um Text einzugeben.

Date

2022-06-13

EURAMET e.V., Bundesallee 100, 38116 Braunschweig, Germany
Phone: +49 531 592 1960 Fax: +49 531 592 1969 E-mail: secretariat@euramet.org
www.euramet.org

Experimental study of blockage effect in wind tunnels for calibrations of anemometers

EURAMET pilot study no. 1431
Final report

J. Geršl[1], J. Sluše[1], P. Busche[2], M. de Huu[3], D. Pachinger[4], H. Müller[5], K. Hölper[6], A. Bertašienė[7], M. Vilbaste[8], I. Care[9], H. Kaykısızlı[10], L. Maar[11], S. Haack[12]

[1]Czech Metrology Institute, Okruzni 31,63800 Brno, Czech Republic
[2]Deutsche WindGuard Wind Tunnel Services GmbH, Varel, Germany
[3]Federal Institute of Metrology METAS, Wabern, Switzerland
[4]BEV/E+E, Engerwitzdorf, Austria
[5]Physikalisch Technische Bundesanstalt, Braunschweig, Germany
[6]Westenberg Engineering, Köln, Germany
[7]Lithuanian Energy Institute, Kaunas, Lithuania
[8]Testing centre, University of Tartu, Tartu, Estonia
[9]CETIAT, Villeurbanne, France
[10]TÜBİTAK UME, Gebze / Kocaeli, Turkey
[11]Czech Hydrometeorological Institute, Prague, Czech Republic
[12]Danish Technological Institute, Aarhus, Denmark
E-mail (corresponding author): jgersl@cmi.cz

May 2022

Contents

1 Introduction

When an anemometer is calibrated in a wind tunnel the velocity indication of the meter is influenced by flow conditions at a boundary of a test section of the wind tunnel leading to the so called blockage effect. The larger is the meter compared to the test section cross-sectional area the more significant the blockage effect is. The effect also depends on the type of the test section (open or closed) and on the type of the anemometer tested. Moreover, it is desirable to place a reference anemometer to a position where the velocity field is not significantly influenced by the meter under test. This may not be possible for large meters leading to another source of systematic errors in anemometer calibrations [1, 2]. These effects were observed also in inter-laboratory comparisons between air speed calibration laboratories. In [3], it was concluded that the results of the comparisons indicate a need for more attention to blockage effects during air speed calibrations and their impact on air speed uncertainty statements.

To make the calibration results from various wind tunnels comparable they should be corrected to values corresponding to certain standardized boundary conditions – e.g. to free stream conditions assuming an infinite asymptotically homogeneous velocity field with reference velocity given by the velocity at infinity (far enough from the anemometer). Or at least the magnitude of such correction should be estimated and included in the uncertainty budget.
Denoting v_M the velocity indication of the meter under test, $v_E(v_M)$ the velocity indication of the reference anemometer in a wind tunnel when the meter under test indicates v_M and $v_\infty(v_M)$ the velocity of the asymptotically homogeneous free stream at infinity when the meter under test inserted to the stream indicates the velocity v_M, we can define a correction factor for the blockage effect given as

$$\alpha(v_M) = \frac{v_\infty(v_M)}{v_E(v_M)}.$$

A theory of velocity corrections of measurements in wind tunnels with closed measurement section to the free stream conditions was developed by Glauert [4] and further extended by Mikkelsen and Sørensen [5]. Their theory for closed measuring sections is reviewed and extended to open measuring sections in [6] or in the monograph [7]. This theory is suitable for horizontal axis wind turbines (vane anemometers) and it contains some simplifying assumptions and therefore its experimental validation is necessary.

In standards, the blockage effect is addressed e.g. in [8] where a relative uncertainty contribution of 1/4 of the blockage ratio for closed measuring sections and 1/16 of the blockage ratio for open measuring sections is recommended in case of cup anemometer calibrations with Pitot tube as a reference, the blockage ratio being the ratio of the area of the anemometer projected to a plane perpendicular to the flow and the cross sectional area of the test section of a wind tunnel. For closed measuring sections, use of the Maskell theorem [9] is recommended. Otherwise we are not aware of quantitative recommendations for blockage corrections or uncertainties. To eliminate these uncertainties the standards [8, 10] recommend not exceeding the blockage ratio of 10 % for wind tunnels with an open test section and 5 % for wind tunnels with a closed test section. The standard [11] recommends not exceeding 5 % in general.

Experimental investigation of influence of the blockage effect on cup anemometer calibrations can be found e.g. in [12]. Overview and experimental verification of methods for blockage effect corrections for propellers can be found e.g. in [13] and for vertical axis wind-turbines in [14]. Insertion depth effects turn out to be important as well for this project. This effect has been investigated in [12] for cup anemometers and in [15] for a hot film anemometer.

The aim of this project was to experimentally determine the blockage effect corrections for vane and cup anemometers especially in case of wind tunnels with an open test section. Such wind tunnels are

widely used by calibration laboratories but the known correction models mostly apply to wind tunnels with a closed test section. Mathematical modelling of processes at a boundary of air stream in open test sections is challenging [6].

Three vane anemometers and two cup anemometers of various sizes have been calibrated by 12 laboratories providing 14 wind tunnels with test sections of various types and sizes and the deviations of the results have been analysed. On top of that a small size thermal anemometer and a small size vane anemometer were calibrated in some of the participating wind tunnels in order to compensate differences which are not caused by the blockage effect. To separate the effect of boundary conditions from the effect of placing the reference meter to an area influenced by the meter under test the velocity fields in front of the 5 large size anemometers have been measured in a wind tunnel of the pilot laboratory (CMI).

References

[1] Care I and Arenas M, "On the impact of anemometer size on the velocity field in a closed wind tunnel", *Flow Measurement and Instrumentation*, **44**, 2-10, 2015.
[2] Sluše J, "Influence of blockage effect on measurement by vane anemometers", in *EPJ Web of Conferences*, **143**, 02110, 2017.
[3] Müller H, "Final report on EURAMET project No. 827: LDA-based intercomparison of anemometers", *Metrologia*, **50**, Technical Supplement, 2013.
[4] Glauert H, *Airplane Propellers, Aerodynamic Theory*, edited by Durand W F (New York, Dover), 1963, Chap. 7, Div. L
[5] Mikkelsen R and Sørensen J N, "Modelling of Wind Tunnel Blockage", in *Proceedings of the 2002 Global Windpower Conference and Exhibition* [CD-ROM], www.ewea.org.
[6] Sørensen J N, Shen W Z and Mikkelsen R, "Wall Correction Model for Wind Tunnels with Open Test Section", *AIAA Journal*, **44**, No. 8, August 2006.
[7] Sørensen J N, *General Momentum Theory for Horizontal Axis Wind Turbines* (Springer), 2016
[8] EN 61400-12-1: *Wind turbines – Part 12-1: Power performance measurements of electricity producing wind turbines, Annex F*, 2005.
[9] Maskell E C, "A Theory of the Blockage Effects on Bluff Bodies and Stalled Wings in a Closed Wind Tunnel", *Aeronautical Research Council Reports and Memoranda no.* 3400, 1963.
[10] ISO 17713-1: *Meteorology – Wind measurements – Part 1: Wind tunnel test methods for rotating anemometer performance*, 2007.
[11] ASTM D 5096-02: *Standard Test Method for Determining the Performance of a Cup Anemometer or Propeller Anemometer*, 2017.
[12] Westermann D, Balaresque N and Busche P, "Systematic deviation of the anemometer calibration due to geometrical interference", *Report of Deutsche WindGuard Wind Tunnel Services GmbH*, 2011.
[13] R. E. Fitzgerald, *Wind tunnel blockage corrections for propellers*, Master Thesis, University of Maryland, 2007.
[14] I. J. Ross, *Wind Tunnel Blockage Corrections: An Application to Vertical-Axis Wind Turbines*, Master Thesis, University of Dayton, 2010.
[15] M. Rohm, Y. Cordier-Duperray, "Influence of the insertion depth on the response of a hot film anemometer in different wind tunnels", *13th International Metrology Congress*, Lille, 2007 and *Transverse Disciplines in Metrology*, ISTE-Wiley, February 2009, p. 89-100

2 Transfer standards

The following anemometers have been circulated among the participating laboratories:

1) Vane anemometer Testo 0635 9340 with measuring unit Testo 445
2) Vane anemometer Schiltknecht MiniAir20 with a probe Macro
3) Vane anemometer RM Young Gill Propeller MODEL 27106D/F
4) Cup anemometer Vaisala WAA151
5) Cup anemometer Thies First Class Advanced type 4.3351.10.000
6) Thermal anemometer Airflow TA440
7) Vane anemometer Schiltknecht MiniAir20 with a probe Mini

In this section we describe the basic parameters of the anemometers including dimensions and their mounting in the wind tunnels.

Vane anemometer Testo 0635 9340 with measuring unit Testo 445

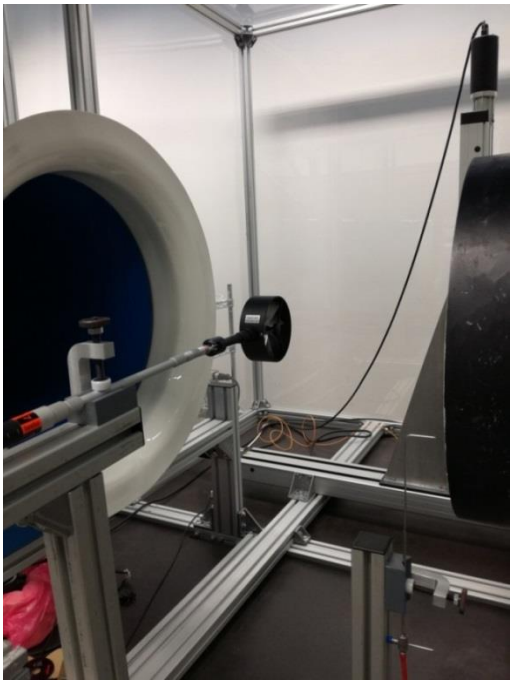

Basic parameters:

Velocity range: (0.1 – 15) m/s
Dimensions:
outer diameter of the rotor head: 10.7 cm
depth of the rotor head: 4.3 cm
length of the telescopic mounting rod: up to 1 m
Velocity indication: reading from the display
Resolution: 0.01 m/s
Serial number: probe: 709, electronics: 61054935

Mounting in a wind tunnel:

The probe is connected to an original telescopic mounting rod provided by Testo. Installation of the probe in the wind tunnel of CMI is shown in Fig. 2.1. Detail of the probe is in the bottom part of Fig. 2.2.

The anemometer was provided by CMI.

Fig. 2.1 Testo probe at CMI

Fig. 2.2 Schiltknecht Macro (top) and Testo 0635 9340 (bottom) probes.

Vane anemometer Schiltknecht MiniAir20 with a probe Macro

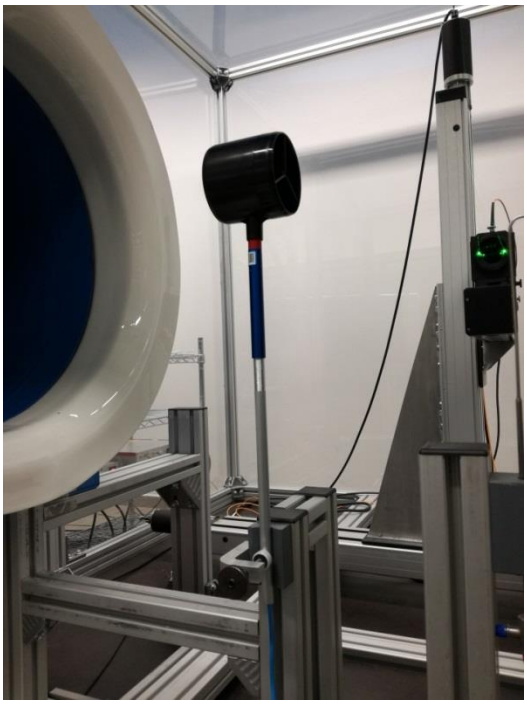

Fig. 2.3 Schiltknecht Makro at CMI

Basic parameters:

Range: (0.3 – 40) m/s
Dimensions:
outer diameter of the rotor head: 8.55 cm
depth of the rotor head: 8 cm
length of the probe from centre of the rotor to bottom of the handrail: 19 cm
Velocity indication: reading from the display
Resolution: 0.01 m/s
Serial number: probe: C-72268,
electronics: 75792

Mounting in a wind tunnel:

The probe is shown in Fig. 2.2. An aluminium tube with outer diameter of 12 mm (Fig. 2.3) is inserted inside the handrail of the probe to mount it into a wind tunnel. Installation in the wind tunnel of CMI is shown in Fig. 2.3. Detail of the probe is in the top part of Fig. 2.2.

The anemometer was provided by METAS.

Vane anemometer RM Young Gill Propeller MODEL 27106D/F

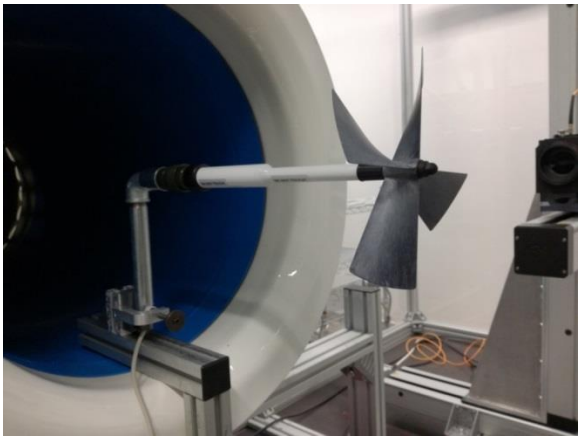

Fig. 2.4 Anemometer RM Young at CMI

Basic parameters:

Range: (0.4 – 35) m/s
Dimensions:
rotor diameter: 20 cm
rotor depth: 3 cm
length from the tip to the mounting elbow: 48 cm
Velocity indication: frequency output with conversion to velocity given by
v (m/s) = 0.03 x f (Hz)
Serial number: 02268

Mounting in a wind tunnel:

The tube in the axis of the anemometer ends with a 90° elbow where a ¾" pipe (outside diameter 27 mm) can be fixed. For some wind tunnels the body of the anemometer is too long to be fixed outside of the wind stream and it must be fixed inside the diffusor. Example of installation in the wind tunnel of CMI is shown in Fig. 2.4.

The anemometer was provided by Deutsche WindGuard.

Cup anemometer Vaisala WAA151

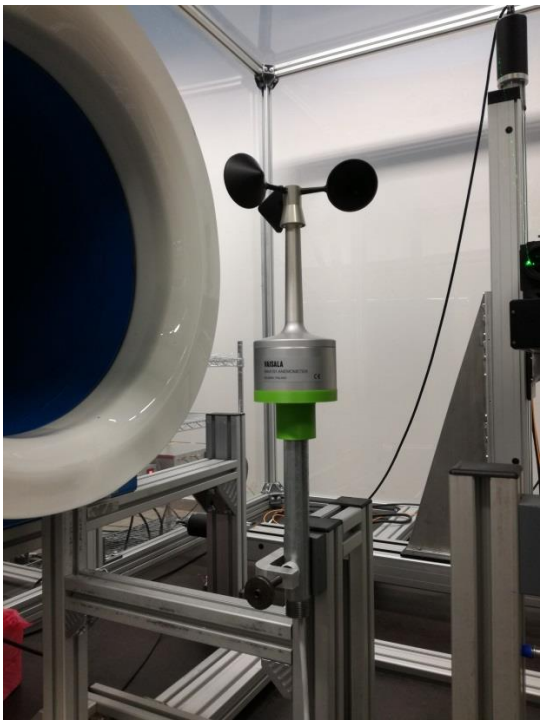

Fig. 2.5 Vaisala WAA151 at CMI

Basic parameters:

Range: (0.4 – 75) m/s
Dimensions:
rotor diameter (2 x distance from axis to outer edge of a cup): 18.2 cm
cup diameter: 5.3 cm
height from bottom to the top of the cups: 24.5 cm
Velocity indication: frequency output with conversion v (m/s) = 0.1007 x f (Hz) + 0.3278
Serial number: N3749498

Mounting in a wind tunnel:

The bottom side of the anemometer is connected to a plastic flange (the plastic flange was damaged and replaced by an aluminium one during the project) where a ¾" pipe (outer diameter 27 mm) is screwed. The installation of the anemometer in the wind tunnel of CMI is shown in Fig. 2.5.

The anemometer was provided by CMI.

Cup anemometer Thies First Class Advanced type 4.3351.10.000

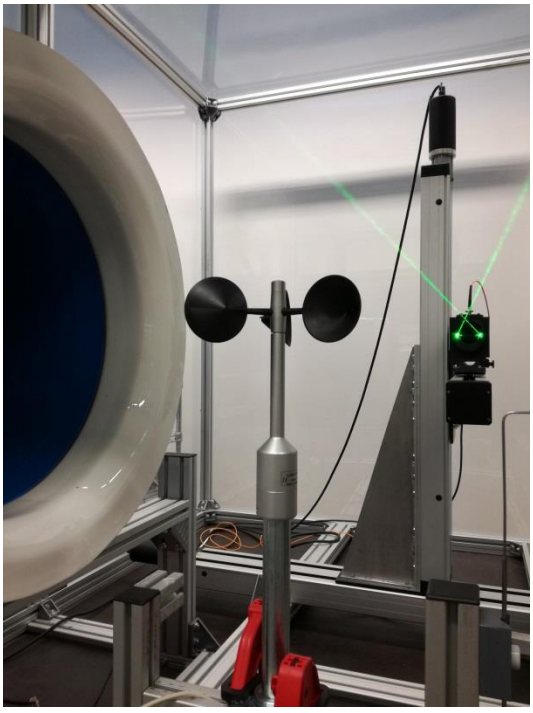

Fig. 2.6 anemometer Thies at CMI

Basic parameters:

Range: (0.3 – 75) m/s
Dimensions: see Fig. 2.7
Velocity indication: frequency output with conversion v (m/s) = 0.0462 x f (Hz) + 0.21
Serial number: 0504057

Mounting in a wind tunnel:

A 1" water pipe (outside diameter 34 mm) was fixed to the bottom of the anemometer. Installation of the anemometer in the wind tunnel of CMI is shown in Fig. 2.6.

The anemometer was provided by Deutsche WindGuard.

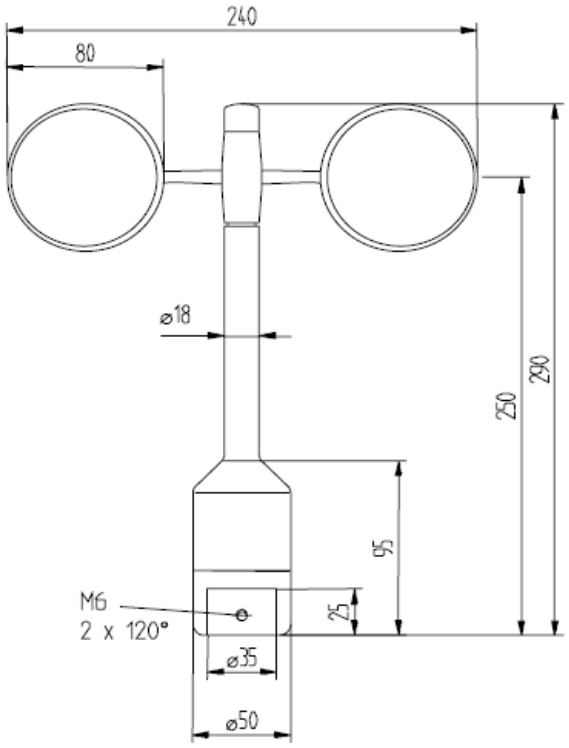

Fig. 2.7 Anemometer Thies First Class Advanced – dimensions

Thermal anemometer Airflow TA440

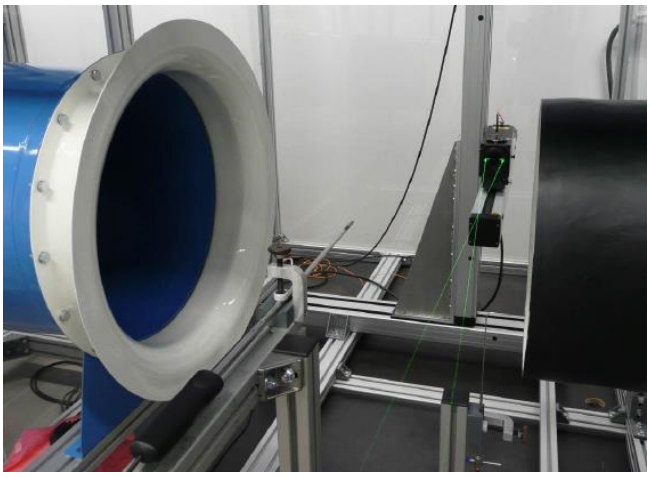

Fig. 2.8 Thermal anemometer Airflow at CMI

Fig. 2.9 The sensor part of the anemometer Airflow

Basic parameters:

Range: (0 – 30) m/s
Dimensions:
diameter of the probe tip: 7 mm
length of the telescopic rod: up to 1 m
Velocity indication: reading from the display
Resolution: 0.01 m/s
Serial number: TA4401237001

Mounting in a wind tunnel and settings:

The sensor is placed at a tip of a telescopic rod. The narrowest part of the telescope has the diameter of 7 mm. This part of the telescope must be pulled out fully since it contains the velocity, temperature and humidity sensors (Fig. 2.9). The actual air pressure in the measuring section is set into the meter manually since the meter does not contain the pressure sensor and the value is needed for the correct velocity reading. The installation of the meter in the wind tunnel of CMI is shown in Fig. 2.8.

Vane anemometer Schiltknecht MiniAir20 with a probe Mini

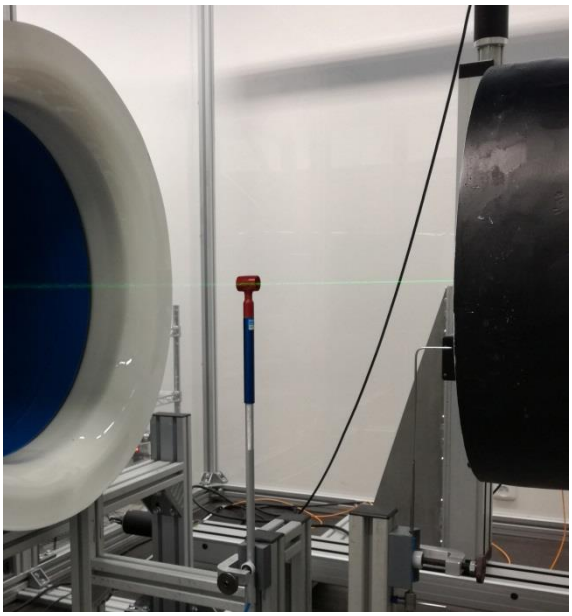

Fig. 2.10 Schiltknecht Mini at CMI

Basic parameters:

Range: (0.5 – 40) m/s
Dimensions:
outer diameter of the rotor head: 22 mm
depth of the rotor head: 28 mm
length of the probe from centre of the rotor to bottom of the handrail: 166 mm
Velocity indication: reading from the display
Resolution: 0.01 m/s
Serial number: probe: 77634, electronics: 75792

Mounting in a wind tunnel:

The mounting is the same as for the probe Schiltknecht Macro, i.e. an aluminium tube with outer diameter of 12 mm is used for mounting the meter. For installation of the meter in the wind tunnel of CMI see Fig. 2.10.

The anemometer was provided by METAS.

3 Participating laboratories

There were 12 laboratories from 9 countries with 14 wind tunnel setups participating in the project. The overview of the laboratories ordered chronologically according to time of measurement can be found in Tab. 3.1 below. A map of participants is presented in Fig. 3.1. Geometrical parameters of the wind tunnels are summarised in Tab. 3.2 including references to photos of the particular wind tunnels in appendix A.

Organisation	Short name	Country	Date of measurement
Czech Metrology Institute	CMI	CZ	1.11.2017-7.1.2018 28.5.-12.8. 2018 8.10.2018-1.2.2019 2.3.-31.4. 2019
E+E Elektronik GesmbH	BEV/E+E	AT	8.1.-21.1. 2018
Physikalisch-Technische Bundesanstalt	PTB	DE	22.1.-11.2. 2018
Deutsche WindGuard Wind Tunnel Services GmbH	DWG	DE	12.2.-25.2. 2018
Westenberg Engineering	WE	DE	26.2.-8.4. 2018
Lithuanian Energy Institute	LEI	LT	9.4.-29.4. 2018
Testing Centre, University of Tartu	TCUT	EST	30.4.-13.5. 2018
CETIAT	CETIAT	FR	14.5.-27.5. 2018
Federal Institute of Metrology METAS	METAS	CH	13.8.-2.9. 2018
TÜBİTAK UME	UME	TR	3.9.-7.10. 2018
Czech Hydrometeorological Institute	CHMI	CZ	4.2.-15.2. 2019
Danish Technological Institute	DTI	DK	18.2.-1.3. 2019

Tab. 3.1 Participating laboratories and time schedule

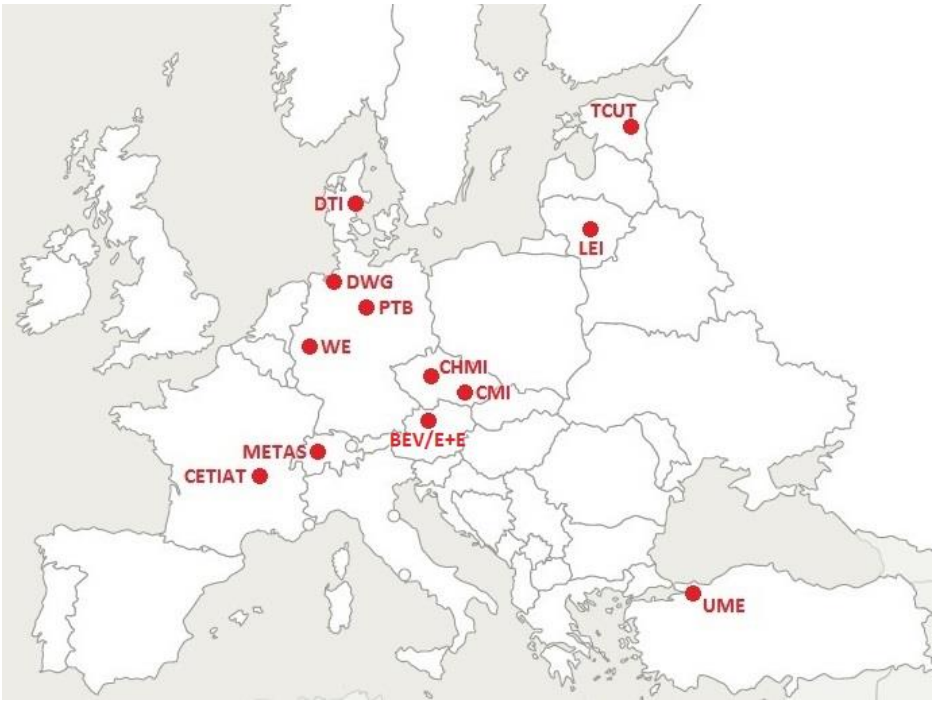

Fig. 3.1 Map of the participating laboratories

wind tunnel no.	lab	wind tunnel type	test section type	nozzle shape	nozzle diameter /width (cm)	test section length (cm)	reference anemometer	Fig. no.
1	DWG	closed	open[1]	square	100	180	Pitot tubes	A.1
2	WE800	open	box	circular	80	100	LDA	A.2
3	CHMI	closed	open	rectang.	50 x 60	100	LDA	A.3
4	CMI	closed	open	circular	45	63	LDA	A.4
5	LEI 1	closed	box	circular	40	100	LDA/US	A.5
6	PTB	closed	open	circular	32	46.8	LDA	A.6
7	UME	open	box	circular	31.5	58	LDA	A.7
8	BEV/E+E	closed	open[2]	circular	25.5	35	LDA	A.8
9	WE255	closed	open	circular	25.5	32	LDA	A.9
10	TCUT	open	box	circular	15.2	27	DP on nozzle	A.10
11	METAS	closed	closed[3]	rectang.	74 x 49	82	Vane/Pitot	A.11
12	CETIAT	closed	closed	square	51	100	LDA	A.12
13	DTI	open	closed	square	50	200	LDA	A.13
14	LEI 2	closed	closed	circular	40		LDA/US	A.5

[1] Bottom and top walls of the test section are present for the DWG wind tunnel
[2] Test section is enclosed to a large size chamber
[3] Bottom wall of the test section is not present for the METAS wind tunnel

Tab. 3.2 Overview of the participating wind tunnels

In Tab. 3.2 the test section type “open” means that any walls surrounding the test section are far enough from the test section, “box” means that the test section is enclosed in a box with walls that are wider than the nozzle of the wind tunnel and “closed” means that the test section is surrounded by walls with the same cross section as the nozzle of the wind tunnel.

Blockage ratios of the transfer standards in the wind tunnels

In Tab. 3.3 below, the blockage ratios of the large size anemometers in the participating wind tunnels are summarised. They are determined as ratio of projected cross-sectional area of the cup wheel or propeller, sensor and support apparatus of an anemometer to the total wind tunnel test section area.
According to ISO 17713-1 and EN 61400-12-1 the recommended blockage ratio of an anemometer is less than 5 % for a wind tunnel with closed test section and less than 10 % for a wind tunnel with open test section. In this work, however, we consider also larger blockage ratios in order to investigate the blockage effect in wider range.

The projected cross-sectional area of the Schiltknecht and Testo anemometers is estimated as $\pi d^2/4$ with d being the outer diameter of the frame surrounding the anemometer propeller (see Fig. 3.2 (a)). The exact cross-sectional area of the propeller parts of these anemometers is smaller than the calculated one since the blades of the vane does not cover all the circle. On the other hand the mounting rod area is not included.
For the cup anemometers Vaisala and Thies we denote d the diameter of a cup and D the diameter of the whole cup wheel. We estimate the cross-sectional area as $A_p + A_s$ with $A_p = \pi d^2/4 + d.(D - d)$ being the cross-sectional area of the propeller part (see Fig. 3.2 (b)) and A_s being a cross-sectional area of the part of a housing of an angular sensor which enters the air stream in the wind tunnel. Again the exact cross-sectional area of the propeller part of the cup anemometers is smaller than the calculated A_p since the cups does not cover all the area as depicted in the Fig. 3.2 (b). On the other hand the area of the thin part of the anemometer body holding the rotor is not included.
For the RM Young vane anemometer we denote d the propeller diameter and we calculate the cross-sectional area as the area of the real propeller projection which is approximately 2/5 of the area of the complete propeller circle (Fig. 3.2 (c)), i.e. it is $\pi d^2/10$. The mounting of the RM Young anemometer is located more than 40 cm behind the propeller so we suppose its role is negligible.

The procedures described above give just an estimate of the blockage ratios avoiding an analysis of the complex shapes of the anemometers with their mounting. The values, however, are not used for any exact calculations further. Also, the blockage ratio only roughly corresponds to the actual blockage effect since, for example, construction elements like frame around an anemometer propeller nearly do not change the front area of the anemometer but change the surrounding velocity field significantly as will be shown in the following tests.

wind tunnel	**test section**	**Schilt. Macro**	**Testo**	**RM Young**	**Vaisala**	**Thies**
		blockage ratio (%)				
DWG	open or box	0.57	0.90	1.3	1.4	2.2
WE800		1.1	1.8	2.5	2.8	4.4
CHMI		1.9	3.0	4.2	4.7	7.4
CMI		3.6	5.7	7.9	8.9	13
LEI 1		4.5	7.2	10	9.8	16
PTB		7.1	11	x	11	22
UME		7.3	12	16	12	23
BEV/E+E		11	18	25	18	35
WE255		11	18	x	x	x
TCUT		31	50	x	x	x
METAS	closed	1.6	2.5	3.5	3.9	6.1
CETIAT		2.2	3.5	4.8	5.4	8.5
DTI		2.3	3.6	5.0	5.7	8.9
LEI 2		4.5	7.2	10	11	x

Tab. 3.3 Blockage ratios of the transfer standards

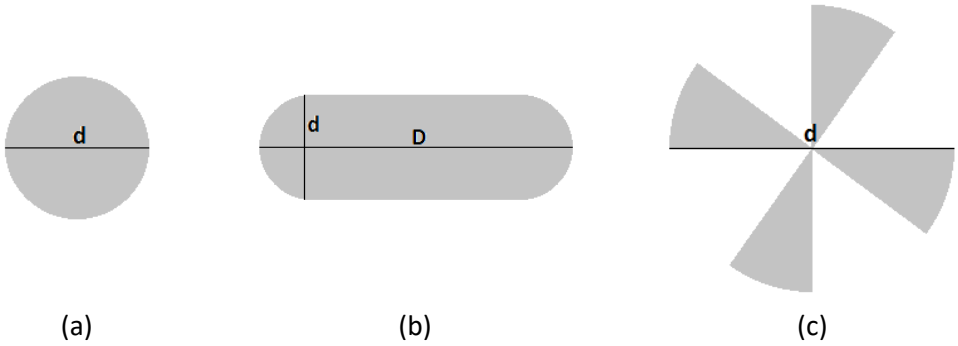

Fig. 3.2 Calculated cross-sectional areas of the anemometers

4 Measurement procedure

The anemometers were calibrated by the participating laboratories according to their standard procedures. The same mounting pipes have been used in all the laboratories. Calibration points are given in Tab. 4.1 below. The calibration velocities are the velocities *indicated by the meter under test* (not by the reference), i.e. the velocity in a wind tunnel was set in a way that the meter under test indicated values as near as possible to the values prescribed in the Tab. 4.1. In case of the anemometer Testo the 20 m/s was skipped since the meter has a range up to 15 m/s. For the anemometer Vaisala the 0.5 m/s was replaced by 1 m/s because of the starting threshold of the meter.

anemometer	calibration points (m/s)
Testo	0.5; 2; 5; 8; 12
Schiltknecht Macro	0.5; 2; 5; 8; 12; 20
RM Young	0.5; 2; 5; 8; 12; 20
Vaisala	1; 2; 5; 8; 12; 20
Thies	0.5; 2; 5; 8; 12; 20
Airflow	0.5; 2; 5; 8; 12; 20
Schiltknecht Mini	0.5; 2; 5; 8; 12; 20

Tab. 4.1 Calibration points

Calibrations at CMI have been performed 6 times during the lifespan of the project for each of the meters in order to evaluate the long-time stability of the meters and reproducibility of the measurements.

In order to find the systematic deviations in calibration results due to boundary conditions in a test section of a wind tunnel it is necessary to have other sources of systematic deviations under control. One such possible source is the influence of a tested anemometer to the velocity field in a position where a reference anemometer is placed. An investigation of this effect is summarised in the next section before we proceed to the calibration results.

5 Velocity fields in front of the anemometers

Velocity fields in front of the 5 tested large size anemometers have been measured in the wind tunnel of CMI for all velocities for which the calibrations have been performed and maps of distribution of the reference meter positions of the participating laboratories have been created. The velocity fields in front of the anemometers may differ in different wind tunnels so the maps presented here, obtained in the wind tunnel of CMI, give just an estimate of a size of the effect of the reference meter position.
The velocity fields have been measured with LDA placed on a 3D traversing system. Only the velocity component parallel to the axis of the test section has been measured. The graphs presented here shows a velocity disturbance caused by the tested meter which is determined as the difference between the velocity field with the anemometer installed and the velocity field measured in an empty test section. Since there can be a small unknown offset between the measurements with and without the anemometer, the velocity disturbance fields are determined up to this offset which means that their absolute value is not exactly known. Therefore, the isolines in the plots are not provided with values. On the other hand gradients of the velocity disturbance fields are not affected by the offset and a step between the isolines is well defined. In all the plots Fig. 5.1-5.7 the step between neighbouring isolines is 0.2 % of a nominal velocity. The plots then enable to estimate velocity differences between the position of the reference meter of all the participants and also enable to determine an area in front of a meter where the influence of the meter is negligible by looking for a negligible gradients of the velocity disturbance field.

In Fig. 5.1-5.3 the velocity disturbance fields in front of the vane anemometers are shown for the maximal velocities in which the anemometers have been calibrated (12 m/s for Testo and 20 m/s for Schiltknecht and RM Young). The fields were measured in a horizontal plane at a height corresponding to the centre of the anemometer's propeller in a 2 cm step grid of points in both axial and transversal directions corresponding to the grid nodes in the plots. The measurement grid starts 2.5 cm behind the wind tunnel nozzle which is circular with a diameter of 45 cm. For the vane anemometers the velocity field in a half of the depicted plane has been measured only. The field in the second half was completed assuming rotational symmetry of the meters and the flow with respect to the wind tunnel axis. The tested anemometers are depicted as the grey blocks above the upper line. The projection of the anemometer shape is rectangular since this is a top view.

In Fig. 5.4-5.7 the velocity disturbance fields in front of the cup anemometers are shown for the maximal velocity 20 m/s. The flow around the cup anemometers is not axially symmetric as in the case of vane anemometers and therefore it is not sufficient to measure the velocity field just in a horizontal half-plane. The Figs. 5.4 and 5.6 again show the velocity disturbance field in a horizontal plane at a height corresponding to the centre of the anemometer's propeller. In this case the field in the whole plane was measured and we can see the flow asymmetry. The Figs. 5.5 and 5.7 then show the velocity disturbance field in a vertical plane given by the axis of the wind tunnel test section and rotation axis of the anemometer. Only a half-plane above the propeller centre was measured since nobody place the reference meter below - in front of the anemometer body. Again, the grid starts 2.5 cm behind the wind tunnel nozzle and the grid step is 2 cm in both directions.

The positions of the reference anemometers of the laboratories are depicted as the red dots which are numbered according to the wind tunnel numbering introduced in the Tab. 3.2. Mutual positions of a reference and MUT are also in Tab. 5.1. The wind tunnel setups LEI 1 and LEI 2 are not included since, in case of LEI 1, the reference meter is placed at least 1.5 m in front of the meter under test and, in case of LEI 2, the ultrasonic flow meter is used as a reference for calibration of the large size anemometers (see Fig. A.5b). In this case the ultrasonic flow meter is calibrated against LDA which is installed near the position for MUT when there is no MUT present. The wind tunnel of TCUT is not included since it uses a differential pressure measurement at the wind tunnel nozzle as a reference. In case of the tested vane anemometers the position of the reference meters which are not placed in the horizontal plane at the level of anemometer centre has been rotated and depicted in this plane taking the axial symmetry into account.

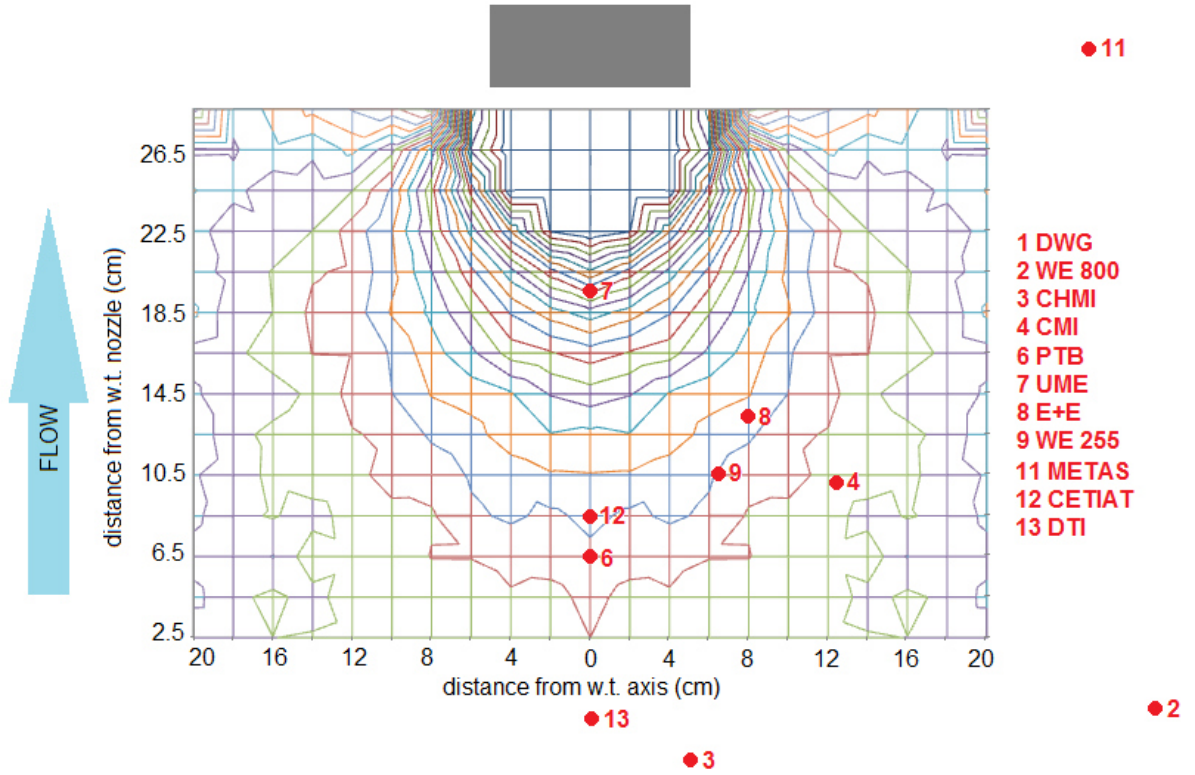

Fig. 5.1 Testo - velocity disturbance field measured in the wind tunnel of CMI; 12 m/s; isolines with step 0.2 % of 12 m/s; dots represent a reference anemometer position relative to the MUT in various wind tunnels (the position of DWG is out of the plot).

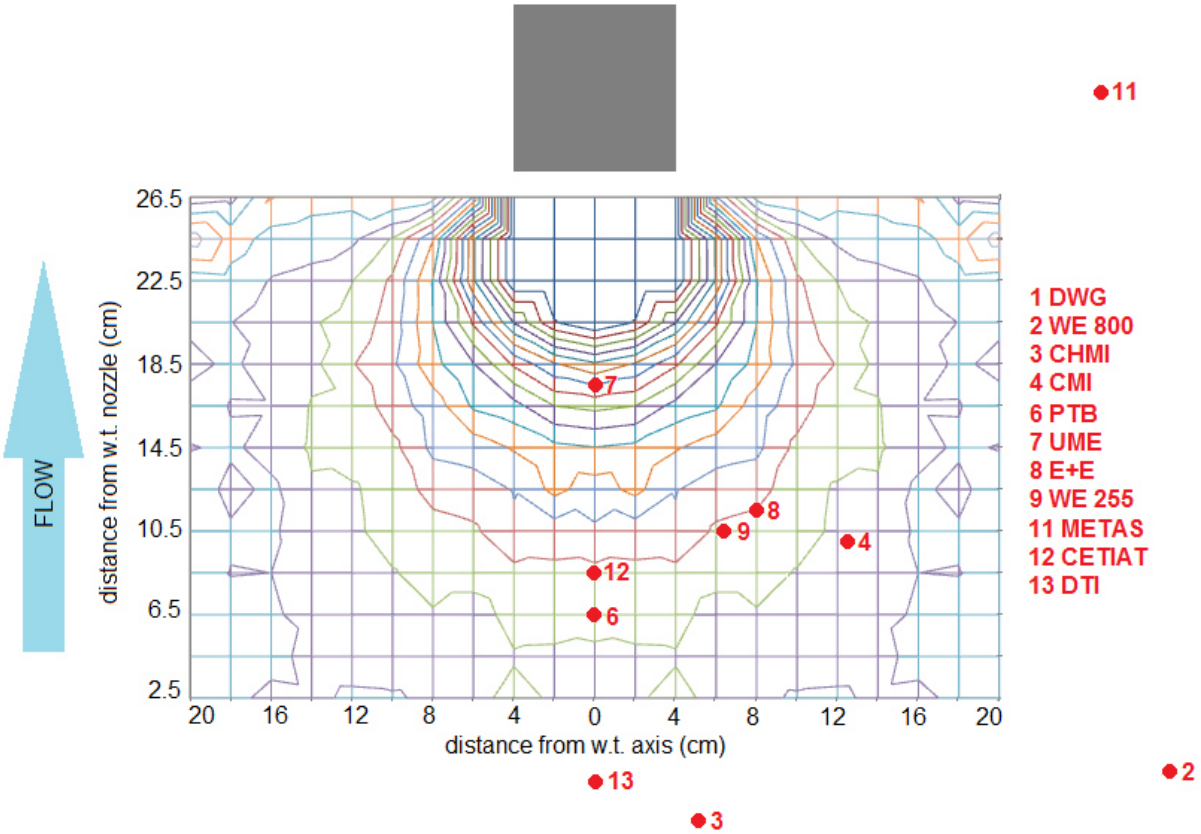

Fig. 5.2 Schiltknecht Macro - velocity disturbance field measured in the wind tunnel of CMI; 20 m/s; isolines with step 0.2 % of 20 m/s; dots represent a reference anemometer position relative to the MUT in various wind tunnels (the position of DWG is out of the plot).

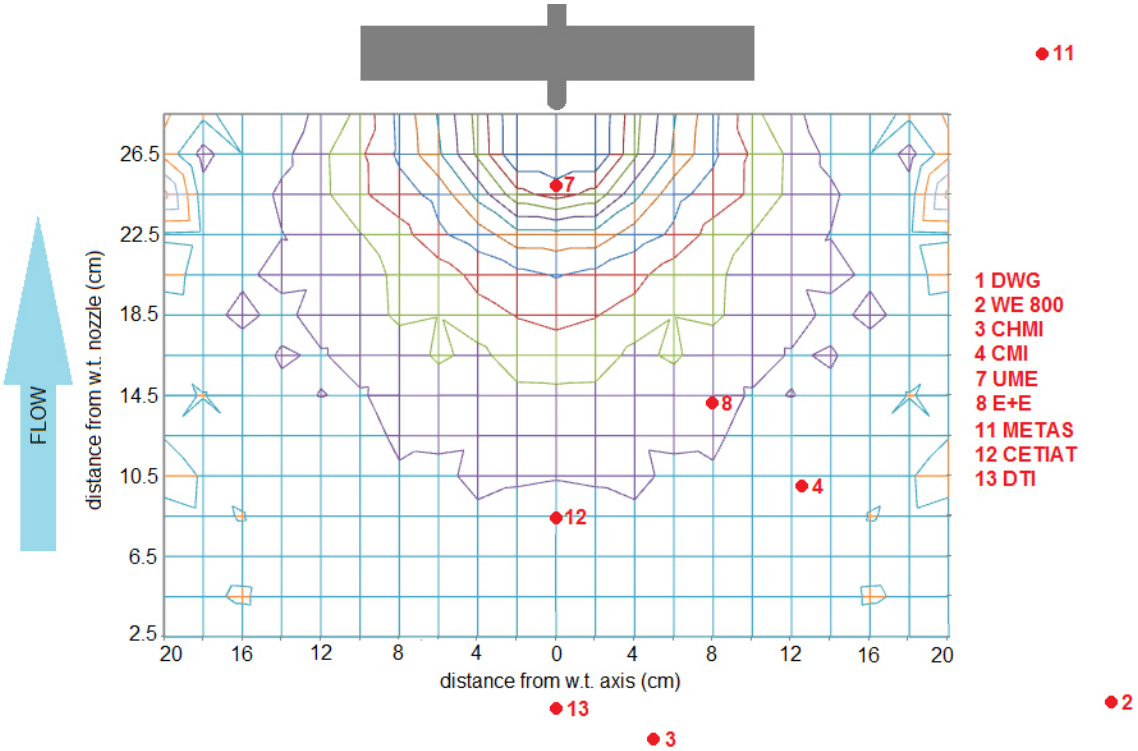

Fig. 5.3 RM Young - velocity disturbance field measured in the wind tunnel of CMI; 20 m/s; isolines with step 0.2 % of 20 m/s; dots represent a reference anemometer position relative to the MUT in various wind tunnels (the position of DWG is out of the plot).

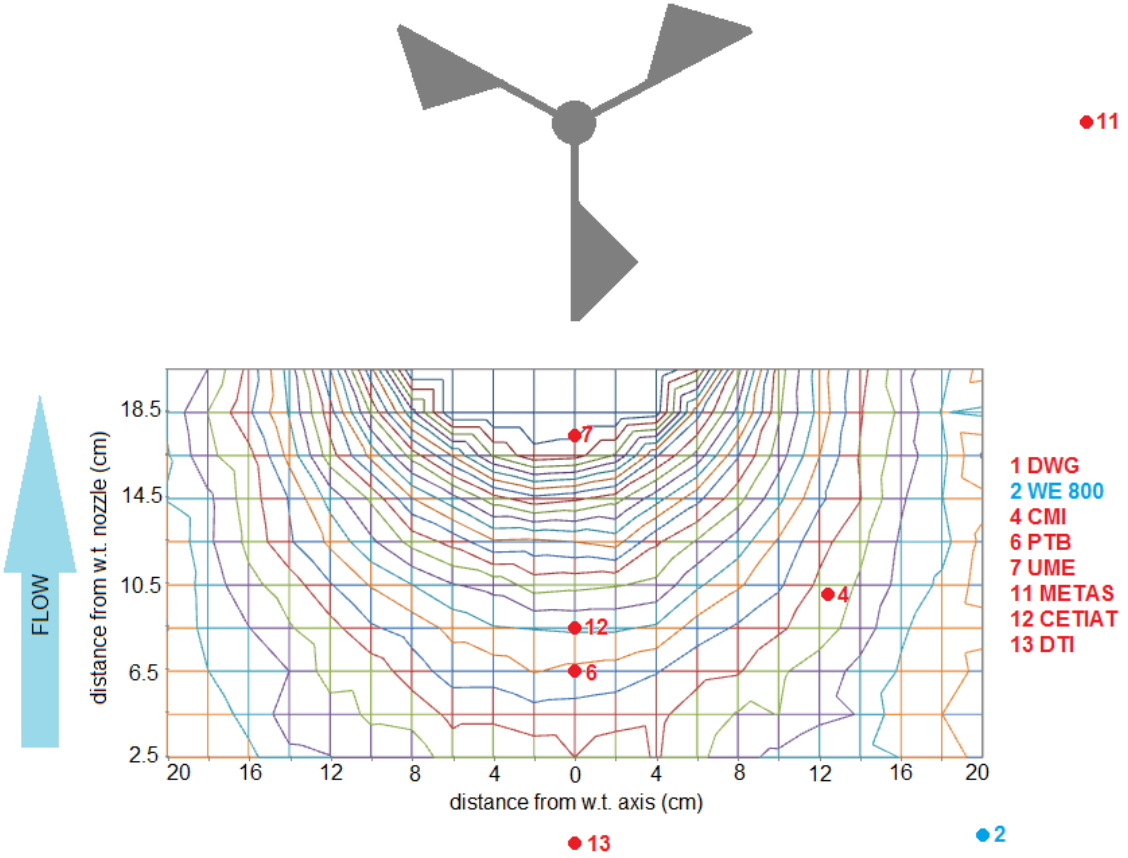

Fig. 5.4 Vaisala - velocity disturbance field in horizontal plane measured in the wind tunnel of CMI; 20 m/s; isolines with step 0.2 % of 20 m/s; dots represent a reference anemometer position relative to the MUT in various wind tunnels (the position of DWG is out of the plot); the blue dot is 20 cm out of the plane towards the reader.

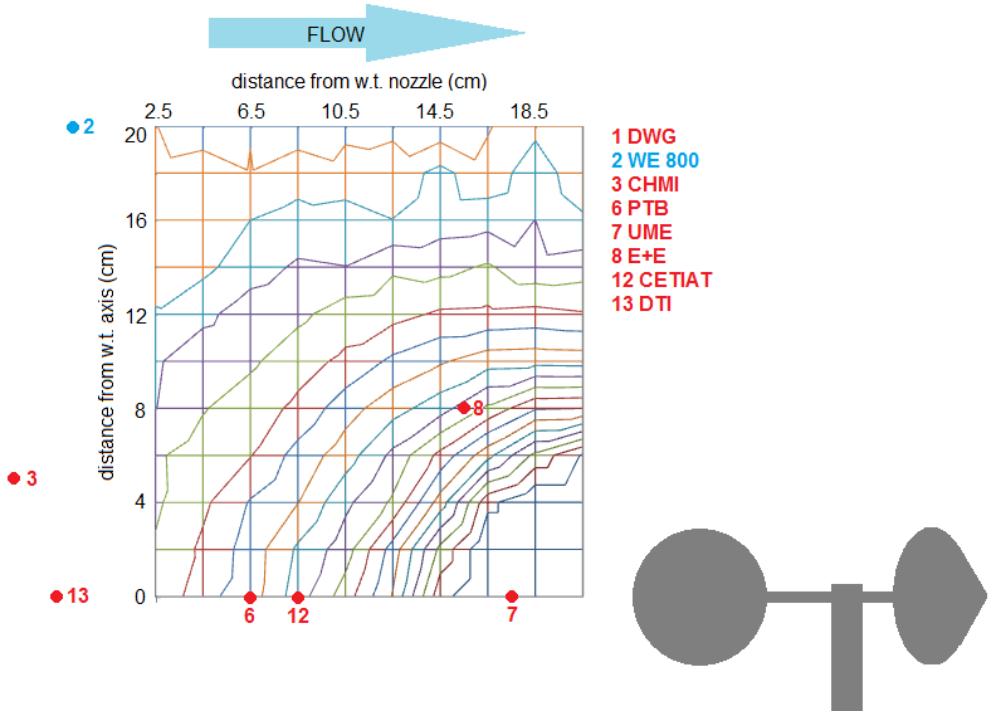

Fig. 5.5 Vaisala - velocity disturbance field in vertical plane measured in the wind tunnel of CMI; 20 m/s; isolines with step 0.2 % of 20 m/s; dots represent a reference anemometer position relative to the MUT in various wind tunnels (the position of DWG is out of the plot); the blue dot is 20 cm out of the plane towards the reader.

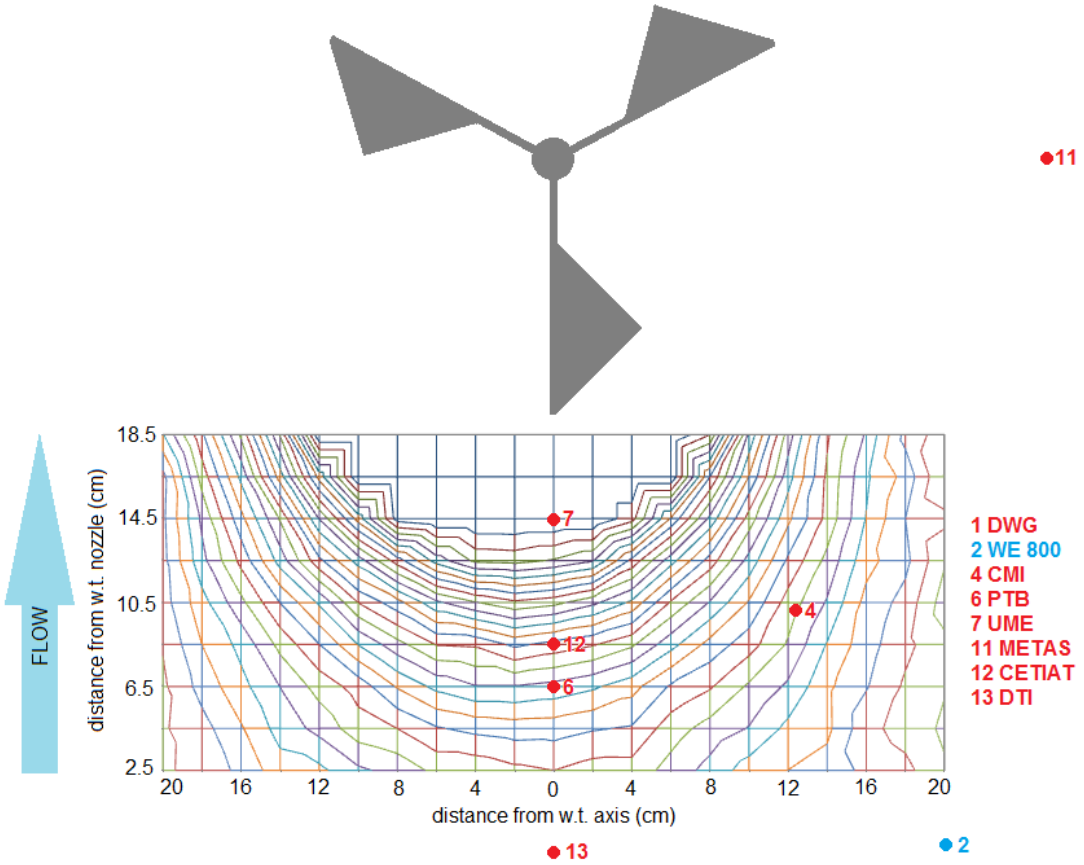

Fig. 5.6 Thies - velocity disturbance field in horizontal plane measured in the wind tunnel of CMI; 20 m/s; isolines with step 0.2 % of 20 m/s; dots represent a reference anemometer position relative to the MUT in various wind tunnels (the position of DWG is out of the plot); the blue dot is 20 cm out of the plane towards the reader.

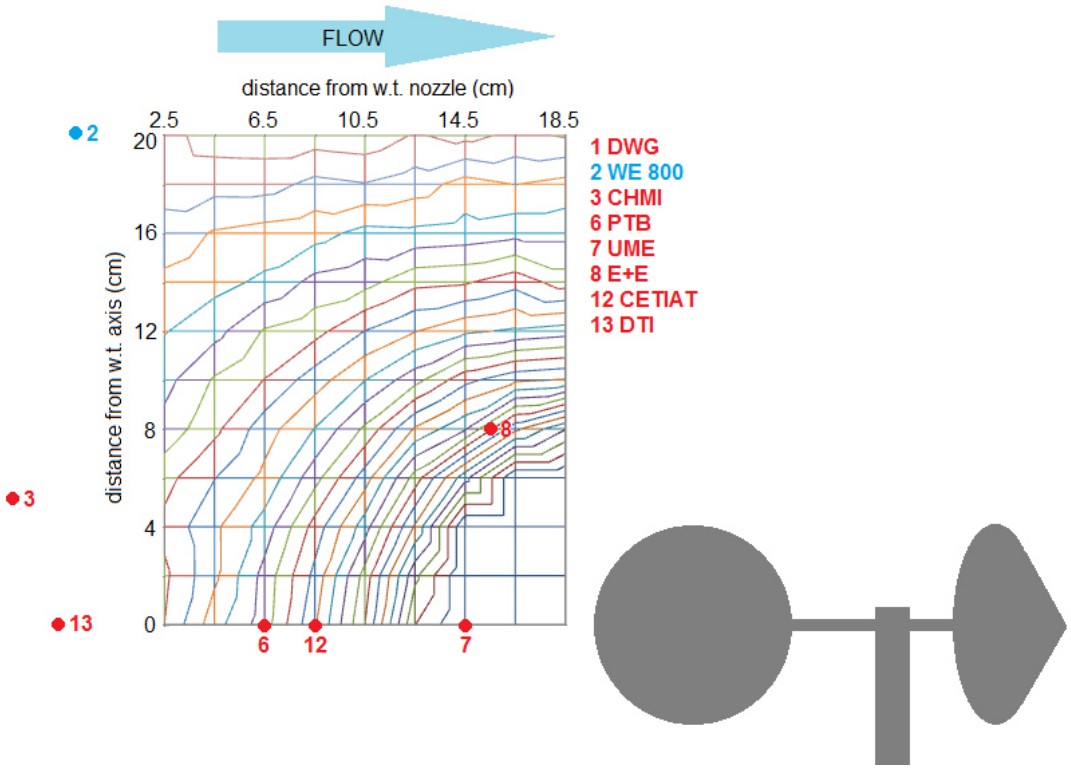

Fig. 5.7 Thies - velocity disturbance field in vertical plane measured in the wind tunnel of CMI; 20 m/s; isolines with step 0.2 % of 20 m/s; dots represent a reference anemometer position relative to the MUT in various wind tunnels (the position of DWG is out of the plot); the blue dot is 20 cm out of the plane towards the reader.

The velocity disturbance fields for lower velocities, expressed in a relative way as percentage of a nominal velocity, look very similar to the ones for the maximal velocities depicted here. The fields for different velocities have been compared at the axis of the test section - see Figs. 5.8-5.12. In these plots the horizontal z-axis gives position along the axis of the test section with zero being 1.5 cm behind the wind tunnel nozzle. At this z-axis the centre of the propeller of the anemometers is always at 30 cm position (31.5 cm behind the nozzle). The velocity disturbance dv at the vertical axis is defined as a difference of velocities with minus without the anemometer installed in the test section. Again the dv is given up to a small unknown offset and the curves for all the velocities are shifted to zero at the $z = 0$ position. We can see that slightly larger velocity gradients have been observed only for the lowest velocity 0.5 m/s and for some of the anemometers (RM Young and Schiltknecht).

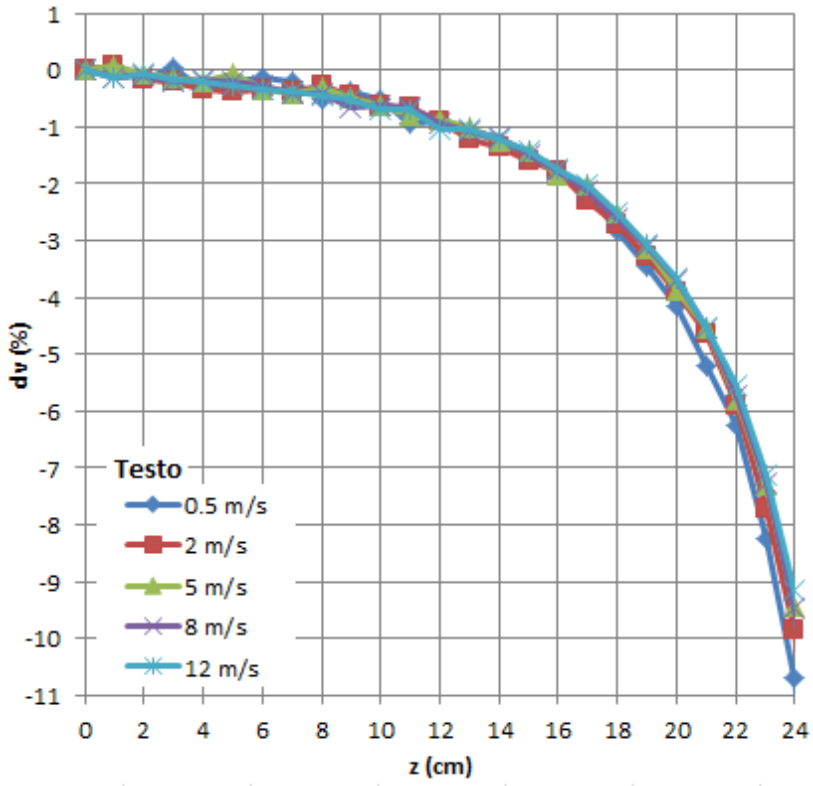

Fig. 5.8 Axial velocity disturbance for various velocities in front of the anemometer Testo

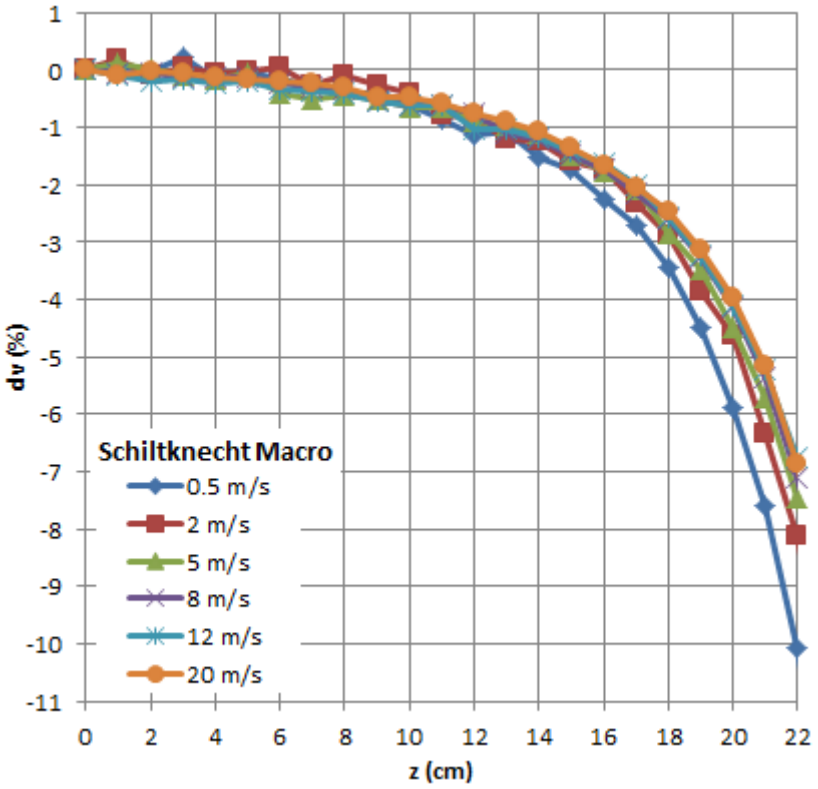

Fig. 5.9 Axial velocity disturbance for various velocities in front of the Schiltknecht Macro probe

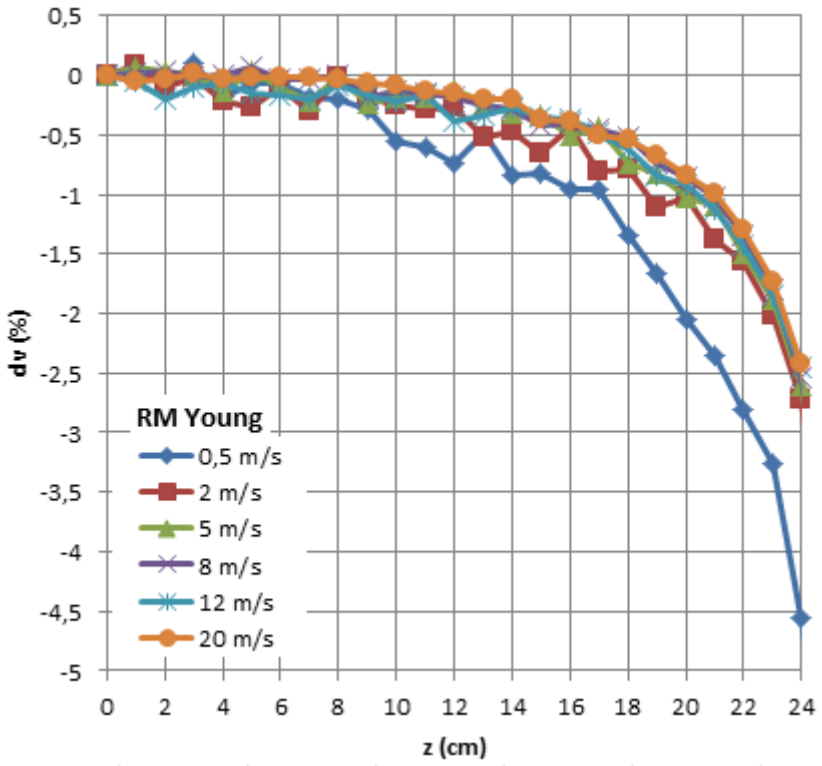

Fig. 5.10 Axial velocity disturbance for various velocities in front of the anemometer RM Young

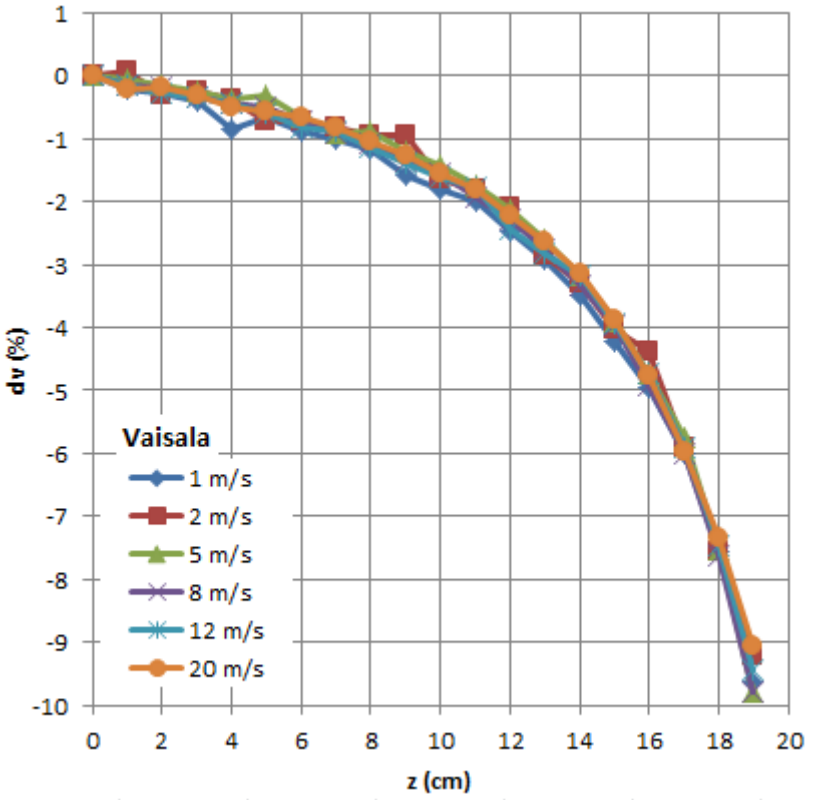

Fig. 5.11 Axial velocity disturbance for various velocities in front of the anemometer Vaisala

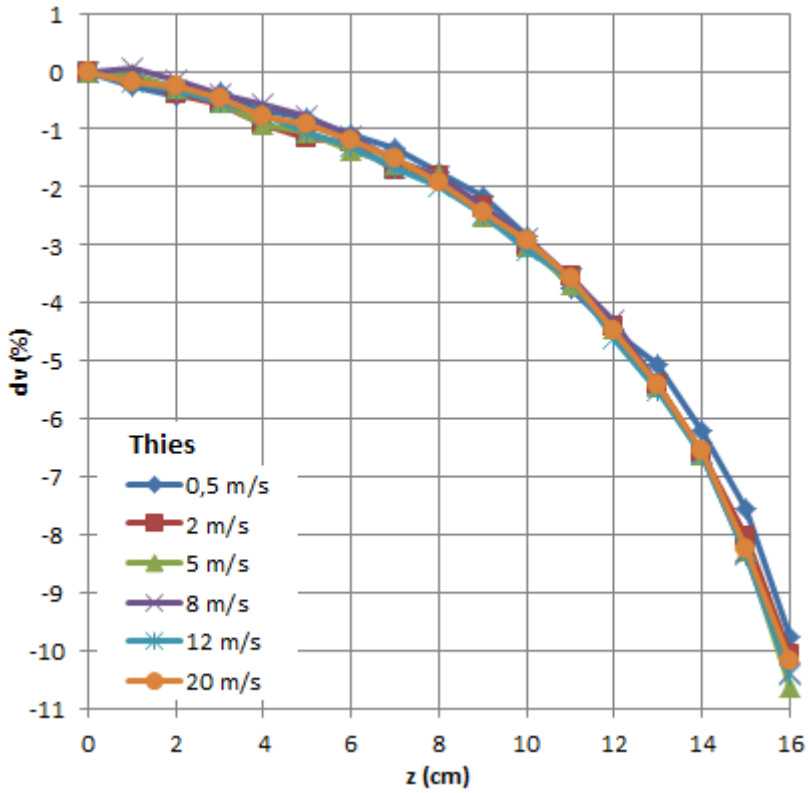

Fig. 5.12 Axial velocity disturbance for various velocities in front of the anemometer Thies

From the measured velocity disturbance fields (Fig. 5.1-5.12) we see that the velocity gradients in front of the anemometers strongly depend not only on the anemometer size but also on the anemometer construction. The lowest influence was observed for the 20 cm vane anemometer RM Young Gill Propeller (Fig. 5.3 and 5.10) even if it has the blockage ratio which is the largest from the vane anemometers and comparable to the blockage ratio of the smaller cup anemometer Vaisala. The smaller vane anemometers Schiltknecht and Testo have a frame around their propellers which is not moving and stops the air causing the larger influence in front of the meters (see Figs. 5.1, 5.2, 5.8, 5.9). For the vane anemometers one can conclude that most of the wind tunnels have a reference meter in an area where the velocity gradient causes systematic deviations of a few tenths of percent between the labs which may be a significant value compared to typical uncertainty values, however, in most cases it is not a leading uncertainty component.
On the other hand for cup anemometers the velocity gradients in front of the meters are larger (see Figs. 5.4-5.7, 5.11, 5.12). The systematic deviations between the labs due to the velocity gradient can exceed 1 % and therefore the velocity gradient becomes one of the dominant uncertainty sources.
Therefore, if we want to investigate the effect of boundary conditions in a wind tunnel and we want to avoid mixing with other effects like this effect of velocity gradient in front of a meter, it seems, that for the vane anemometers in this project it will be viable but for the cup anemometers it will be challenging.
Further discussion of the measured velocity disturbance fields follows in the next section with calibration results.

	(mm)	Airflow	Schilt. Mini	Schilt. Macro	Testo	RM Young	Vaisala	Thies
DWG	dx	350	350	350	350	350	350	350
	dy	350	350	350	350	350	350	350
	dz	1050	1050	1050	1050	1050	1050	1050
WE 800	dx	200		200	200	200	200	200
	dy	-200		-200	-200	-200	-200	-200
	dz	325		325	325	325	325	325
CHMI	dx	0	0	0	0	0	0	0
	dy	-50	-50	-50	-50	-50	-50	-50
	dz	350	350	350	350	350	350	350
CMI	dx	125	125	125	125	125	125	125
	dy	0	0	0	0	0	0	0
	dz	215	215	215	215	215	215	215
LEI 1	dx			0	0	0	0	0
	dy			0	0	0	0	0
	dz			1500	1500	1500	1500	1500
PTB	dx	0	0	0	0		0	0
	dy	0	0	0	0		0	0
	dz	250	250	250	250		250	250
UME	dx	0		0	0	0	0	0
	dy	0		0	0	0	0	0
	dz	100		140	121	65	141	170
BEV/E+E	dx	0	0	0	0	0	0	0
	dy	-80	-80	-80	-80	-80	-80	-80
	dz	160	175	200	181	175	160	160
WE 255	dx	45	45	45	45			
	dy	-45	-45	-45	-45			
	dz	110	210	210	210			
METAS	dx	250		250	250	250	250	250
	dy	0		0	0	0	0	0
	dz	0		0	0	0	0	0
CETIAT	dx	0		0	0	0	0	0
	dy	0		0	0	0	0	0
	dz	230		230	230	230	230	230
DTI	dx	0	0	0	0	0	0	0
	dy	0	0	0	0	0	0	0
	dz	330	330	330	330	330	330	330

Tab. 5.1 Mutual positions of a reference anemometer and a tested anemometer; *x,y,z* axes form an orthonormal right-handed basis, *z*-axis is pointing in the wind stream direction, *y*-axis is vertical pointing upwards, *x*-axis is horizontal; $(dx, dy, dz) = (x, y, z)_{MUT} - (x, y, z)_{REF}$ where the coordinates of MUT are coordinates of the geometrical centre of the propeller head in case of the vane or cup anemometers or coordinates of the thermal element in case of the thermo-anemometer.

6 Stability tests

All the tested anemometers have been calibrated 6 times at CMI during the lifetime of the project in order to test their stability and reproducibility of measurement at CMI. The 6 calibration curves for each meter including the calibration dates are shown in the graphs Fig. 6.1-6.7 below. Span of the errors defined as a difference of the maximum and the minimum error is for each meter and velocity summarised in Tab. 6.1. We see that the stability of the meters is good besides a few cases in the lowest velocities near to the lower range of the meters and besides the thermo-anemometer Airflow for higher velocities. The reason for instability of the anemometer Airflow is not known but one of the possibilities is contamination of the heated element by LDA seeding. The instability of the anemometer Airflow was the reason for additional measurements with the anemometer Schiltknecht Mini in order to have data from a stable meter with negligible blockage effect. However, another issues with the probe Schiltknecht Mini arose as will be discussed in the following sections.

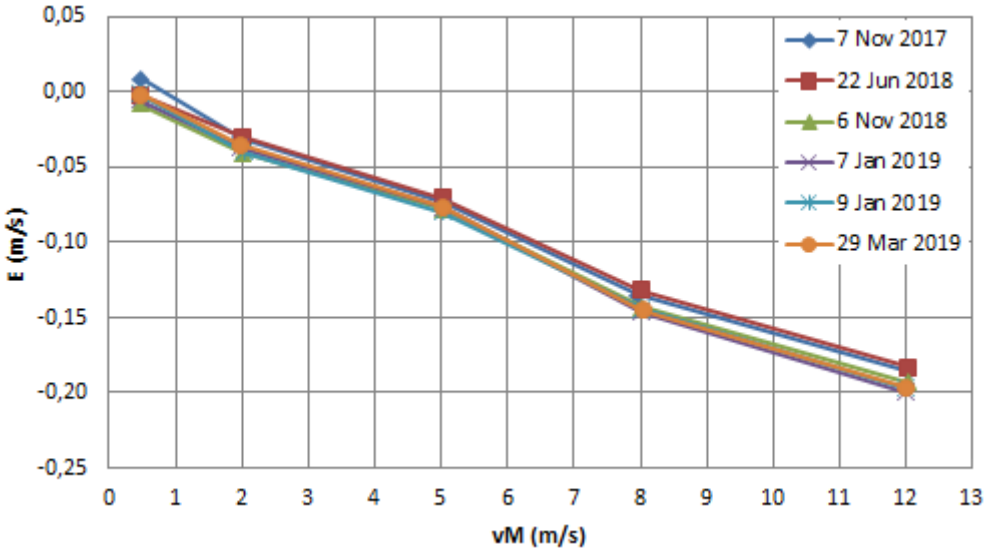

Fig. 6.1 Repeated calibration curves for the anemometer Testo

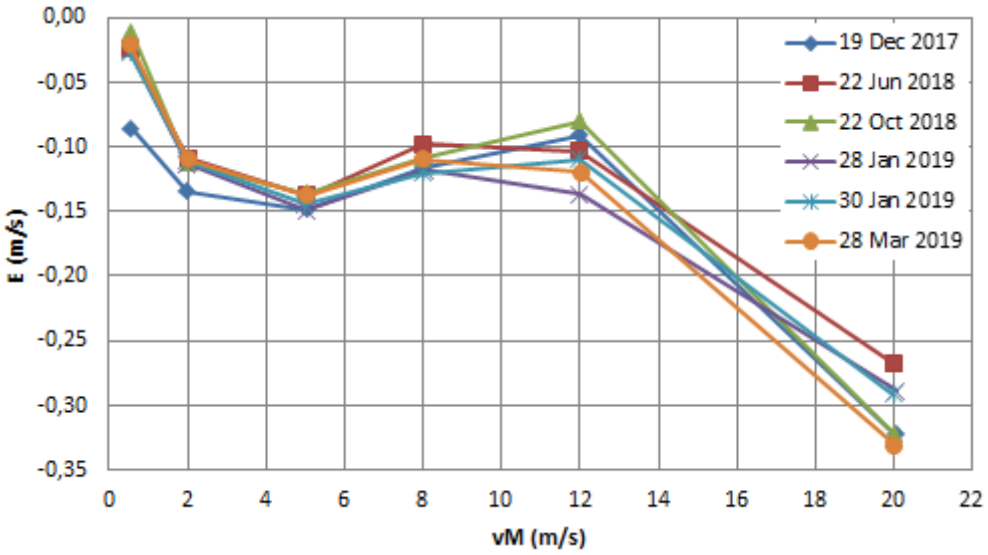

Fig. 6.2 Repeated calibration curves for the anemometer Schiltknecht Macro

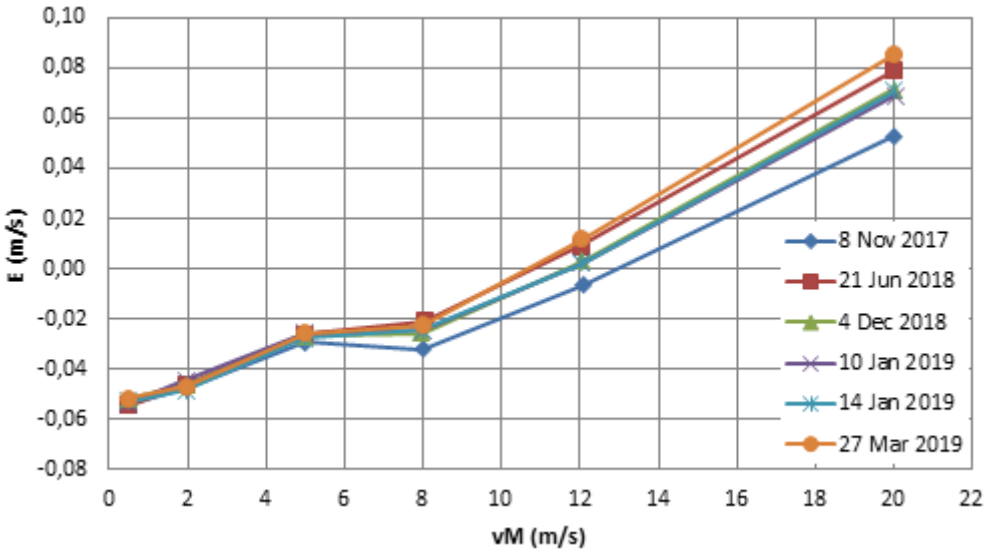

Fig. 6.3 Repeated calibration curves for the anemometer RM Young

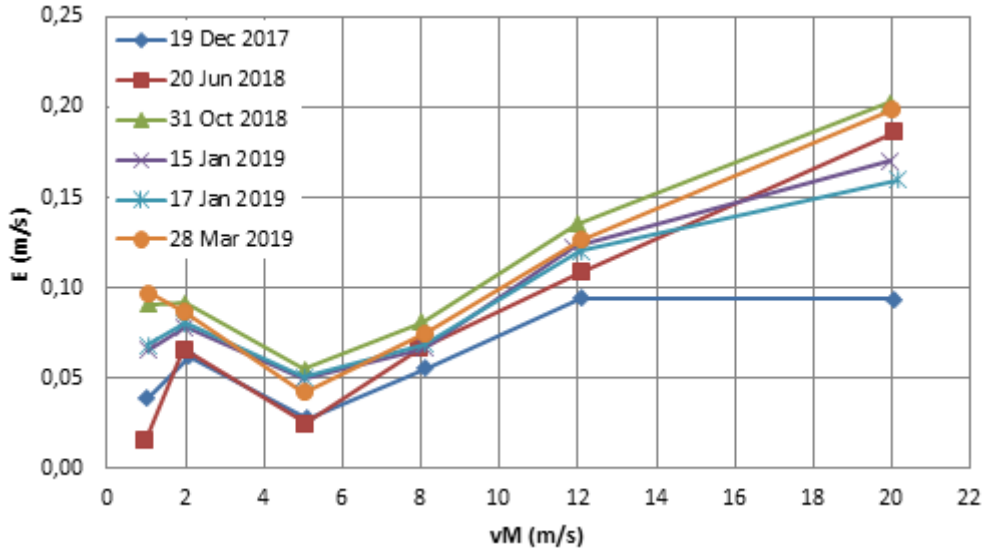

Fig. 6.4 Repeated calibration curves for the anemometer Vaisala

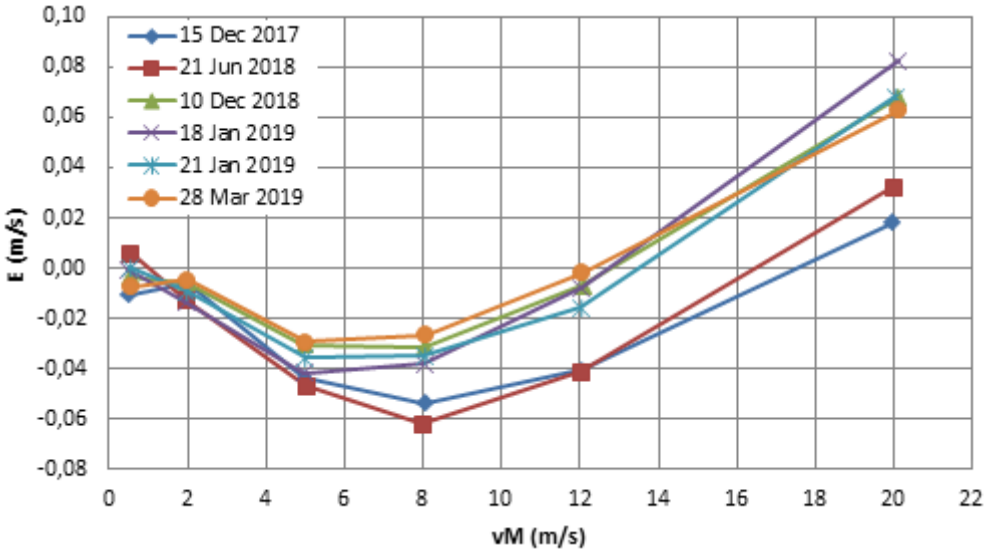

Fig. 6.5 Repeated calibration curves for the anemometer Thies

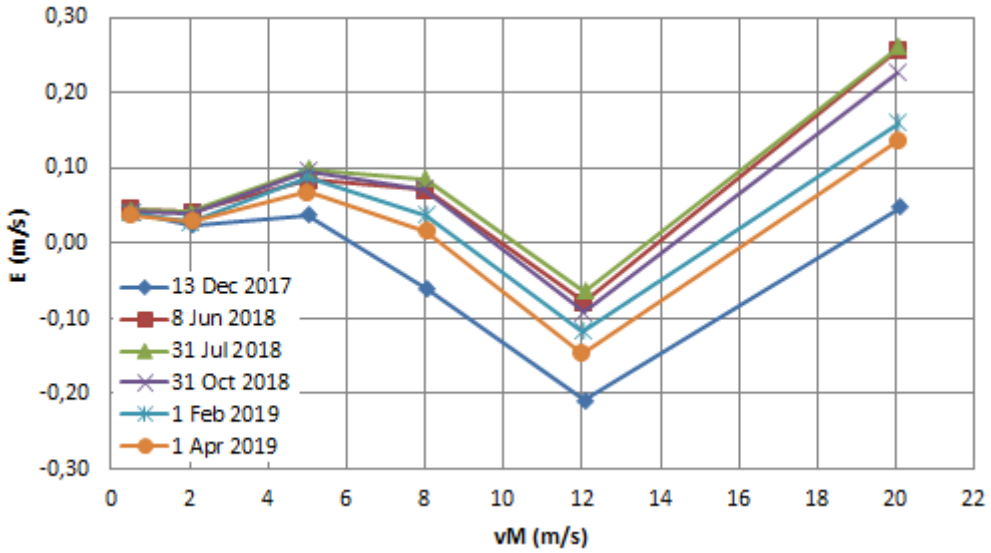

Fig. 6.6 Repeated calibration curves for the anemometer Airflow

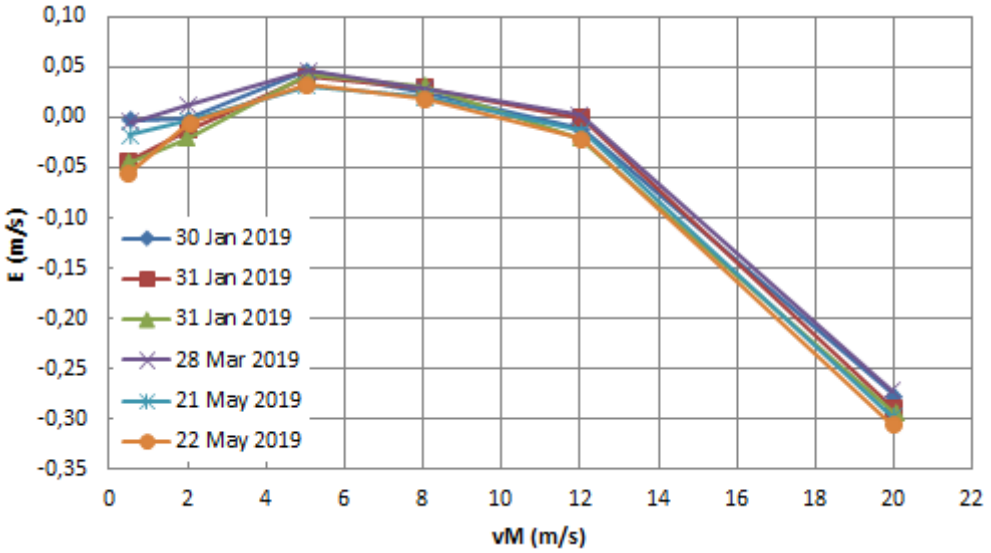

Fig. 6.7 Repeated calibration curves for the anemometer Schiltknecht Mini

	Testo	Schilt. Macro	RM Young	Vaisala	Thies	Airflow	Schilt. Mini
v (m/s)	E_max – E_min (m/s)						
0.5	0.017	0.074	0.003		0.016	0.008	0.053
1				0.081			
2	0.011	0.025	0.004	0.030	0.009	0.018	0.033
5	0.010	0.013	0.004	0.030	0.017	0.061	0.015
8	0.015	0.022	0.011	0.026	0.035	0.147	0.013
12	0.016	0.057	0.018	0.041	0.039	0.146	0.024
20		0.063	0.033	0.109	0.064	0.212	0.034

Tab. 6.1 Span of errors from 6 repeated calibrations at CMI

7 Calibration results

The complete calibration data are summarised in Appendix B. As some laboratories apply a correction to their reference velocity and/or an uncertainty component related to the blockage effect and the methods of evaluation of such corrections and uncertainties differ from lab to lab (see section 7.3 for details) the calibration data in the Appendix B include both – anemometer errors including and not-including the blockage effect correction (if applied) and expanded uncertainties ($k = 2$) including and not-including a blockage effect component (if applied).
The data exposition below is divided into two main parts. In section 7.1 a comparison of the classical calibration curves is shown which include all the blockage effect corrections and uncertainties of the participating laboratories. In section 7.2 dependencies of the obtained anemometer errors on the wind tunnel size (reciprocal cross-sectional area of the test section) are shown for both data sets – with and without the blockage effect corrections and uncertainties.

7.1 Errors as functions of air-speed – comparison of classical calibration curves

In graphs Fig. 7.1-7.7 error curves of the 7 anemometers in the participating wind tunnels are shown. The v_M axis displays a velocity indicated by a meter under test. The E axis displays the error of a meter, i.e. $E = v_M - v_{ref}$ with v_{ref} being a reference velocity. The curves drawn by a full line belong to wind tunnels satisfying the criteria of [8, 10] on the blockage ratio, i.e. less than 10 % for open test sections and less than 5 % for closed test sections. For test sections bounded by a box the 10 % criterion was used. The curves drawn by a dashed line belong to wind tunnels which exceed these limits. Uncertainty bars are not included for all the error curves in the Figs. 7.1-7.7, however, for each velocity there is a pair of lines showing stability of the meter and typical expanded uncertainty of the calibrations. The span of the left line from a pair is given as difference between maximal and minimal error of the meter obtained during the six repeated calibrations at CMI (Tab. 6.1). The span of the right line from a pair is given as median of all expanded uncertainty intervals as reported by the participating laboratories. Only the span of the lines plays a role. The position of the lines in the plots has just a graphical justification.

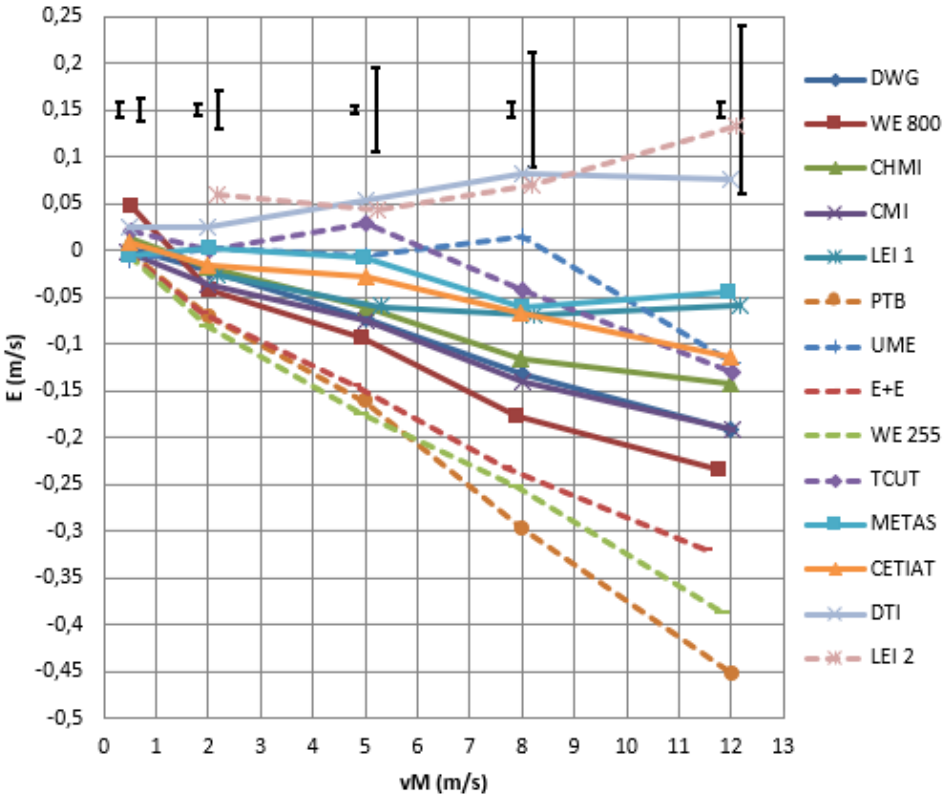

Fig. 7.1 Error curves – Testo; for explanation of the graphical elements see the text

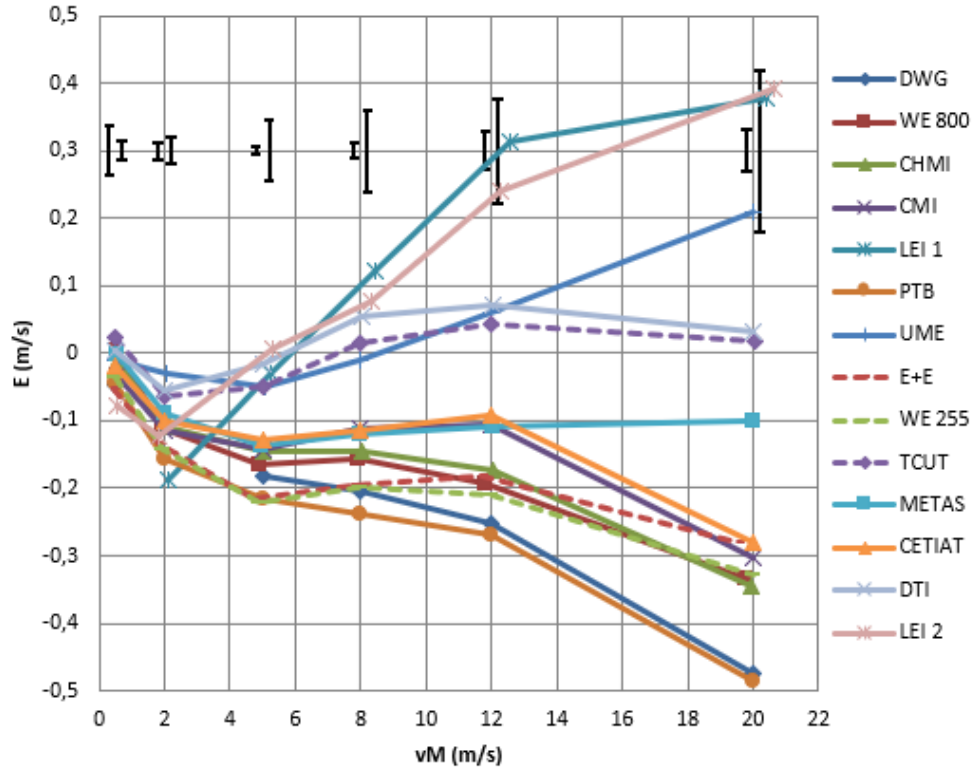

Fig. 7.2 Error curves – Schiltknecht Macro; for explanation of the graphical elements see the text

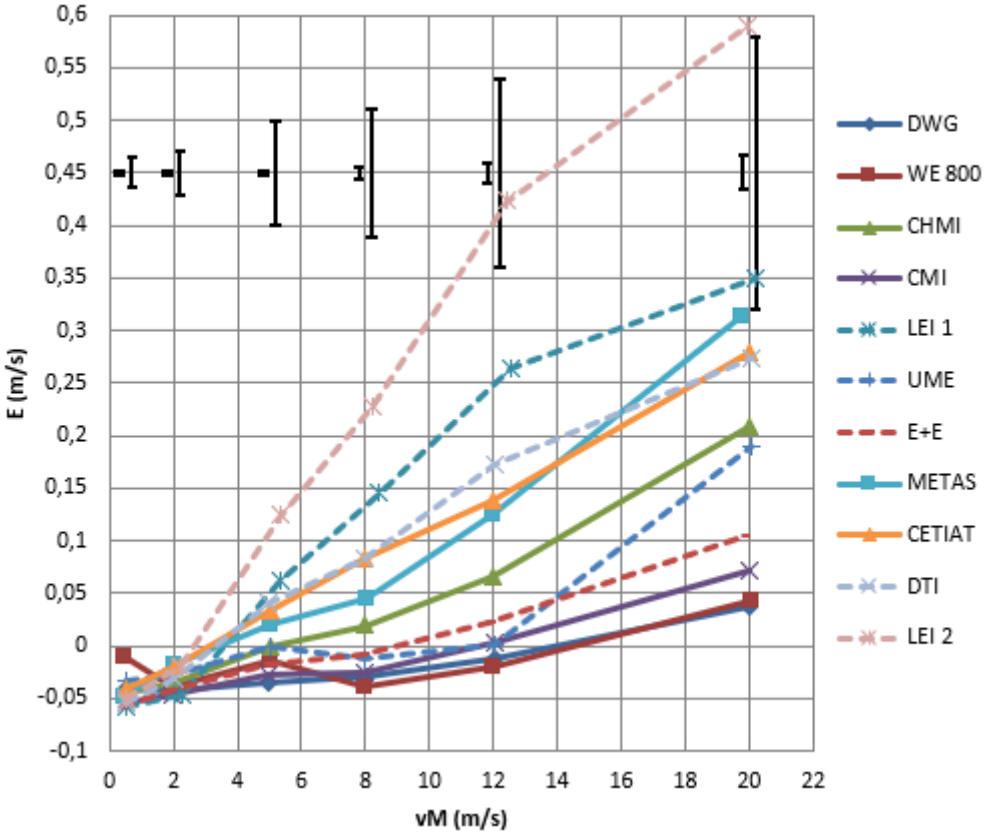

Fig.7.3 Error curves – RM Young; for explanation of the graphical elements see the text

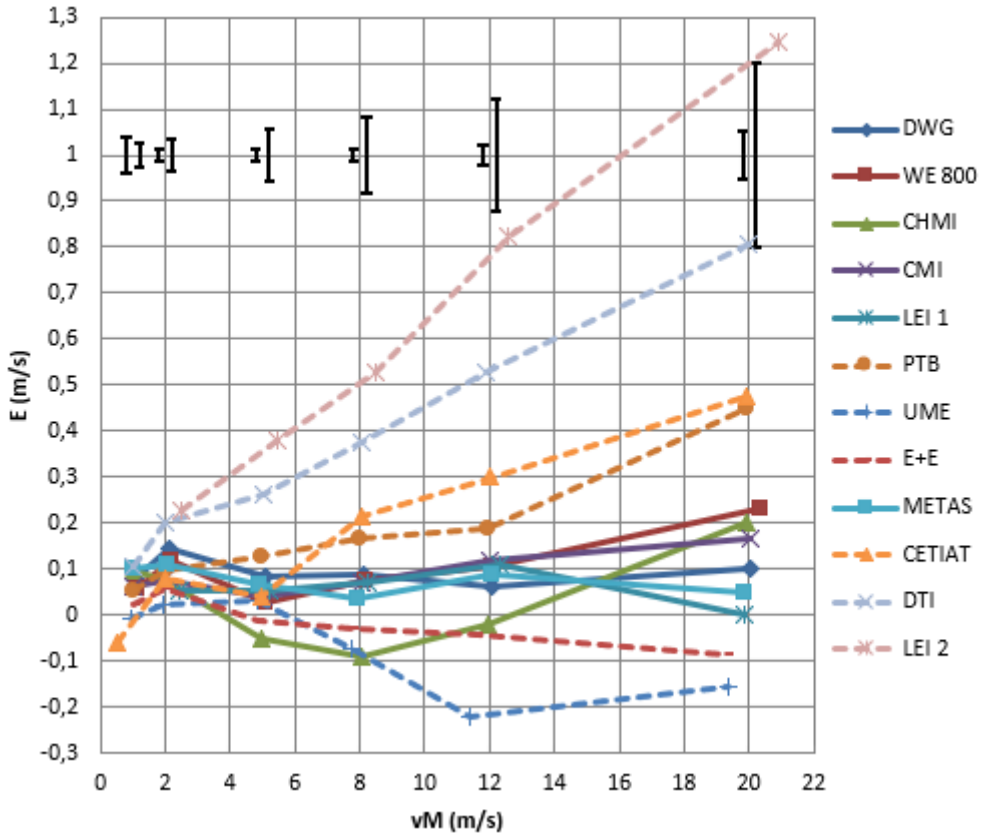

Fig. 7.4 Error curves – Vaisala; for explanation of the graphical elements see the text

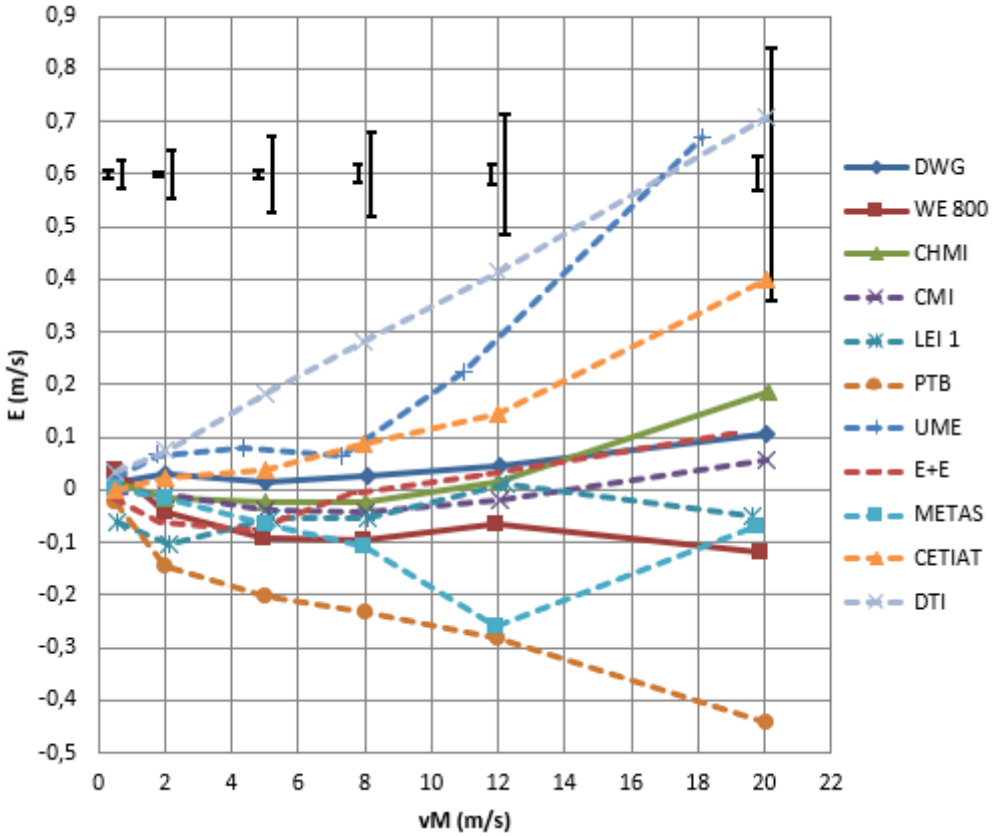

Fig. 7.5 Error curves – Thies; for explanation of the graphical elements see the text

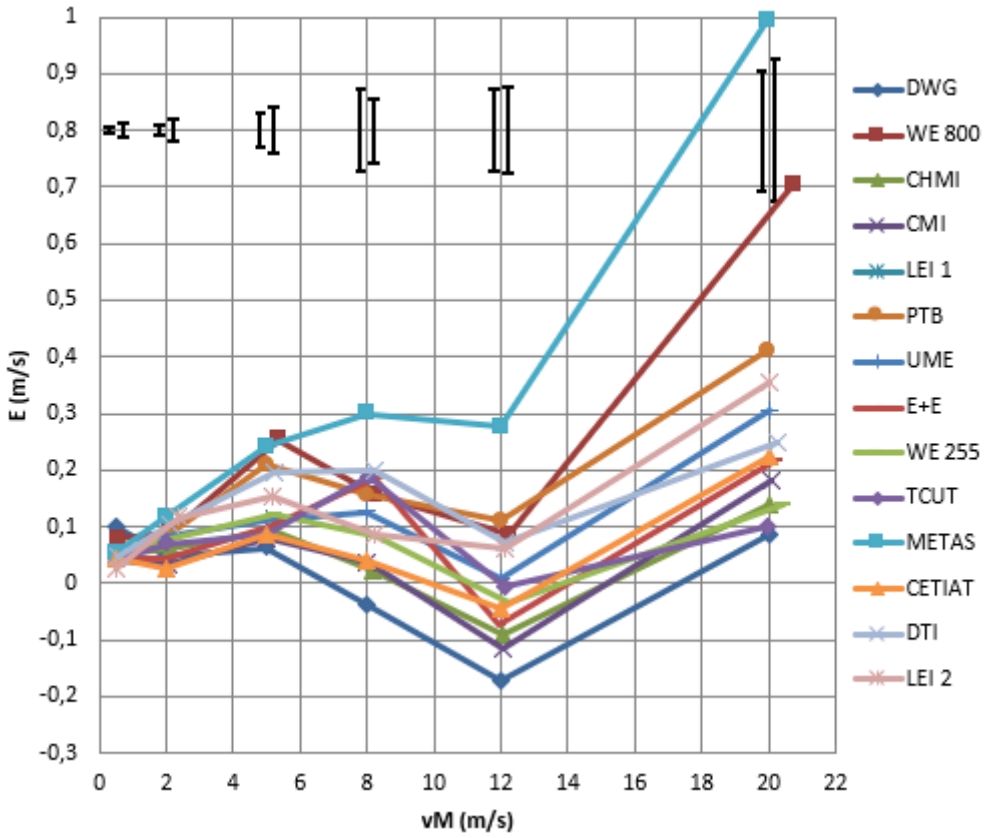

Fig. 7.6 Error curves – Airflow; for explanation of the graphical elements see the text

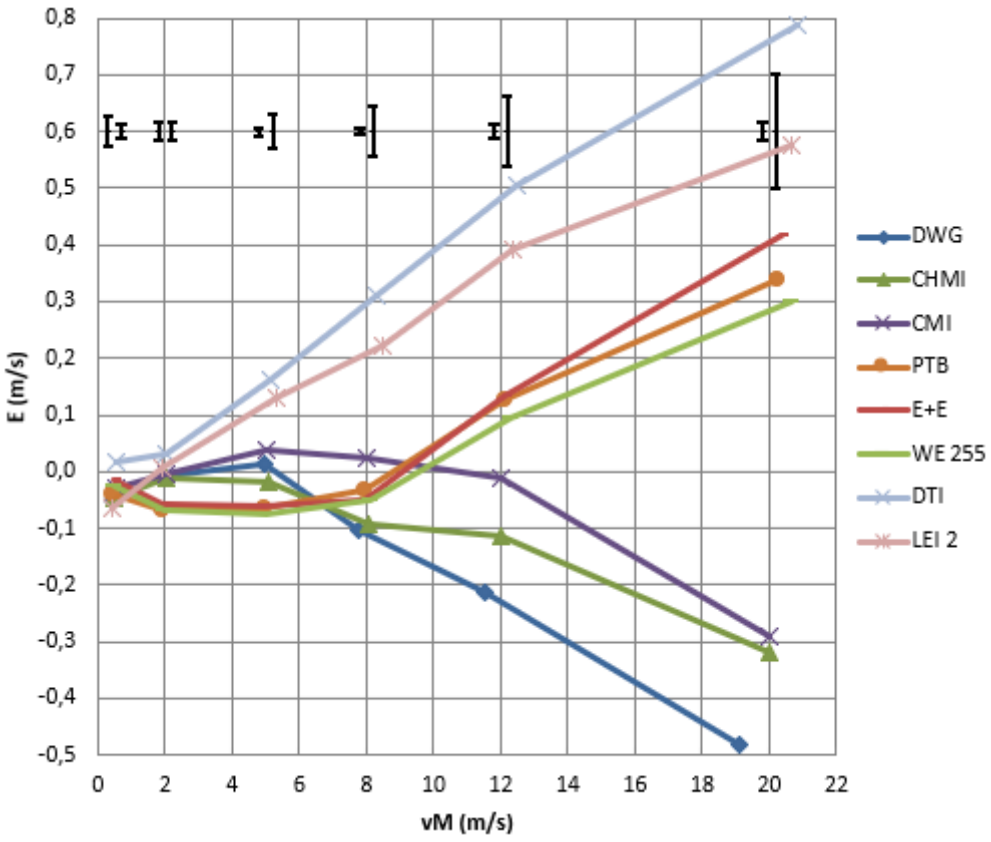

Fig. 7.7 Error curves – Schiltknecht Mini; for explanation of the graphical elements see the text

In Fig. 7.2 with calibration results of the vane anemometer Schiltknecht Macro we see a group of error curves at lower error values and then several curves above them. The shift of the wind tunnel of UME to the larger error values can be explained by the close position of the reference meter (see Fig. 5.2 – lab no. 7). The shifts of LEI 1, LEI 2 and DTI are probably caused by a different kind of systematic error. The shift of DTI and LEI 2 to the larger error values repeats also for the other meters. The curve of TCUT is heavily dependent on the applied blockage effect correction.

In Fig. 7.1 with calibration results of the vane anemometer Testo we can see the error curves of the larger wind tunnels (full lines) grouped in the middle except DTI which is shifted similarly as for the Schiltknecht Macro anemometer. The calibration curves of the smaller wind tunnels (dashed lines) are scattered around them.

In Fig. 7.3 with calibration results of the largest vane anemometer RM Young Gill Propeller we see quite good agreement between the error curves besides the curve of LEI 2 which is deviated also for the other meters. We cannot see a clear distinction between smaller wind tunnels (dashed lines) and larger wind tunnels (full lines). The reason could be that in spite of the large size of the meter the interaction with air stream is not so strong as follows from the Figs. 5.3 and 5.10.

In Fig. 7.4 with calibration results of the smaller cup anemometer Vaisala we can see a clear grouping of the error curves belonging to the large wind tunnels (full lines) and the curves of the smaller wind tunnels (dashed lines) scattered around them. Similar behaviour can be seen also in Fig. 7.5 with the calibration results of the larger cup anemometer Thies.

In Fig. 7.6 with calibration results of the thermal anemometer Airflow we see that the instability of the meter is comparable with a typical expanded uncertainty of calibration for this meter. Large errors deviating from most of the calibration curves are observed in case of METAS and for higher velocities also for WE 800. Excluding these wind tunnels and taking the instability of the meter into account the agreement of the calibration results is quite good. However, because of the instability of the meter another small meter has been selected – the vane anemometer Schilknecht Mini – and additional measurements have been performed in several laboratories in order to be able to compensate possible systematic deviations between the wind tunnels which are not caused by the blockage effect.

In Fig. 7.7 with calibration results of the small vane anemometer Schiltknecht Mini we see a dramatic disagreement of the measured error curves. Two effects have been further investigated in order to clarify these deviations – effect of insertion depth of the anemometer in a test section of a wind tunnel (details in section 8) and effect of inclination angles of the anemometer with respect to the air stream direction (details in section 9).

7.2 Errors as functions of a test section size and type

To see more clearly how the meter errors obtained by the participants depend on their test section size and type and to evaluate if there are any systematic trends in these dependencies we plot relative errors for each meter and each air-speed as a function of $1/A$ with A being a cross-sectional area of nozzle outlet of the participants' wind tunnels. Moreover, we distinguish the test section type (open, box, closed – see Tab. 3.2) by different colours of the plotted data.
The dependencies on $1/A$ are to certain extent equivalent to dependencies on the blockage ratio A_M/A with A_M being the front area of the anemometer under test (including mounting) exposed to flow. The difference is only in rescaling by the factor A_M which is constant for a given anemometer, assuming that the variations of the mounting area exposed to flow in various wind tunnels are not significant.
Also, if a clear function dependence $E(1/A)$ would appear in the measured data, extrapolating the function $E(1/A)$ to $1/A \rightarrow 0$ could give an error under "ideal" conditions of unbounded flow and the deviations from this error could be defined for particular labs with given boundary conditions in their test section.

The values of $1/A$ for the participating wind tunnels together with hydraulic diameter d and area A of their outlet nozzle are summarised in Tab. 7.1.

	Open test section						Box test section				Closed test section			
	DWG	CHMI	CMI	PTB	WE255	E+E	WE800	LEI 1	UME	TCUT	METAS	CETIAT	DTI	LEI 2
d (m)	1	0.55	0.45	0.32	0.255	0.255	0.80	0.4	0.315	0.152	0.59	0.51	0.50	0.40
A (m^2)	1	0.30	0.159	0.08	0.051	0.051	0.50	0.126	0.078	0.018	0.363	0.26	0.25	0.126
1/A (m^{-2})	1	3.33	6.29	12.4	19.6	19.6	1.99	7.96	12.8	55.1	2.76	3.84	4.0	7.96

Tab. 7.1 Hydraulic diameter, area and reciprocal area of the wind tunnels' outlet nozzles

In order to investigate the deviations caused by the different test sections, calibration data *not* including the blockage effect corrections and uncertainties are needed. Justification of the blockage effect corrections and uncertainties applied by the participating laboratories can then be discussed based on comparison of the data *with* and *without* the corrections and uncertainties. Therefore, plots of both data sets – including and not-including the blockage effect corrections and uncertainties – are shown.

Since the goal is to investigate the differences in reference velocities v_E leading to a given MUT indication v_M in various wind tunnels, the participants were asked to calibrate the anemometers in prescribed values of v_M. Therefore, it will be practical to define the relative error as

$$E(\%) = \frac{v_M - v_E}{v_M}.100$$

i.e. with v_M in the denominator (instead of v_E as it is usual). However, the differences from the usual definition are much smaller than the reported uncertainties.

The plots of this relative error including the expanded uncertainty bars are in the Figs. 7.8 – 7.12 below. Interpreting the plots one should be aware that the reported errors are influenced by a mixture of effects – the blockage effect, varying mutual position of MUT and a reference anemometer, systematic errors not related to the MUT-tunnel interaction and also by the insertion depth effect which is discussed in more detail in the section 8.

In the Figs. 7.8 – 7.12 we see that the $E(1/A)$ dependencies can hardly be expressed by a simple function. Therefore, it is difficult to draw any general quantitative conclusions on how the anemometers' error depends on the test section size and type.

For the wind tunnels with closed test section there is typically quite steep error increase with increasing $1/A$ (decreasing test section cross-section). However, it should be checked what is the cause of these error differences – if it is related to the blockage effect or not. For example, the test sections of CETIAT and DTI are nearly identical but at the same time large deviations occur in many cases.

Some errors are significantly influenced by close position of a reference anemometer to a MUT, e.g. for the results of UME (see Figs. 5.1-5.7).

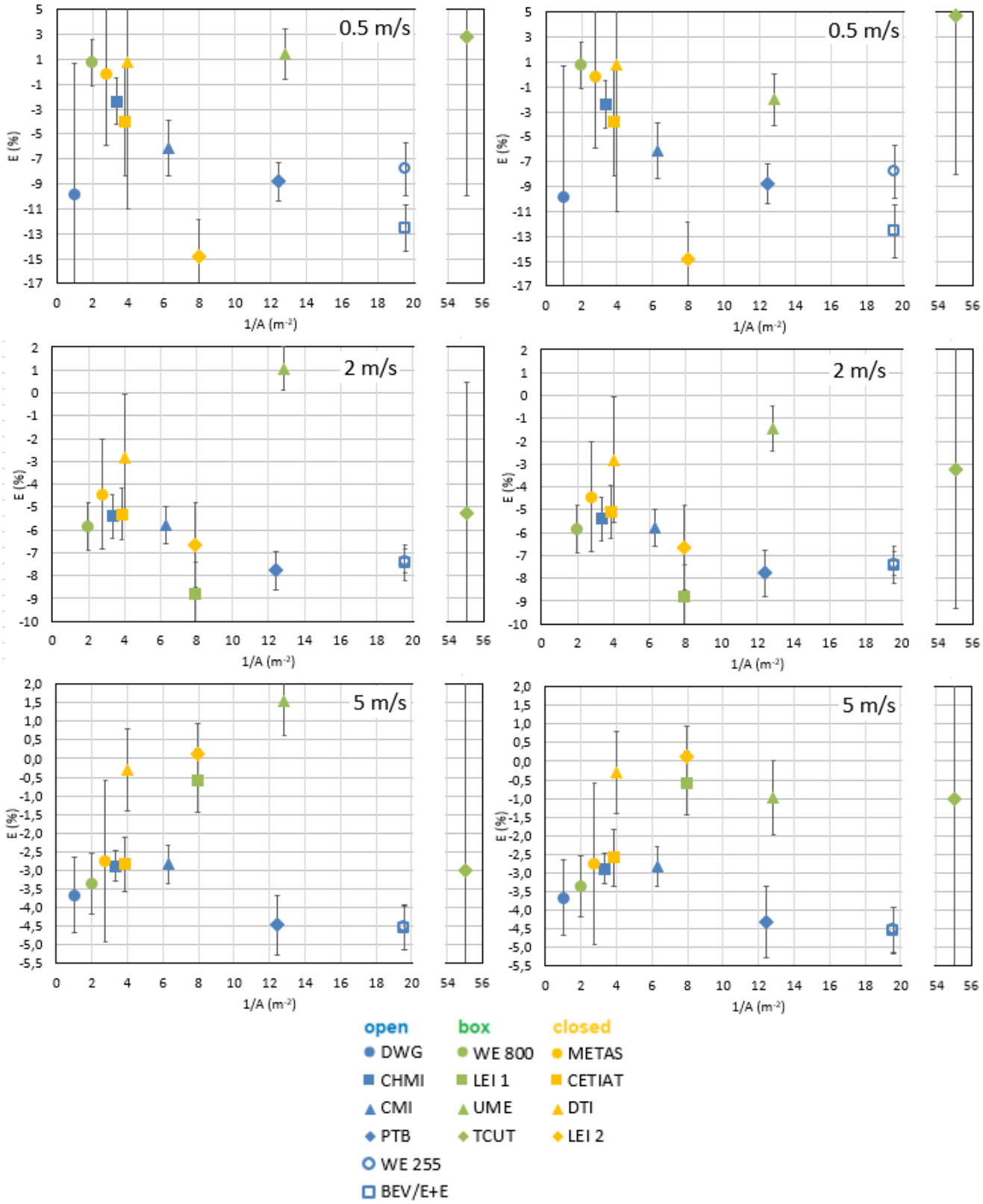

Fig. 7.8 (a) Schiltknecht Macro – anemometer errors with expanded uncertainties as functions of the reciprocal nozzle area for velocities (0.5-5) m/s. Data not-including / including blockage effect corrections and uncertainty components are shown in the left / right column.

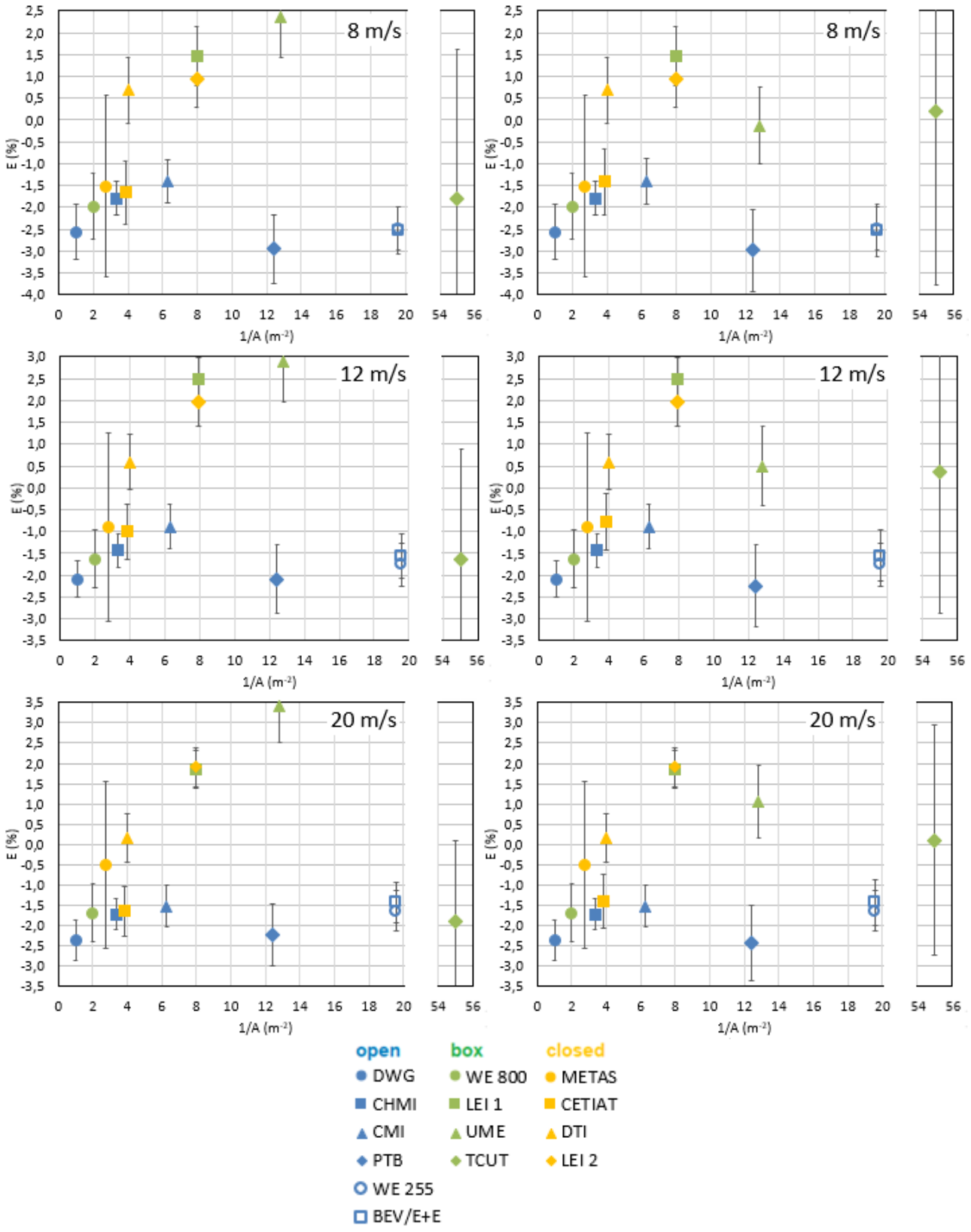

Fig. 7.8 (b) Schiltknecht Macro – anemometer errors with expanded uncertainties as functions of the reciprocal nozzle area for velocities (8-20) m/s. Data not-including / including blockage effect corrections and uncertainty components are shown in the left / right column.

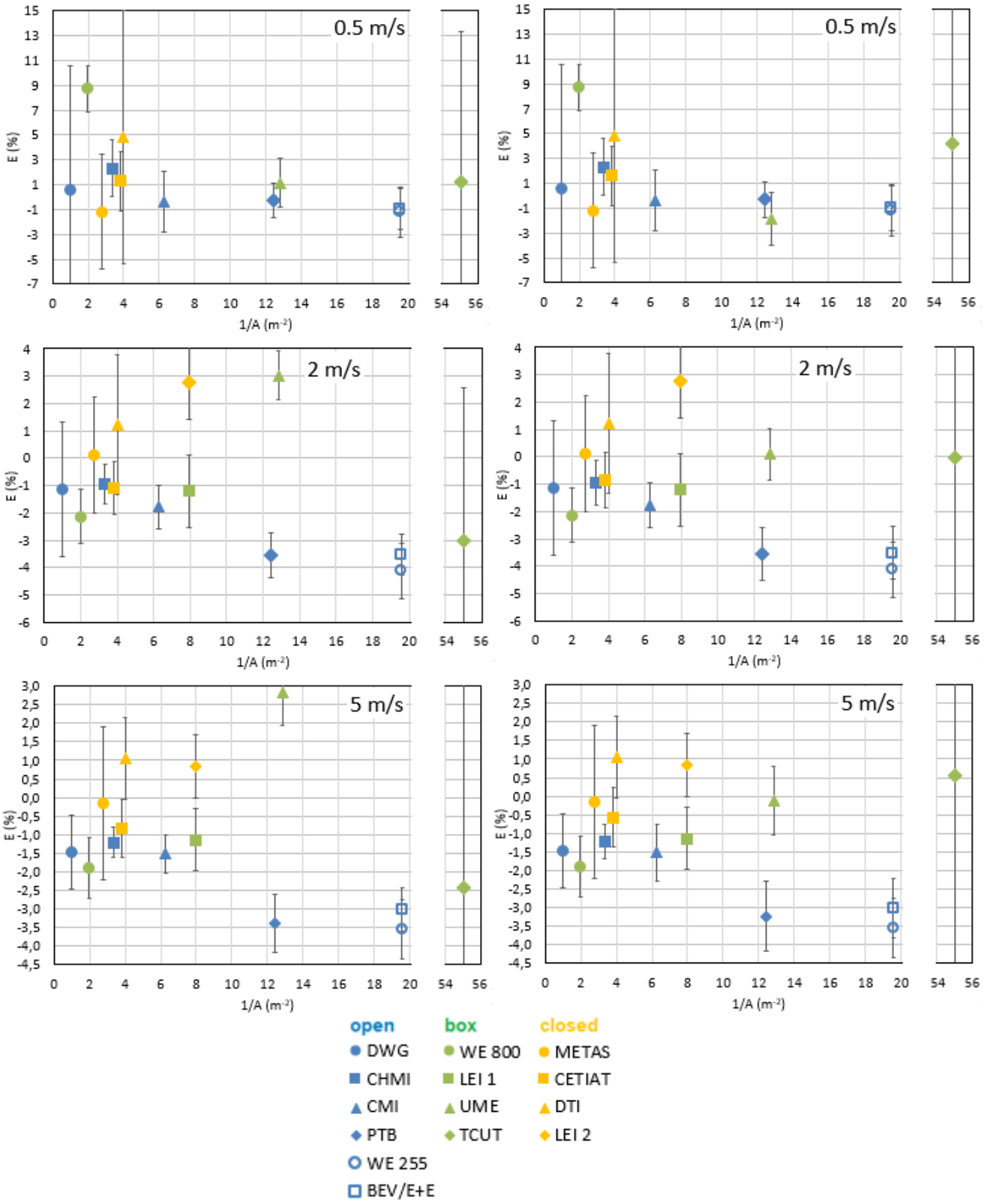

Fig. 7.9 (a) Testo – anemometer errors with expanded uncertainties as functions of the reciprocal nozzle area for velocities (0.5-5) m/s. Data not-including / including blockage effect corrections and uncertainty components are shown in the left / right column.

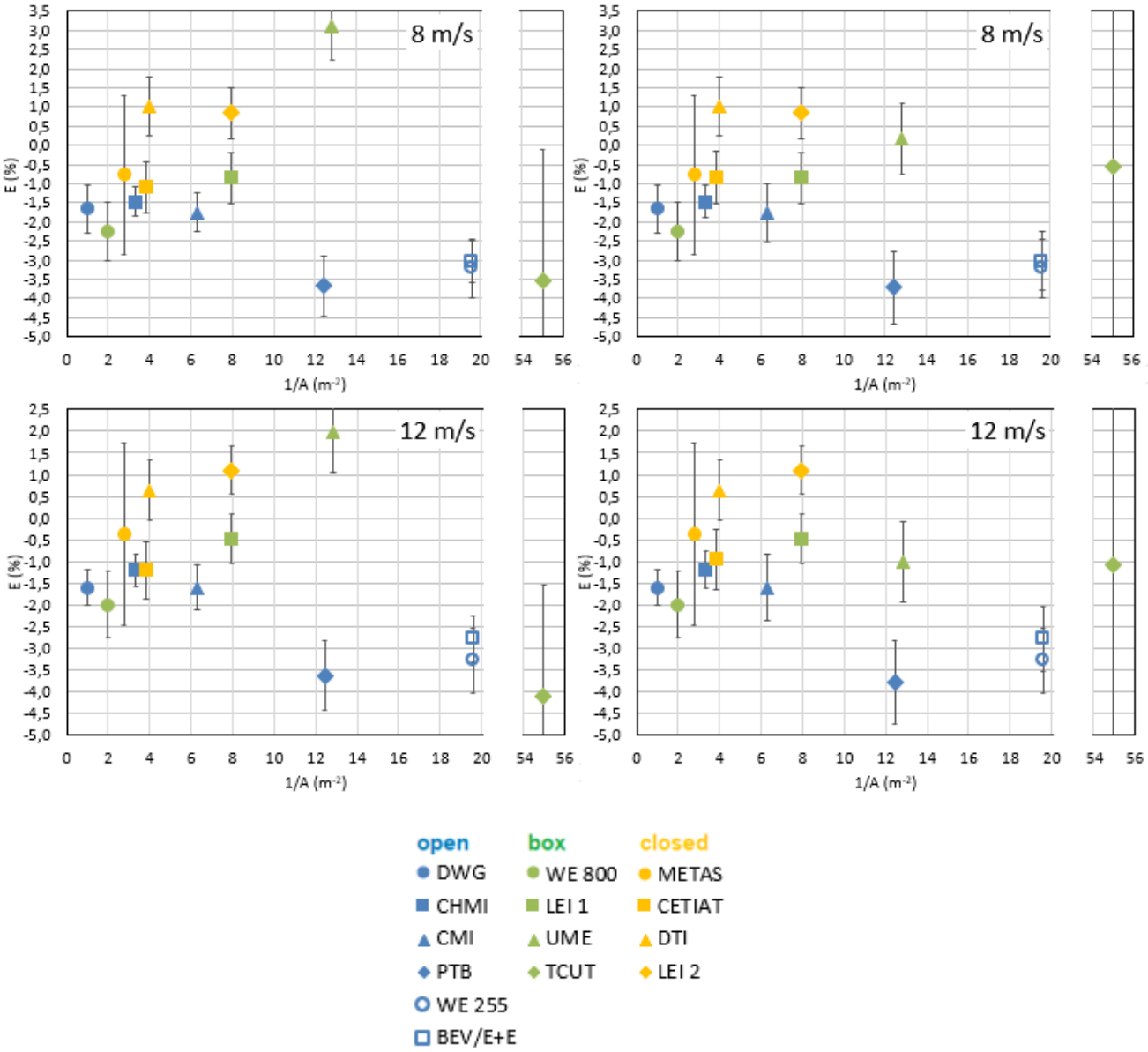

Fig. 7.9 (b) Testo – anemometer errors with expanded uncertainties as functions of the reciprocal nozzle area for velocities (8-12) m/s. Data not-including / including blockage effect corrections and uncertainty components are shown in the left / right column.

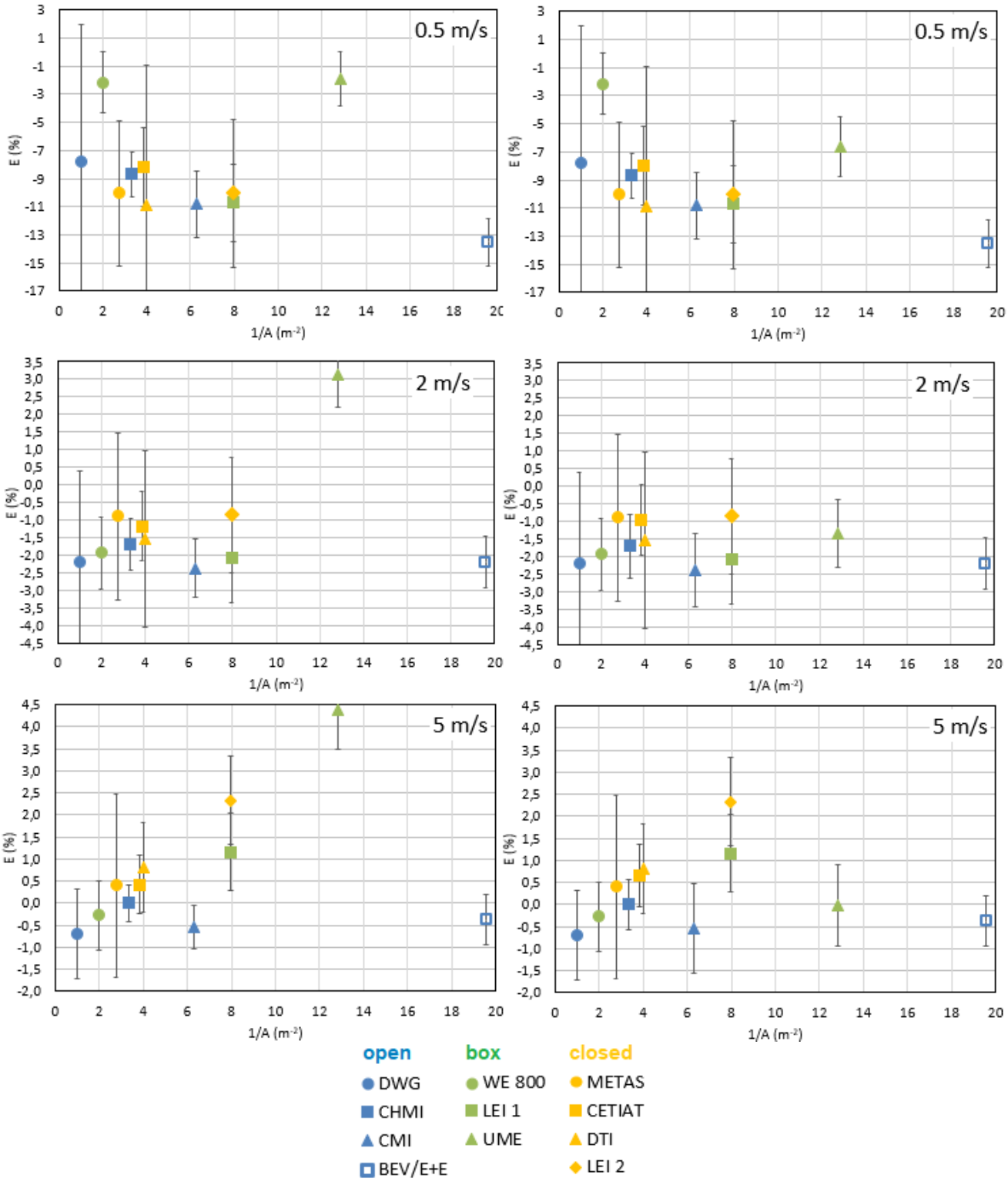

Fig. 7.10 (a) RM Young – anemometer errors with expanded uncertainties as functions of the reciprocal nozzle area for velocities (0.5-5) m/s. Data not-including / including blockage effect corrections and uncertainty components are shown in the left / right column.

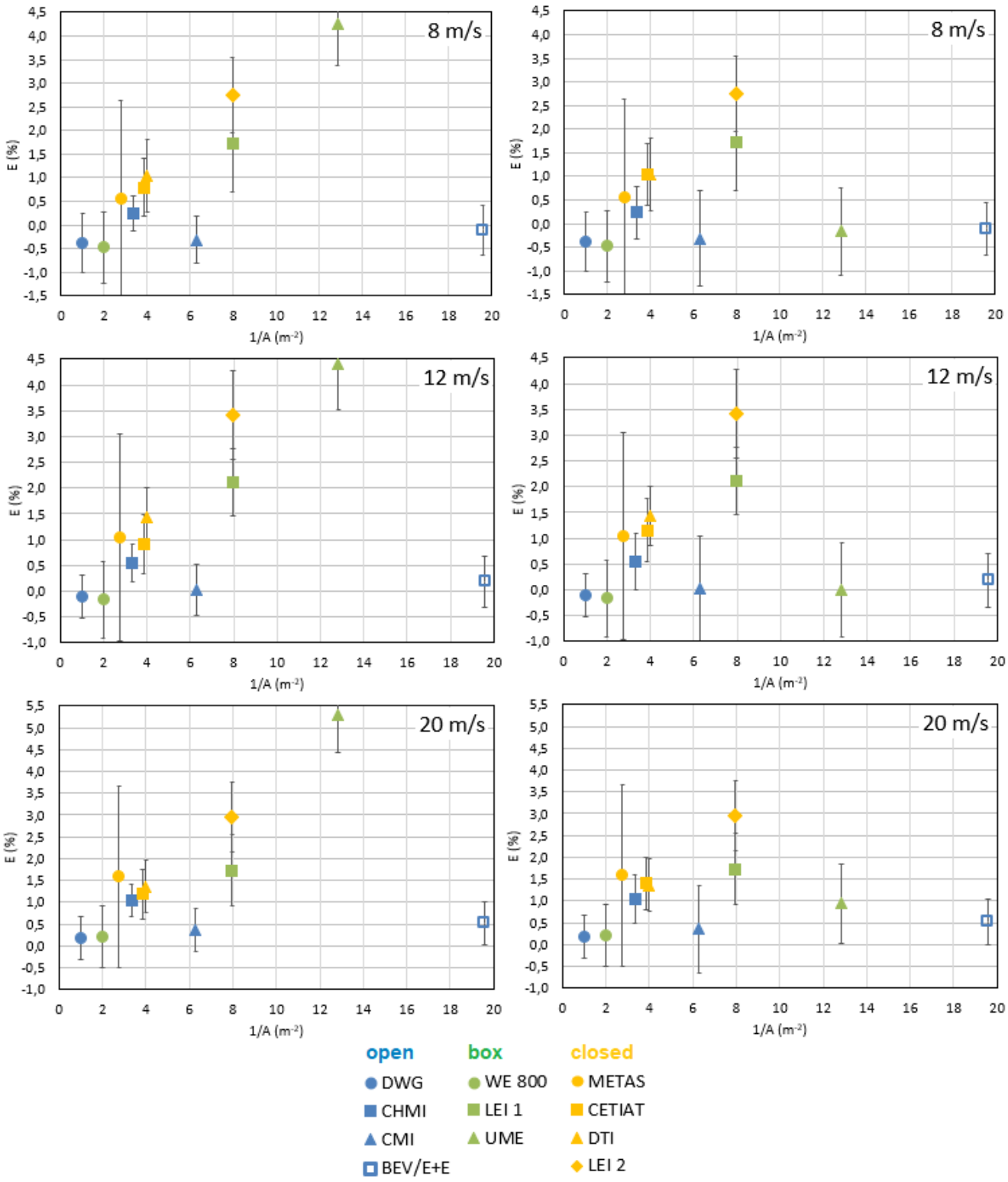

Fig. 7.10 (b) RM Young – anemometer errors with expanded uncertainties as functions of the reciprocal nozzle area for velocities (8-20) m/s. Data not-including / including blockage effect corrections and uncertainty components are shown in the left / right column.

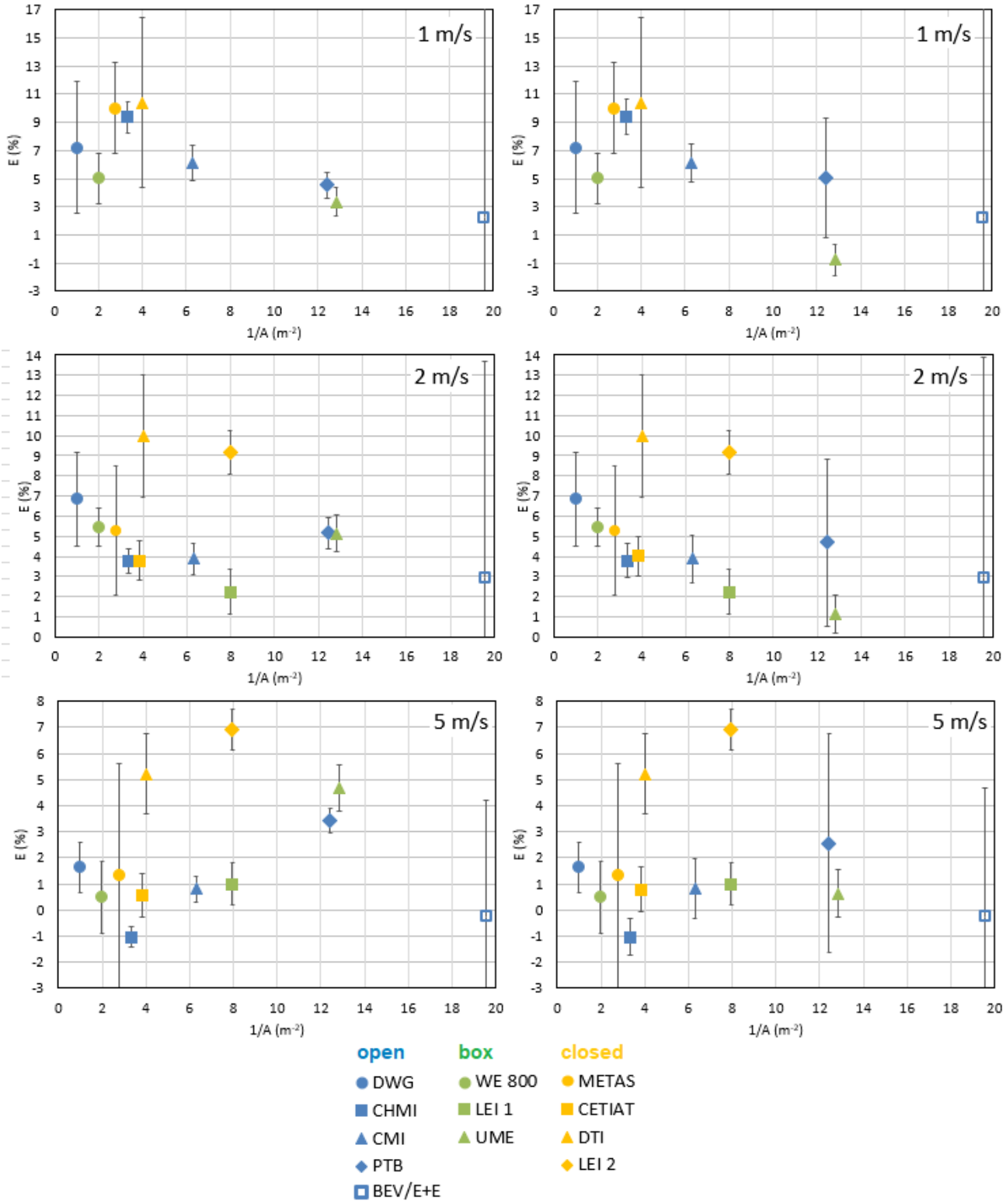

Fig. 7.11 (a) Vaisala – anemometer errors with expanded uncertainties as functions of the reciprocal nozzle area for velocities (1-5) m/s. Data not-including / including blockage effect corrections and uncertainty components are shown in the left / right column.

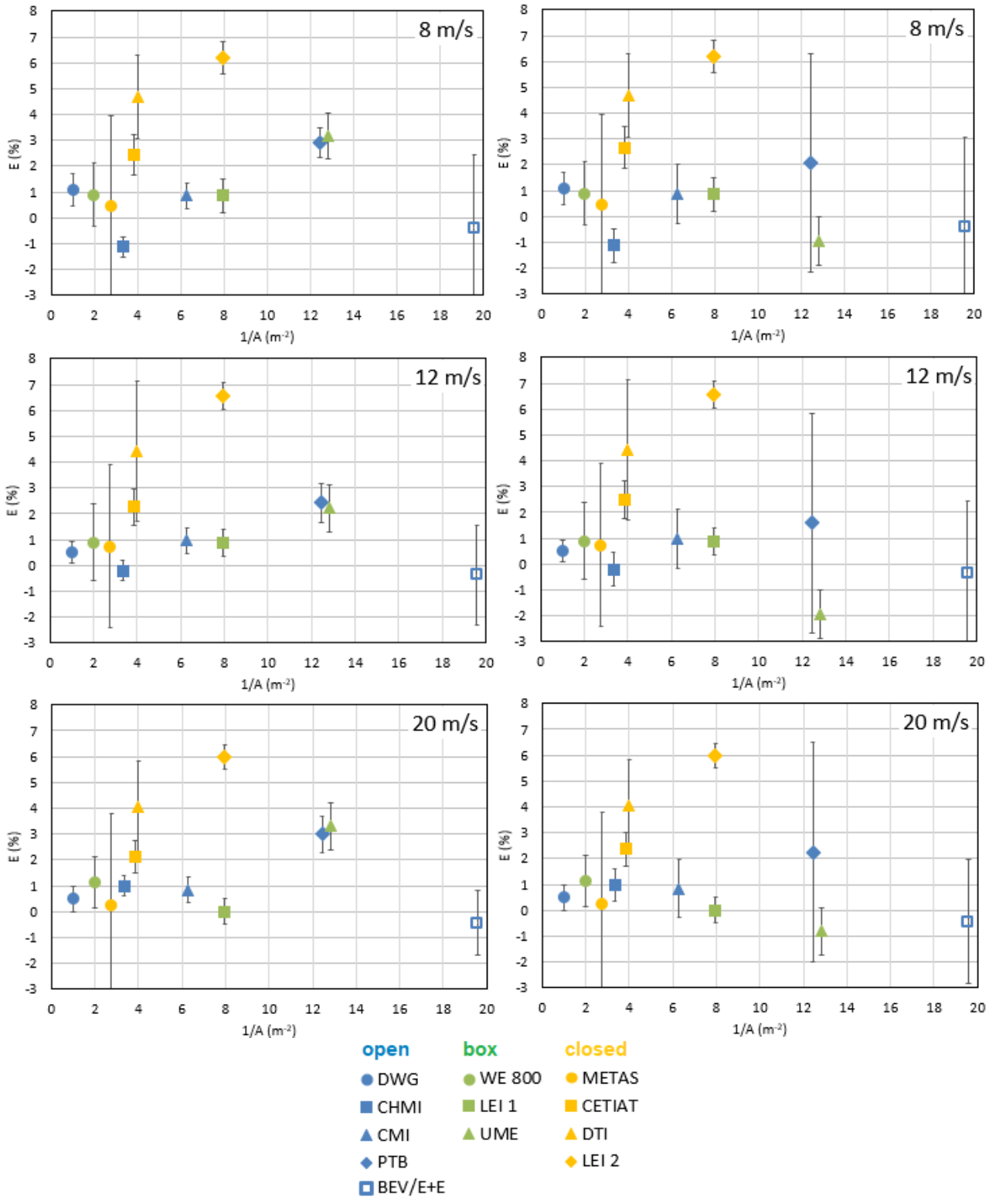

Fig. 7.11 (b) Vaisala – anemometer errors with expanded uncertainties as functions of the reciprocal nozzle area for velocities (8-20) m/s. Data not-including / including blockage effect corrections and uncertainty components are shown in the left / right column.

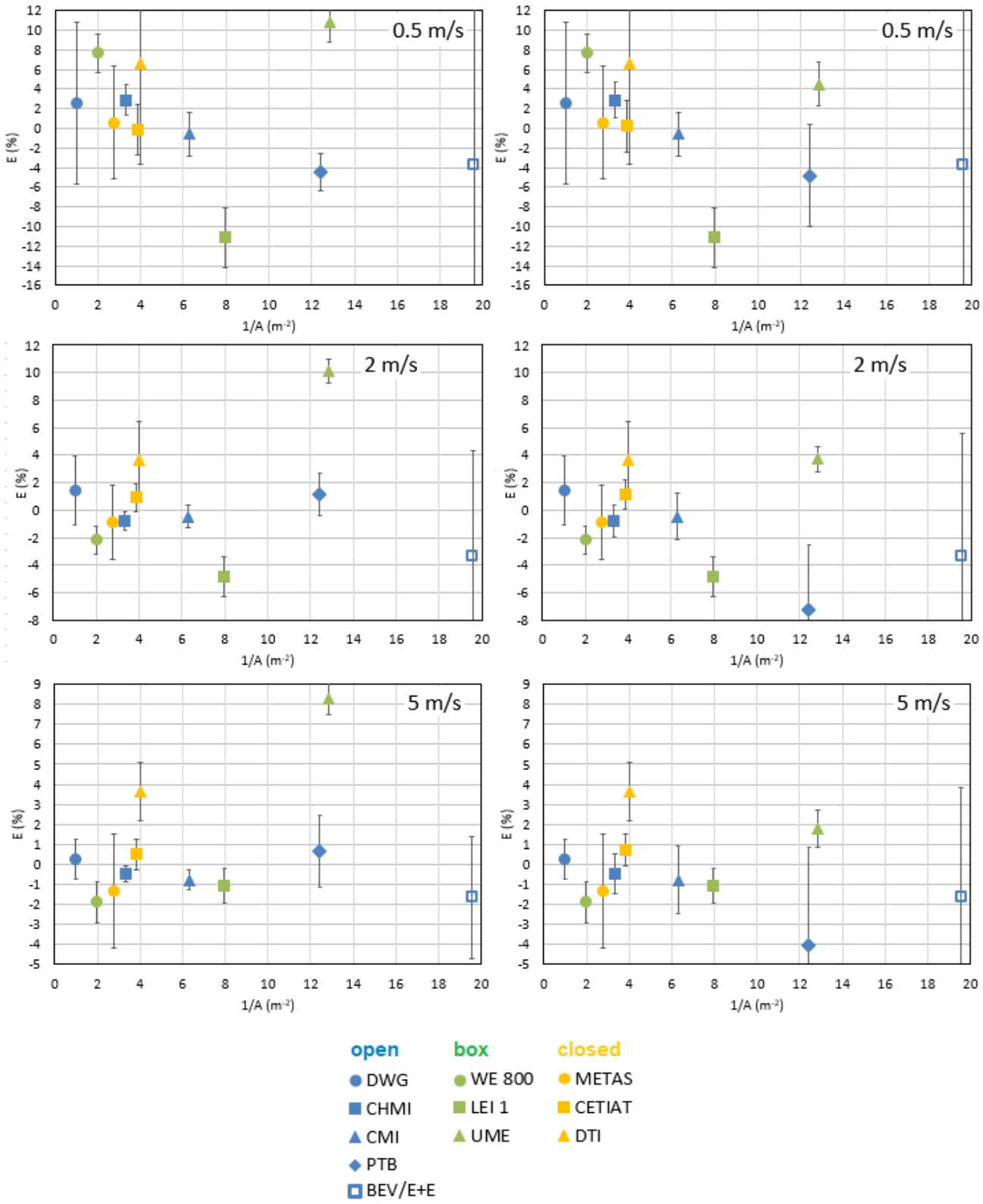

Fig. 7.12 (a) Thies – anemometer errors with expanded uncertainties as functions of the reciprocal nozzle area for velocities (0.5-5) m/s. Data not-including / including blockage effect corrections and uncertainty components are shown in the left / right column.

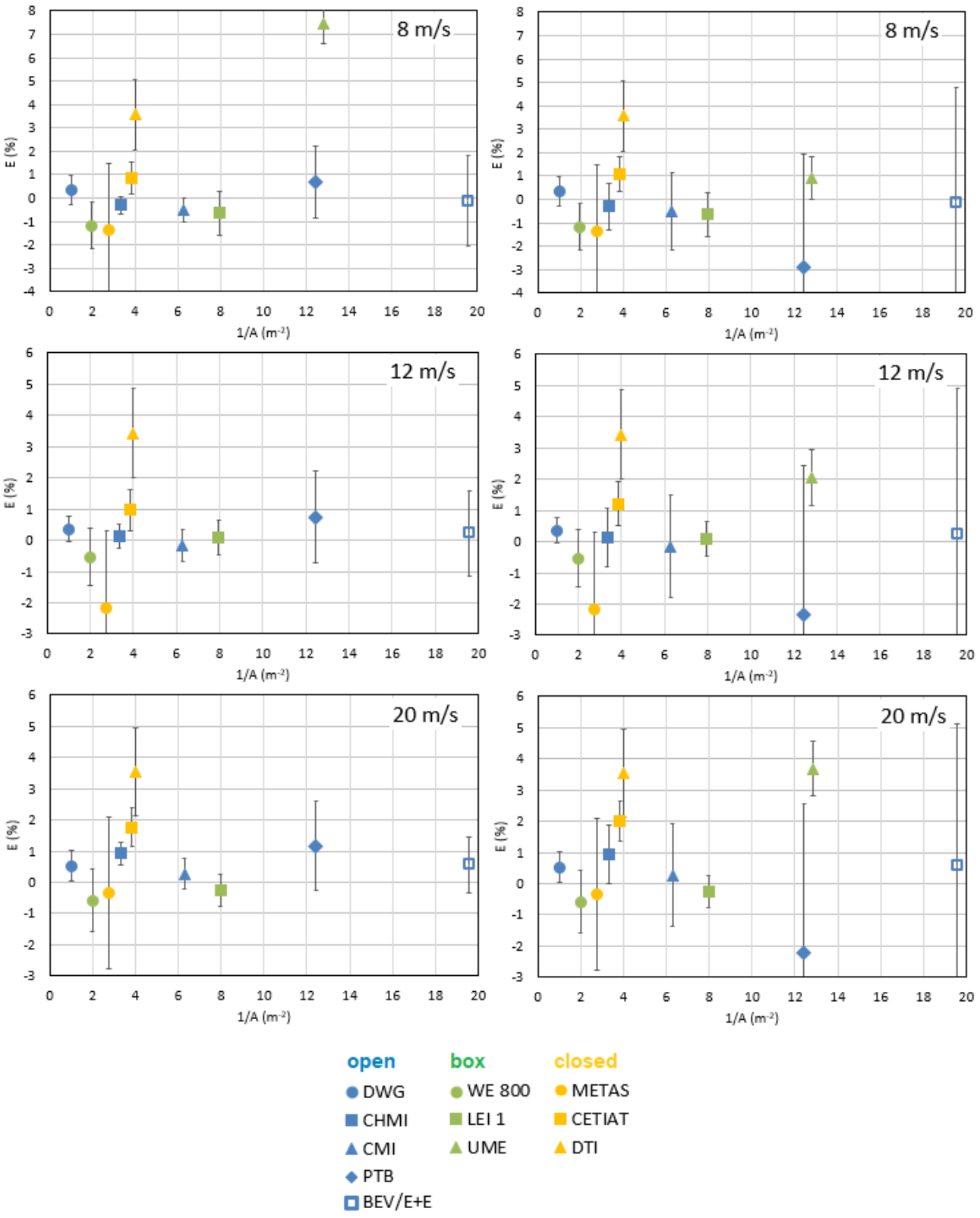

Fig. 7.12 (b) Thies – anemometer errors with expanded uncertainties as functions of the reciprocal nozzle area for velocities (8-20) m/s. Data not-including / including blockage effect corrections and uncertainty components are shown in the left / right column.

7.3 Corrections and uncertainty components related to the blockage effect

This section gives an overview of corrections to the reference velocity and of the uncertainty components related to the blockage effect. Tab. 7.2 below summarises if such corrections or uncertainty components are applied by the participating laboratories or not. Full calibration data with and without the corrections of the reference velocity and the uncertainty component related to the blockage effect are included in Appendix B.

laboratory	Correction of reference velocity applied	Uncertainty component applied
DWG	no	no
WE	no	no
CHMI	no	yes
CMI	no	yes
LEI	no	no
PTB	yes	yes
UME	yes	yes
BEV/E+E	no	yes
TCUT	yes	yes
METAS	no	no
CETIAT	yes	yes
DTI	no	no

Tab. 7.2 Application of corrections and uncertainties related to the blockage effect by the participating laboratories.

There is, however, no unified approach in determining such corrections or uncertainties. The methods of expressing them vary from lab to lab and it is instructive to mention several of them.

BEV/E+E

The determination of the blockage contribution at BEV/E+E is done according to the Appendix A of the EURAMET Calibration Guide No. 24 – "Guidelines on the Calibration of Solid Anemometers Part 1: Pitot Static Tubes". Usually, the influence of the Device under Test (DUT) on the flow profile has to be determined. Therefore, two flow profiles are recorded over the entire cross section in front of the DUT, namely one with and one without a DUT mounted in the measuring section. The two flow profiles differ by an offset, by a change in flow profile over the entire cross-section, or a combination of both. The offset component is automatically corrected by the LDA based on the measurement method. The remaining change of flow profile is evaluated and quadratically add as a rectangular distributed contribution to the measurement uncertainty budget.

CETIAT

The blockage effect is taken into account by a correction of the reference velocity and an uncertainty associated to this correction. This one has been evaluated by performing tests in the wind tunnel. For different type and size of anemometers, the velocity measured by the reference anemometer at its reference location is compared to the same value measured when the instrument under test is far (when the reference value is not affected by the instrument). A correction is applied when the correction is significant (i.e. for vane anemometer with a diameter greater than 80 mm and cup anemometers, mainly) and an uncertainty component based on repeatability tests is applied.

CMI

The percentual standard uncertainty component related to the blockage effect is calculated as 1/16 of the blockage ratio of an anemometer in the test section of the wind tunnel of CMI, following recommendation of the standard EN 61400-12-1, which is, however, meant for cup anemometers only.

PTB

The reported uncertainties include a component related to the blockage effect, except for the thermal anemometer Airflow TA440. For this device no correction for blockage effect was made here. As a rule, sensors whose diameter exceeds 40 mm are not calibrated in the wind tunnel used for this study.

In detail, the following corrections were made during these examinations:
a) Schiltknecht Makro: Additional uncertainty of 0.5 % related to blockage effect, no considerable corrections made
b) Testo 445: Additional uncertainty of 0.5 % related to blockage effect, no considerable corrections made
c) Vaisala Cup Anemometer: Additional uncertainty of 1.5 % related to blockage effect, correction of the reference velocity by up to 1 % made
d) Thies Cup Anemometer: Additional uncertainty of 1.5 % related to blockage effect, correction of the reference velocity by up to 2 % made

TCUT

A blockage effect correction of the reference velocity is determined based on a comparison of calibrations with a larger wind tunnel of LEI using a vane anemometer with a propeller diameter of 80 mm as a transfer standard.

8 Insertion depth effect for the Schiltknecht vane anemometers

Flow patterns in surroundings of anemometers' mounting rod may influence performance of the anemometers' sensing element and this influence may be dependent on a length of the mounting rod exposed to flow, thus, leading to the so called insertion depth effect. Significant dependence of indication of anemometers on the insertion depth have been observed earlier for cup anemometers [12] and hot film anemometers [15].
We define the insertion depth d of an anemometer probe as a distance of the centre of the anemometer probe (axis of vane) from intersection of the anemometer's mounting rod with a prolonged inner wall of the wind tunnel nozzle (see Fig. 8.1).

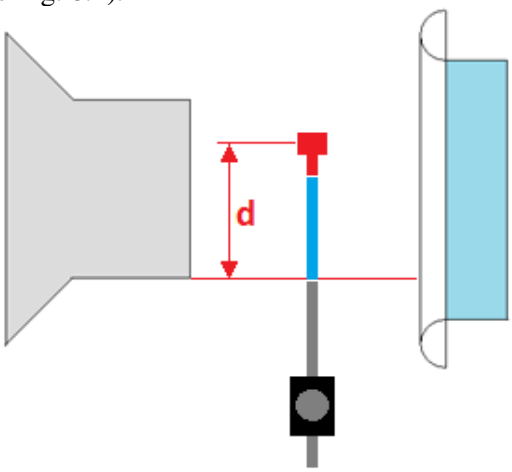

Fig. 8.1 Definition of the insertion depth d

The insertion depth dependency of the vane anemometers Schiltknecht Mini and Schiltknecht Macro has been measured in the wind tunnel of CMI using the same mounting rod as for the calibrations reported above. The anemometers have been installed 31.5 cm behind the wind tunnel nozzle (as for the CMI calibrations reported above) and placed on a construction enabling shifts of their insertion depth d without changes in their inclination with respect to the air stream.
Indication of the anemometers has been recorded for insertion depths from 60 mm to 390 mm with 15 mm step. The measurements have been performed for the six nominal velocities 0.5, 2, 5, 8, 12 and 20 m/s.

In order to exclude variations of the anemometer indication which are caused by inhomogeneity of the air velocity field in the wind tunnel, the air velocity field in the empty test section have been measured using LDA in the same positions as used for the tested vane anemometers. The result of this measurement is shown in Fig. 8.2 where the quantity Δv_{rel} on the vertical axis is defined as relative percentual deviation of air velocity $v(d)$ in a position corresponding to the insertion depth d from a velocity in the test section centre v_c ($= v(d)$ with $d = 225$ mm), i.e.

$$\Delta v(d) = v(d) - v_c, \qquad \Delta v_{rel}(d) = \frac{v(d) - v_c}{v_c} \times 100.$$

As we will see later the velocity variations in Fig. 8.2 in the empty test section are order of magnitude smaller than the variations in indication of the vane anemometers, however, the data in Fig. 8.2 are used to remove the air flow inhomogeneity from the insertion depth dependencies of the vane anemometers.

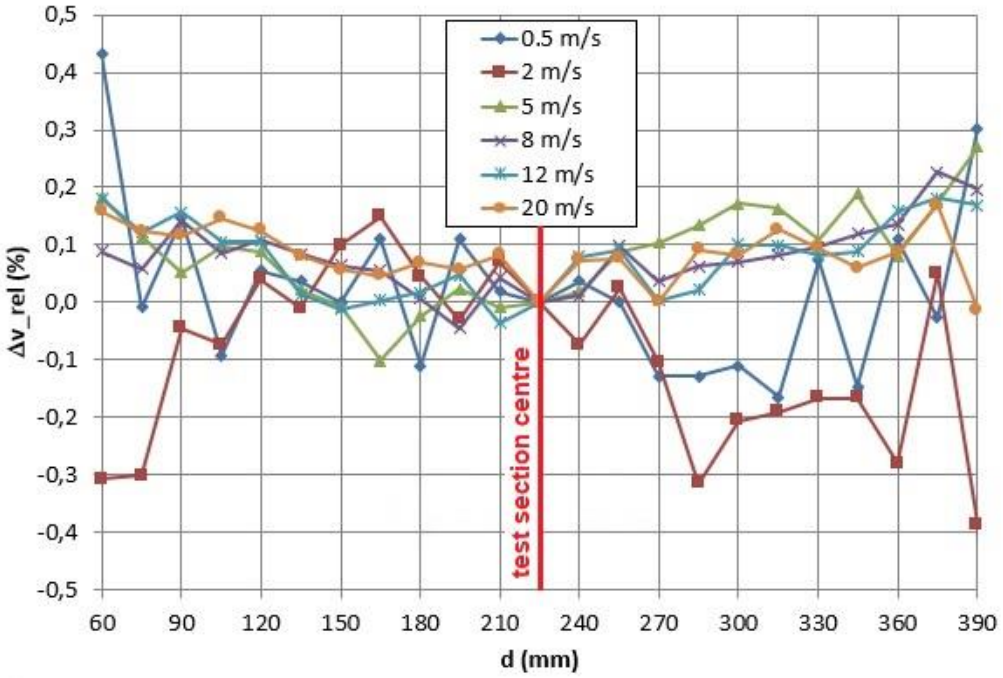

Fig. 8.2 Velocity profiles in empty test section of the wind tunnel of CMI measured by LDA. The test section boundary given by a prolonged outlet nozzle wall is at d = 0 mm and d = 450 mm.

The measurement for each anemometer and each velocity set in the wind tunnel consisted from the following steps: a) install a vane anemometer with a proper angular alignment with respect to the air flow and set the zero position of the insertion depth measurement system, b) set the LDA position to a point which is normally used for anemometer calibrations (10 cm behind the nozzle, 10 cm from the nozzle wall), c) set a required velocity value in the wind tunnel, d) move the tested anemometer to the centre of the test section (d = 225 mm) and read the LDA velocity value (60 s average), e) move the tested anemometer to the lowest insertion depth (d = 60 mm) and read the velocity indicated by the anemometer (average from 20 readings during 60 s period), f) shift the anemometer with increment of 15 mm and read the velocity indicated by the anemometer (average from 20 readings during 60 s period) for each position, g) after each 4-5 increments return the anemometer to the centre (d = 225 mm) and read the LDA velocity value (60 s average).

The purpose of the LDA measurements is to determine a reference value of the velocity in the wind tunnel and its stability during the period when the tested anemometer is shifted from one side of the test section to the other. Therefore, six repeated LDA measurements are taken equally distributed during the whole measurement period. The reason why the tested anemometer is moved to the centre of the test section always when the LDA record is taken is that the anemometer position itself influences the velocity field in the wind tunnel and therefore also the LDA reading. This holds especially for the large size anemometers. Therefore, to eliminate this effect and to be able to evaluate the air velocity stability from the LDA data, the tested anemometer is placed always to the same position when LDA velocity is measured.

We denote v_{LDA} the average of the six repeated LDA measurements. A reference velocity $v_{REF}(d)$ for each position of a tested anemometer is then determined as a velocity of air in empty test section in the position d when the velocity in the position where LDA is placed for calibrations is v_{LDA}, i.e. it is given as

$$v_{REF}(d) = v_{LDA} + (v_c - v_{cal}) + \Delta v(d)$$

where $\Delta v(d)$ is the correction discussed above (given by Fig. 8.2 in %) and $v_c - v_{cal}$ is an additional correction given by velocity difference in empty test section between the centre of the test section and the position where LDA is placed for calibrations.

The absolute and relative errors of a meter under test (MUT) are then defined as

$$E(d) = v_{MUT}(d) - v_{REF}(d), \qquad E_{rel}(d) = \frac{v_{MUT}(d) - v_{REF}(d)}{v_{REF}(d)} \times 100.$$

In these errors as functions of the insertion depth the velocity profile of the empty test section is subtracted by definition of $v_{REF}(d)$.
The measured dependencies $E_{rel}(d)$ for various velocities are shown in Fig. 8.3 for the Mini probe and Fig. 8.4 for the Macro probe. We see that the determined errors are very sensitive to the insertion depth and therefore various insertion depths used for calibrations in various participating labs might lead to significant deviations in calibration results.

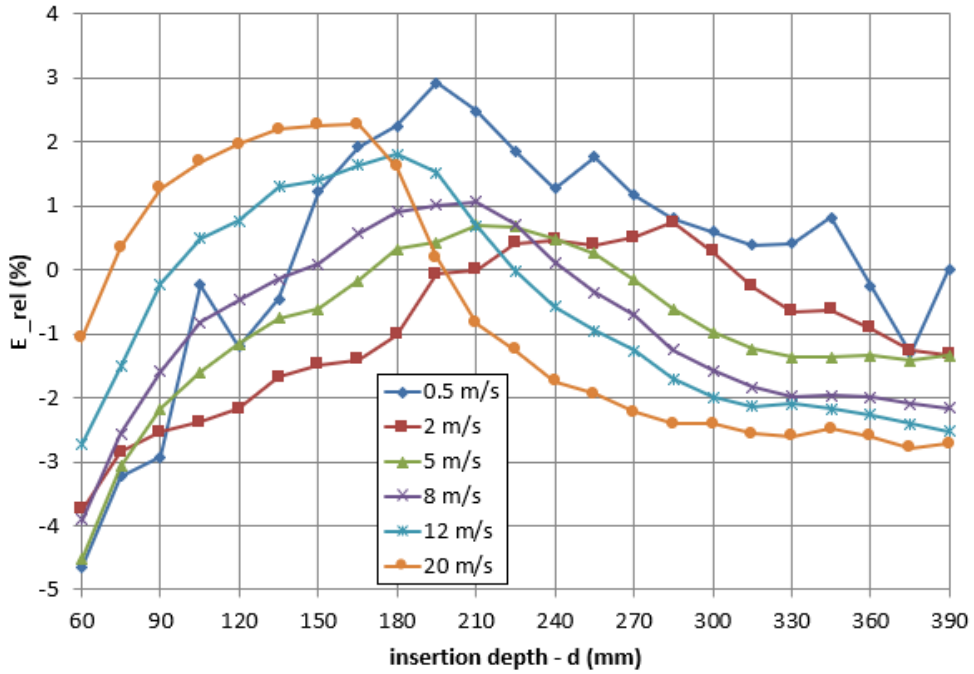

Fig. 8.3 Error of the anemometer Schiltknecht Mini as a function of the insertion depth in the wind tunnel of CMI. The test section boundary given by a prolonged outlet nozzle wall is at d = 0 mm and d = 450 mm.

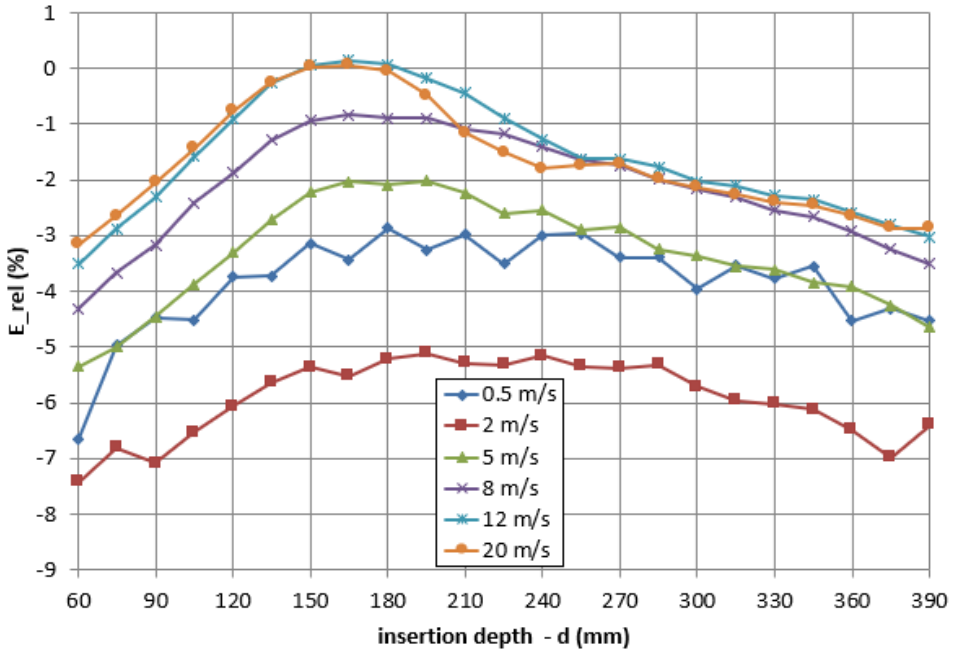

Fig. 8.4 Error of the anemometer Schiltknecht Macro as a function of the insertion depth in the wind tunnel of CMI. The test section boundary given by a prolonged outlet nozzle wall is at $d = 0$ mm and $d = 450$ mm.

To see if the deviations of the calibration curves between various participants reported in Fig. 7.7 (Mini probe) and Fig. 7.2 (Macro probe) correspond to the varying insertion depth we need to recalculate the reported calibration curves to a unified value of the insertion depth d_0. We select $d_0 = 225$ mm corresponding to the insertion depth used by CMI. Assuming that similar insertion depth dependencies as shown in Figs. 8.3 and 8.4 would be obtained in all the participating wind tunnels (this assumption might not be true in reality and must be validated experimentally) these curves, obtained in the wind tunnel of CMI, are used to calculate a correction

$$\Delta E(d) = E(d_0) - E(d)$$

which can be used to recalculate an error $E_{lab}(d)$ of a lab using the insertion depth d to the unified insertion depth d_0 by simply adding $E_{lab}(d_0) = E_{lab}(d) + \Delta E(d)$.

The tables 8.1 and 8.2 below summarise the insertion depths used by various labs and the corresponding corrections $\Delta E(d)$ for the anemometers Schiltknecht Mini and Schiltknecht Macro. In case of DWG wind tunnel with insertion depth of 500 mm exceeding the measurement range of CMI the correction has been estimated as $\Delta E = E(d_0) - E(d_{max})$ with $d_{max} = 390$ mm being the maximum tested insertion depth at CMI. This is relevant when the $E(d)$ curve already does not change much for the high values of d, however, it might lead to deviations when this is not the case.

The corrected calibration curves are shown in Fig. 8.5 for the Mini probe and in Fig. 8.7 for the Macro probe. It is also instructive to see a comparison of the uncorrected and corrected calibration curves for wind tunnels with open test section only. The comparison for the Mini probe is in Fig. 8.6 and for the Macro probe in Fig. 8.8.
For the Mini probe we see great improvement of the agreement between participants with open test sections, i.e. all participants except DTI and LEI 2 where the deviations are probably caused by other kind of systematic error. It means that the effect of the insertion depth is most likely the cause of the large deviations between the calibration curves of the Mini probe in Fig. 7.7, at least in case of the wind tunnels with open test section.
On the other hand, for the Macro probe we can't see any improvement in the agreement. In case of wind tunnels with open test section where originally the agreement was good we actually see larger deviations

between the calibration curves when the correction is applied. This indicates that for the larger Macro probe the insertion depth dependencies $E(d)$ could differ in various wind tunnels.
A follow-up Euramet project has been agreed to further investigate this effect.

lab	d (mm)	v (m/s)	0,5	2	5	8	12	20
DWG	500	ΔE (m/s)	0,010	0,035	0,10	0,23	0,30	0,30
CHMI	250		0,0014	0,0000	0,017	0,072	0,098	0,13
CMI	225		0	0	0	0	0	0
PTB	160		0,0009	0,038	0,050	0,024	-0,19	-0,71
E+E	127,5		0,015	0,047	0,081	0,081	-0,13	-0,68
WE	127,5		0,015	0,047	0,081	0,081	-0,13	-0,68
DTI	250		0,0014	0,0000	0,017	0,072	0,098	0,13
LEI 2	200		-0,0051	0,0094	0,0078	-0,026	-0,15	-0,22

Tab. 8.1 Insertion depths used for calibrations by participants and the corresponding correction for Schiltknecht Mini.

lab	d (mm)	v (m/s)	0,5	2	5	8	12	20
DWG	500	ΔE (m/s)	0,0056	0,022	0,11	0,19	0,26	0,27
WE 800	400		0,0056	0,022	0,11	0,19	0,26	0,27
CHMI	250		-0,0029	-0,0008	0,009	0,032	0,074	0,050
CMI	225		0	0	0	0	0	0
LEI 1	200		-0,0019	-0,0033	-0,027	-0,017	-0,076	-0,16
PTB	160		-0,0009	0,0033	-0,027	-0,025	-0,12	-0,32
UME	157,5		-0,0012	0,0028	-0,025	-0,023	-0,12	-0,32
E+E	127,5		0,0013	0,011	0,021	0,033	-0,038	-0,20
WE 255	127,5		0,0013	0,011	0,021	0,033	-0,038	-0,20
TCUT	76		0,0080	0,031	0,12	0,20	0,24	0,23
METAS	245		-0,0029	-0,0022	0,003	0,025	0,060	0,054
CETIAT	255		-0,0030	0,0005	0,015	0,038	0,088	0,047
DTI	250		-0,0029	-0,0008	0,009	0,032	0,074	0,050
LEI 2	200		-0,0019	-0,0033	-0,027	-0,017	-0,076	-0,16

Tab. 8.2 Insertion depths used for calibrations by participants and the corresponding correction for Schiltknecht Macro.

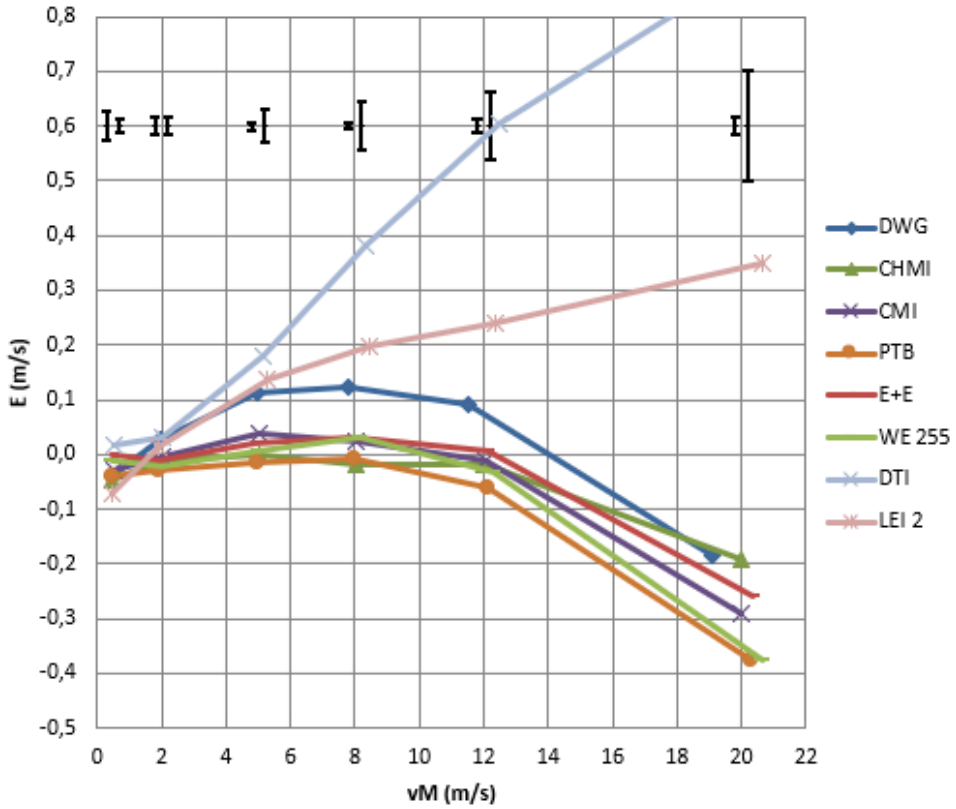

Fig. 8.5 Corrected calibration curves for Schiltknecht Mini

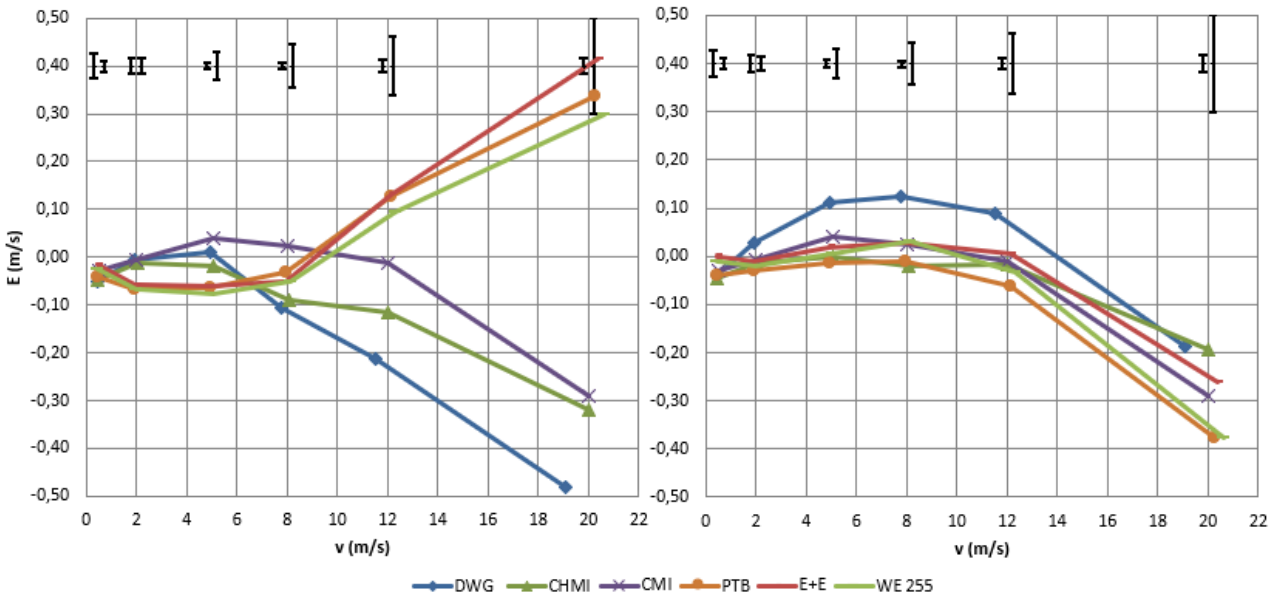

Fig. 8.6 Comparison of uncorrected (left) and corrected (right) calibration curves for wind tunnels with open test section – anemometer Schiltknecht Mini

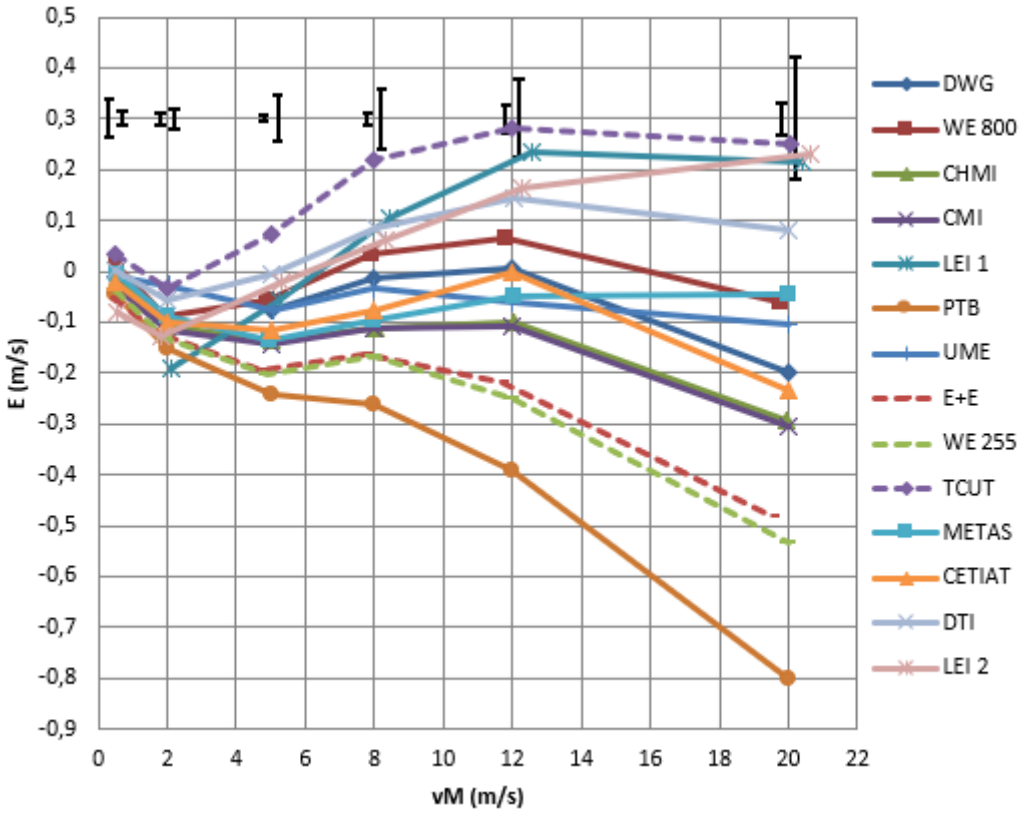

Fig. 8.7 Corrected calibration curves for Schiltknecht Macro

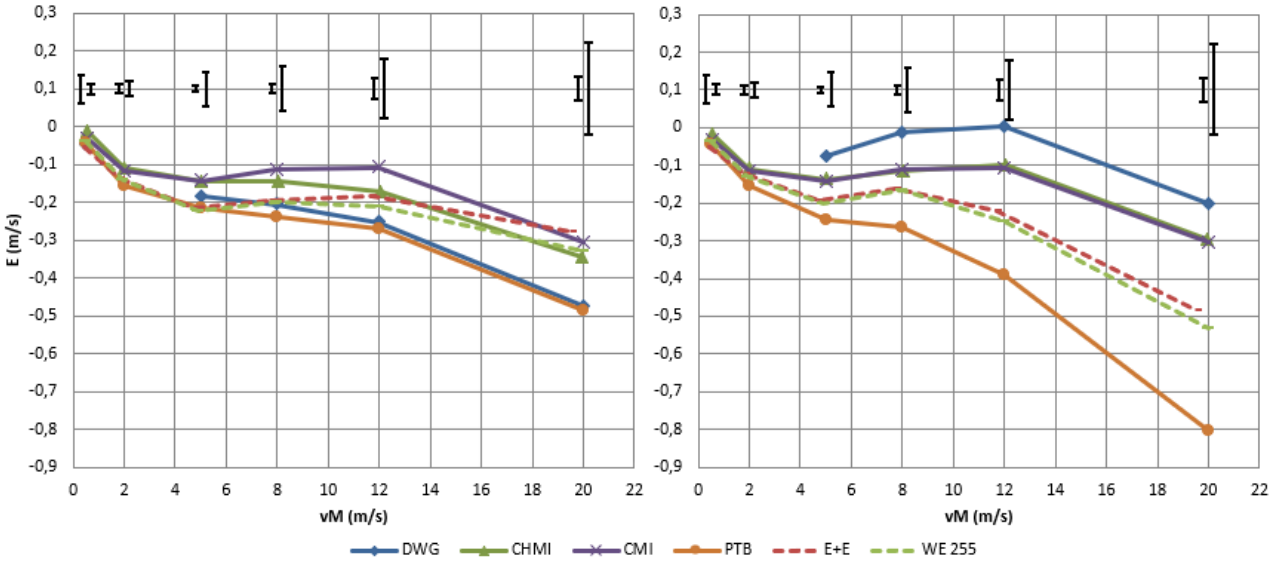

Fig. 8.8 Comparison of uncorrected (left) and corrected (right) calibration curves for wind tunnels with open test section – anemometer Schiltknecht Macro

9 Angular sensitivity of the Schiltknecht MINI anemometer

The angle dependencies of the anemometer Schiltknecht Mini have been measured at DWG wind tunnel for air speed 8 m/s. Yaw angle dependence is shown in Fig. 9.1 and tilt angle dependence in Fig. 9.2. At this moment we have not collected data on angle accuracies of the participating labs but if we suppose angle deviations not exceeding 2° the meter indication deviates by several tenths of percent which is

relevant for the uncertainty budgets but probably it is not the major cause of the deviations observed in Fig. 7.7 which are larger.

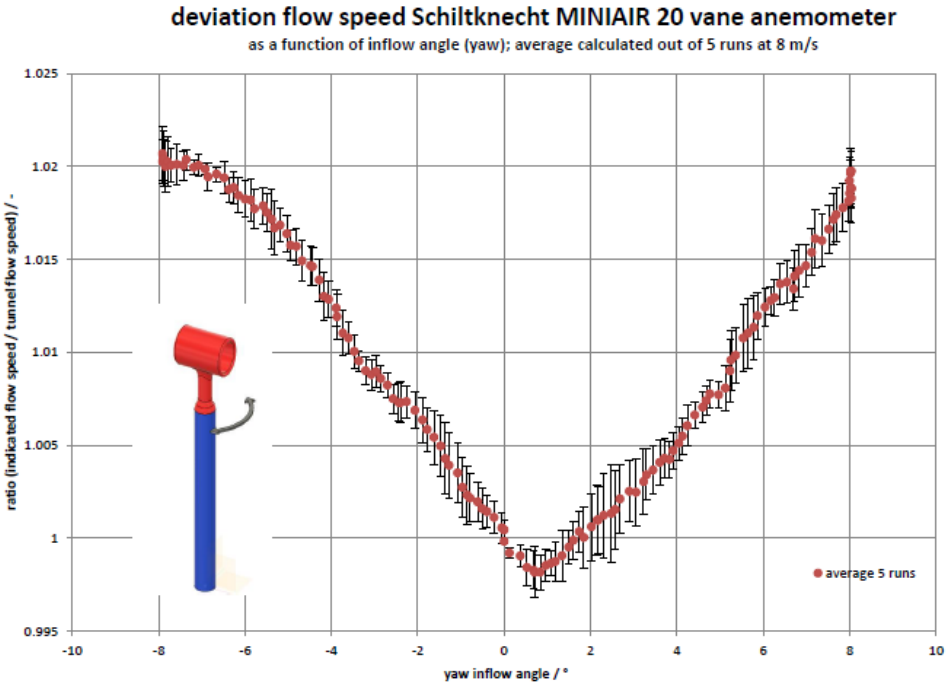

Fig. 9.1 Yaw angle dependence of Schiltknecht Mini indication

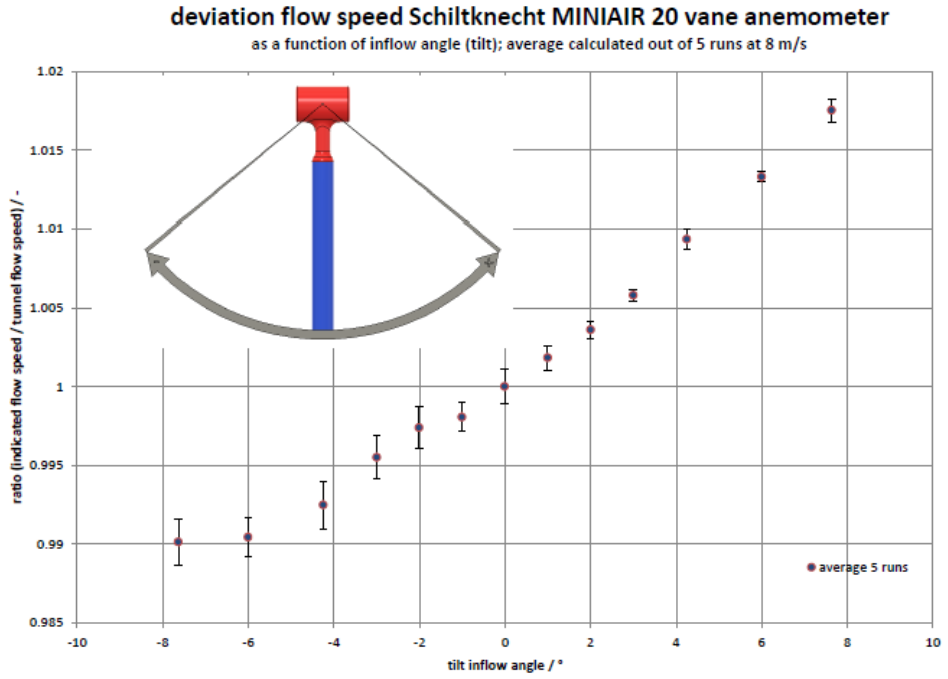

Fig. 9.2 Tilt angle dependence of Schiltknecht Mini indication

10 Conclusions and future work

Velocity field around a given type of anemometer indicating a given velocity value v_M in a wind tunnel depends on boundary conditions imposed by a construction and size of the wind tunnel's test section – on presence of walls (open or closed test section), shape (circular, rectangular), etc.

Also, for the anemometer calibration a reference anemometer is usually placed to certain position in the velocity field in front of the meter under test (MUT), indications of the two instruments are compared and the MUT error is calculated. The mutual position of the MUT and the reference meter is to certain extent arbitrary choice of the testing laboratory which is given by dimensions of the wind tunnel.

Therefore, in laboratories with various wind tunnels different calibration results can be obtained due to both – different velocity field corresponding to the MUT indication v_M and different mutual position of the MUT and the reference anemometer. The choice of the position of the reference with respect to the MUT should be well justified, the mutual interactions should be minimized and the corresponding corrections or uncertainties should be documented.

For large anemometers the modified velocity field in various wind tunnels is usually assigned to the blockage effect which was also the main intended focus of this work. When an obstacle is put in a wind tunnel's test section the air speed decreases in front of the obstacle and increases in the space between the obstacle and the test section boundary. The effect depends on the front area of the obstacle compared to the cross-sectional area of the test section (blockage ratio) but also on the construction of the anemometer since, for example, a presence of a frame around the anemometer's propeller does not increase the blockage ratio significantly but increases the drag force acting on the anemometer and causes significant changes in the surrounding velocity field. Also cup and vane anemometers with the same blockage ratio can have considerably different effect on the velocity field in a wind tunnel's test section.

During the tests in this project, however, it turned out that the blockage effect is not the only important aspect of the velocity field around the anemometer under test. Tests of a small vane anemometer with propeller diameter of 22 mm showed large deviations between participating laboratories which are caused by another type of the wind tunnel – anemometer interaction than the blockage effect. It turned out that processes behind the mounting rod of the anemometer, even thin (12 mm in this case), influence the sensor which is placed at the tip of the mounting rod (plus handrail) and this influence significantly and non-trivially depends on the length of the mounting rod exposed to flow. Similar effect was observed already in past for thermo-anemometers [15] and cup anemometers [12] and is called the insertion depth effect. As shown in this report, this effect is not only important for the small vane anemometers but also the larger ones, even if the size of the effect decreases with the size of the anemometer's sensing element. The reported tests in the wind tunnel of CMI for example showed, that shifting the 22 mm vane anemometer (Schiltknecht Mini) by 15 cm deeper into the air stream may lead to change in anemometer indication up to 5 % whereas for 80 mm vane (Schiltknecht Macro) it is up to 2 %.

In summary, the calibration curves obtained in various participating laboratories are influenced at least by a mixture of the blockage effect, insertion depth effect, varying reference anemometer positions and possibly by other systematic errors which are not related to the wind tunnel – anemometer interaction. In order to evaluate the blockage effect separately the other effects would have to be eliminated or corrected.

The mutual positions of the MUTs and the reference anemometers have not been prescribed in this project, every laboratory used its own standard procedure and reported the positions of the meters in the wind tunnel. An attempt to evaluate the effect of varying reference anemometer position was made by measuring the velocity fields in front of all the 5 large tested anemometers in the wind tunnel of CMI. Maps of the velocity disturbance fields in front of the MUTs including the reference positions of all the

participants have been created, however, it gives a rough estimate of possible differences only, since the velocity fields themselves can differ in various wind tunnels.

Also an attempt to get the other systematic errors under control was made by circulating two small size anemometers (thermo-anemometer and vane) with negligible blockage ratio. However, both of the meters are heavily affected by the insertion depth effect, which was not known before the measurements, and moreover the long-term stability of the thermo-anemometer was not satisfactory. Therefore, the goal of excluding the other systematic errors was not completely achieved. To achieve this goal a circulation of a small anemometer not suffering from the insertion depth effect, would be needed. Results of the currently running Euramet comparison F1515 where an L-type Pitot tube and an ultrasonic anemometer are used as transfer standards could provide additional information.

Even in case of having the mutual MUT-reference positions fixed and eliminating the other systematic errors we still remain with a mixture of the blockage effect and insertion depth effect. For the anemometers' construction with a sensing element at a tip of a mounting rod, which is perpendicular to air flow, the two effects will always appear together. Therefore, it is a question if it makes sense to try to investigate them separately.

Since it is not possible to extract the blockage effect from the current measurement data, the main goal of this project – quantifying deviations of calibration results of vane and cup anemometers due to the blockage effect, especially in wind tunnels with open test section – has not been fully achieved. It is difficult to draw any general quantitative conclusions, e.g. in terms of the blockage ratio, from the data obtained.

However, the insertion depth effect turned out to be of a great importance and therefore a follow-up Euramet project has been agreed by the participants with focus to this effect in various wind tunnels. Based on the new measurements the results contained in this report could be revised.

Appendix A – Photos and schemes of the wind tunnels

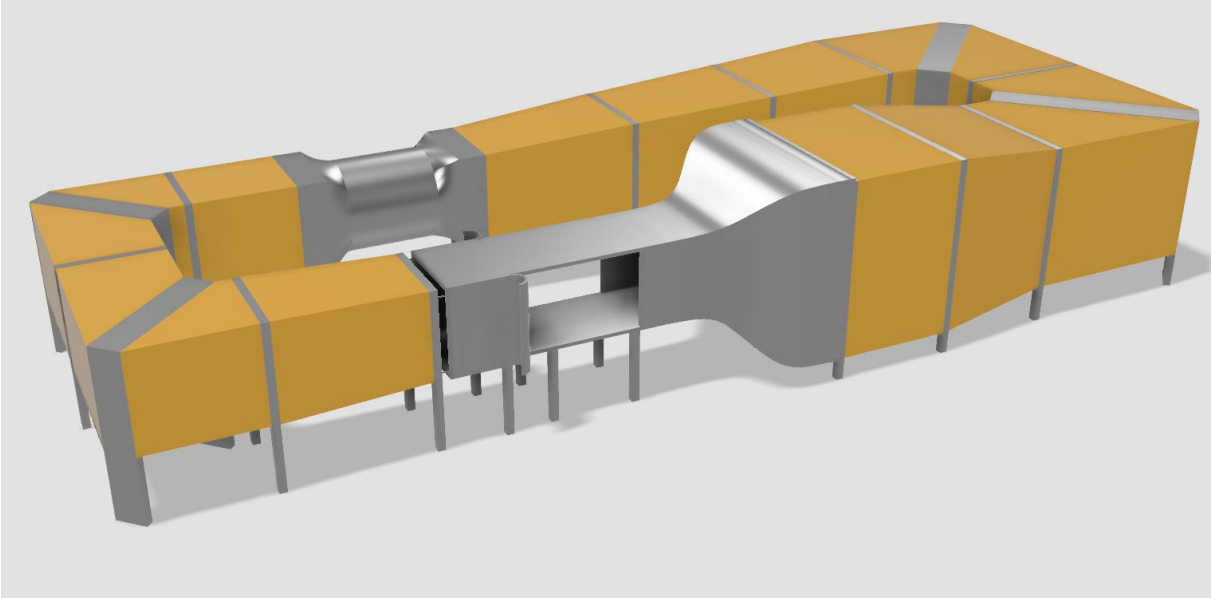

Fig. A.1a Wind tunnel of DWG

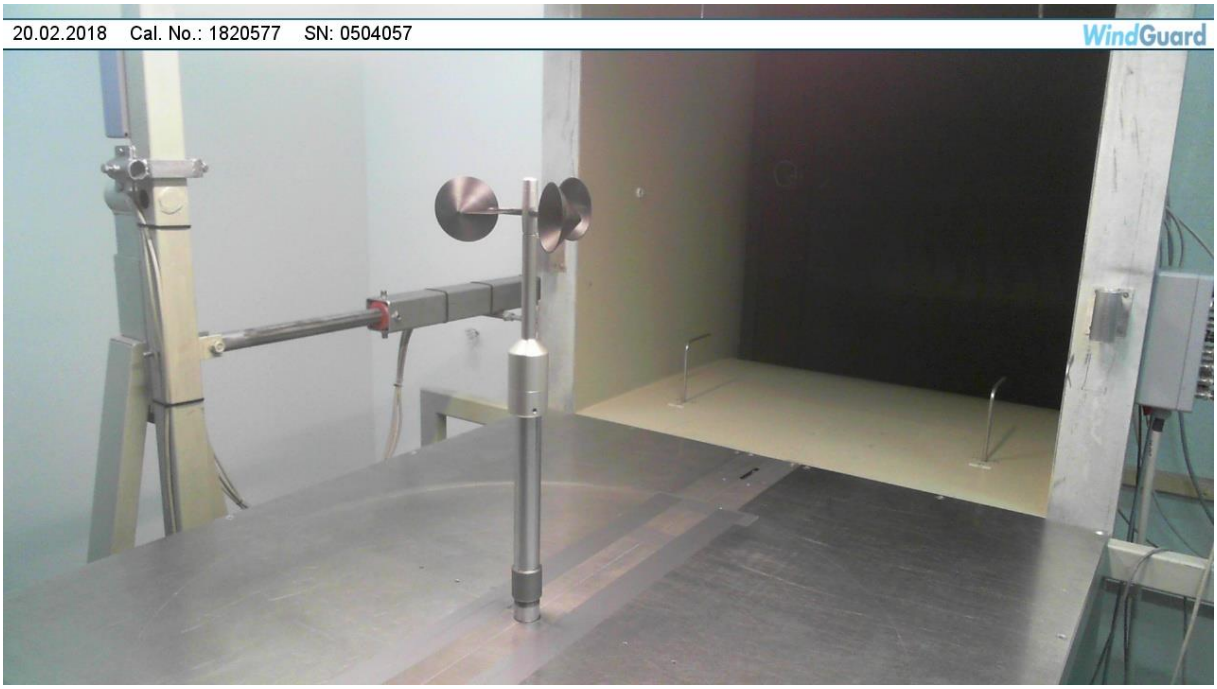

Fig. A.1b Wind tunnel of DWG – test section detail

Fig. A.2 Wind tunnel WE, nozzle diameter 800 mm

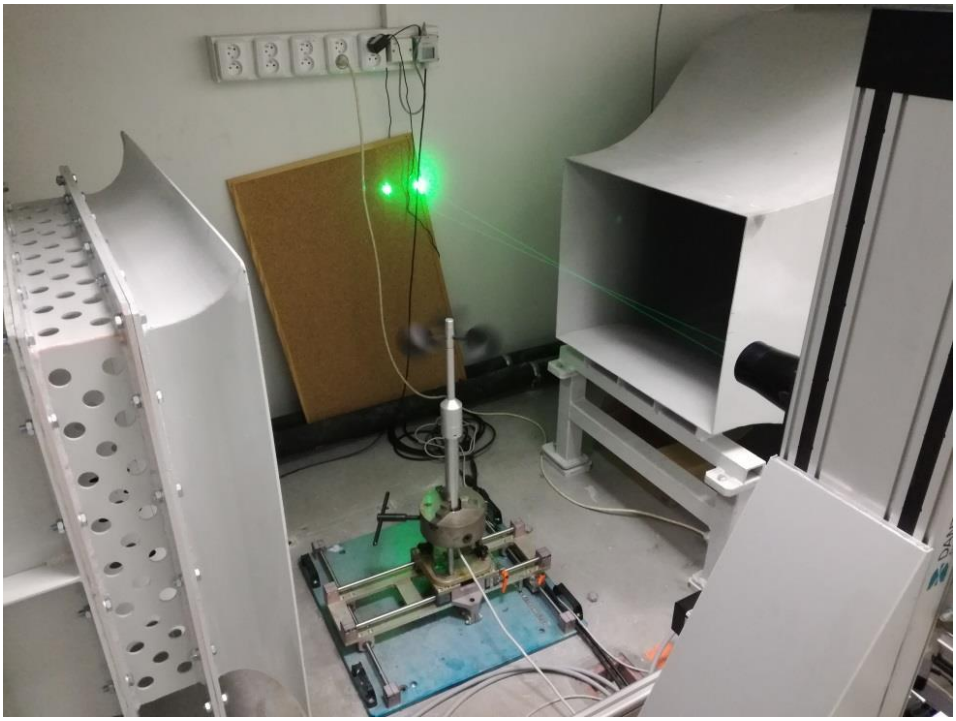

Fig. A.3 Wind tunnel of CHMI

Fig. A.4 Wind tunnel of CMI

Fig. A.5a Wind tunnel of LEI – general view

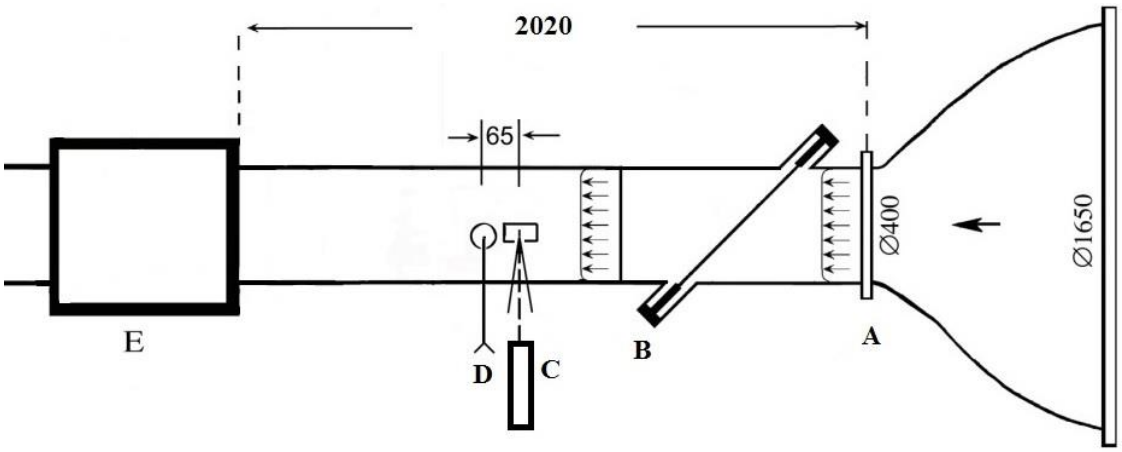

Fig. A.5b Wind tunnel of LEI – test section detail: A – test channel inlet; B – ultrasonic anemometer; C – test section for LDA; D – test section for MUT (for setup denoted as LEI 2); E – test chamber for MUT (for setup denoted as LEI 1)

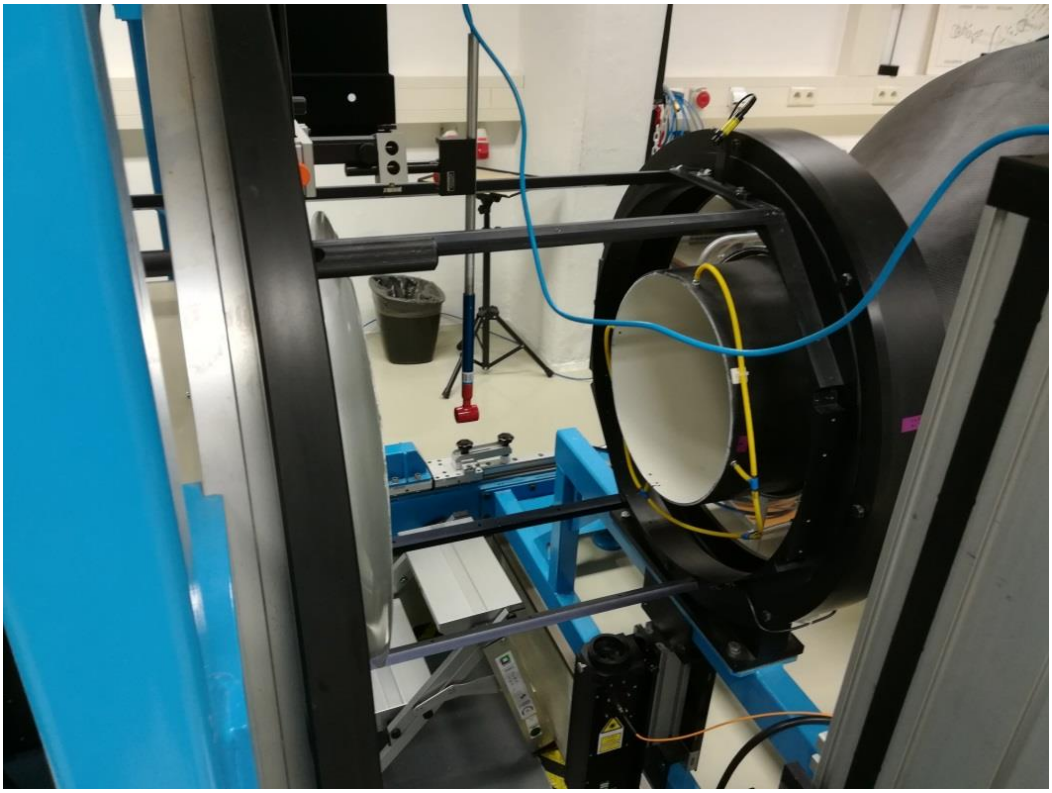

Fig. A.6 Wind tunnel of PTB – test section detail

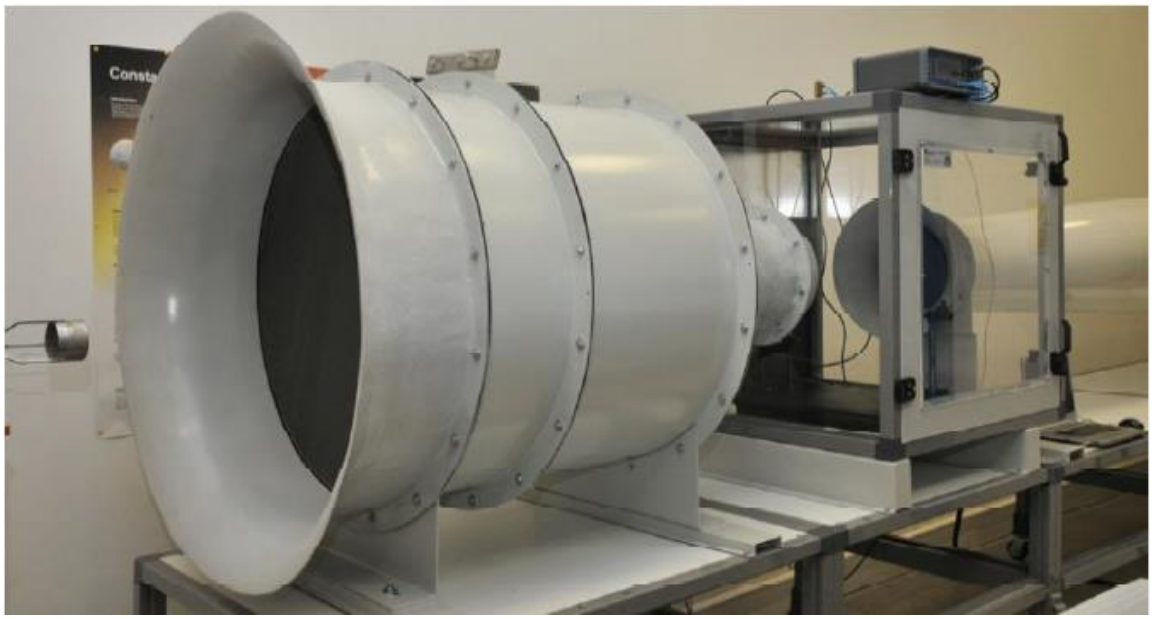

Fig. A.7 Wind tunnel of TÜBİTAK UME

Fig. A.8 Wind tunnel of BEV/E+E

Fig. A.9 Wind tunnel of WE, nozzle diameter 255 mm

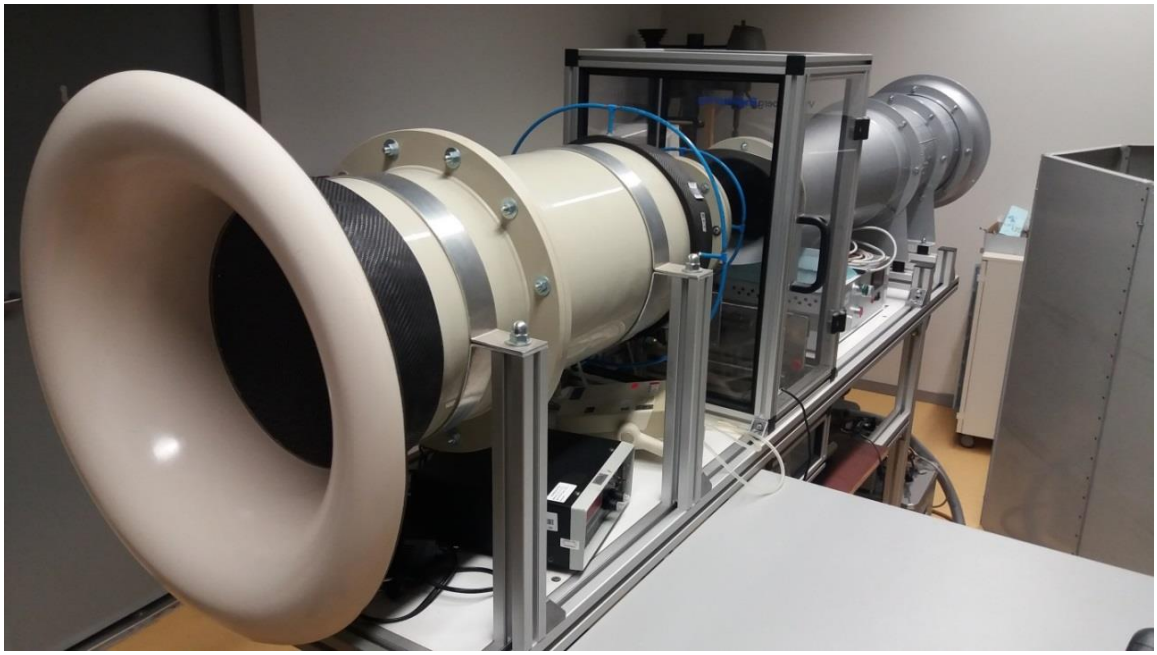

Fig. A.10 Wind tunnel of TCUT

Fig. A.11 Wind tunnel of METAS

Fig. A.12 Wind tunnel of CETIAT

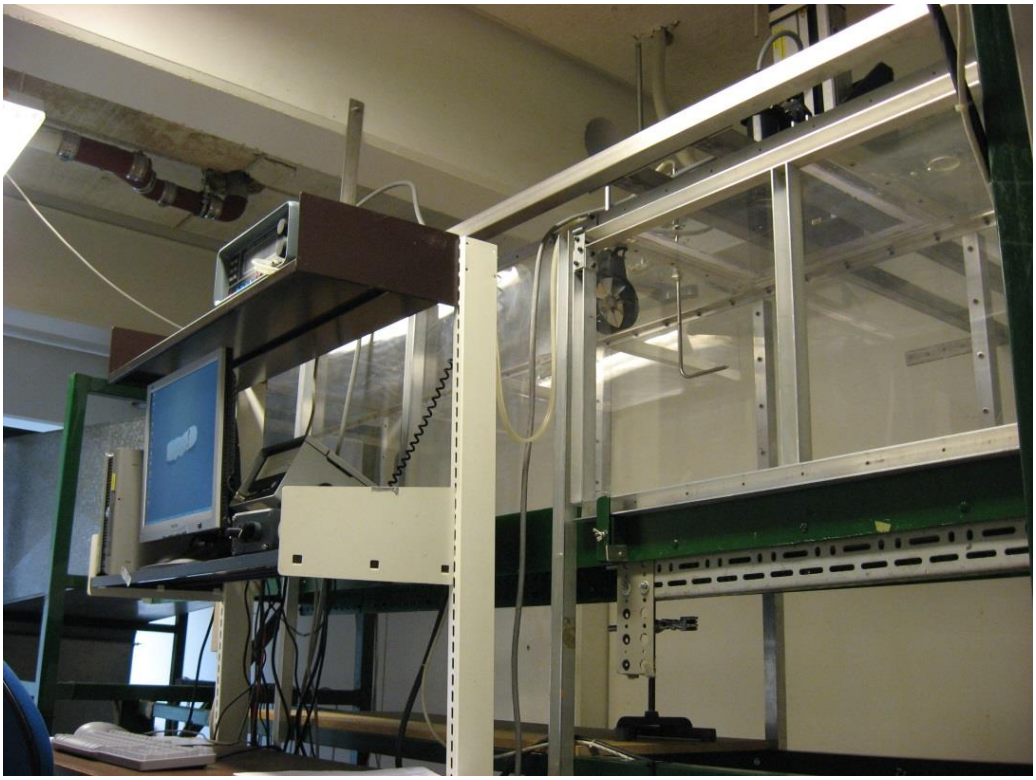

Fig. A.13 Wind tunnel of DTI

Appendix B – Complete calibration data

lab	v_{NOM}	(m/s)	0.5	2	5	8	12	20
DWG	v_M	(m/s)	0,501	2,033	5,006	8,015	11,992	
	E	(m/s)	0,003	-0,023	-0,074	-0,132	-0,192	
	U(E)	(m/s)	0,050	0,050	0,050	0,050	0,050	
WE 800	v_M	(m/s)	0,540	2,008	4,936	7,903	11,782	
	E	(m/s)	0,047	-0,043	-0,094	-0,177	-0,234	
	U(E)	(m/s)	0,010	0,020	0,040	0,060	0,090	
CHMI	v_M	(m/s)	0,534	1,989	5,014	7,987	11,990	
	E	(m/s)	0,012	-0,019	-0,061	-0,117	-0,143	
	U(E)	(m/s)	0,012	0,015	0,020	0,031	0,045	
	$U(E)_{BE}$	(m/s)	0,012	0,017	0,023	0,035	0,051	
CMI	v_M	(m/s)	0,466	1,996	5,019	8,014	12,020	
	E	(m/s)	-0,002	-0,036	-0,076	-0,141	-0,192	
	U(E)	(m/s)	0,011	0,016	0,025	0,041	0,061	
	$U(E)_{BE}$	(m/s)	0,011	0,016	0,039	0,061	0,092	
LEI 1	v_M	(m/s)		2,175	5,289	8,227	12,165	
	E	(m/s)		-0,026	-0,060	-0,070	-0,059	
	U(E)	(m/s)		0,029	0,044	0,055	0,069	
PTB	v_M	(m/s)	0,500	2,003	5,003	8,009	12,014	
	E	(m/s)	-0,002	-0,071	-0,170	-0,294	-0,436	
	E_{BE}	(m/s)	-0,002	-0,071	-0,162	-0,297	-0,454	
	U(E)	(m/s)	0,007	0,016	0,039	0,064	0,096	
	$U(E)_{BE}$	(m/s)	0,007	0,019	0,047	0,076	0,114	
UME	v_M	(m/s)	0,500	2,040	5,000	8,002	12,02	
	E	(m/s)	0,006	0,062	0,141	0,248	0,24	
	E_{BE}	(m/s)	-0,01	0,00	-0,01	0,01	-0,12	
	U(E)	(m/s)	0,010	0,018	0,045	0,071	0,11	
	$U(E)_{BE}$	(m/s)	0,010	0,019	0,046	0,074	0,11	
E+E	v_M	(m/s)	0,475	1,886	4,797	7,689	11,528	
	E	(m/s)	-0,005	-0,066	-0,145	-0,233	-0,320	
	U(E)	(m/s)	0,008	0,014	0,028	0,042	0,060	
	$U(E)_{BE}$	(m/s)	0,009	0,018	0,038	0,059	0,087	
WE 255	v_M	(m/s)	0,500	1,968	4,933	7,896	11,835	
	E	(m/s)	-0,006	-0,081	-0,175	-0,253	-0,388	
	U(E)	(m/s)	0,010	0,020	0,040	0,060	0,090	
TCUT	v_M	(m/s)	0,505	2,01	5,01	8,01	12,03	
	E	(m/s)	0,006	-0,06	-0,12	-0,28	-0,49	
	E_{BE}	(m/s)	0,02	0,00	0,03	-0,04	-0,13	
	U(E)	(m/s)	0,061	0,11	0,29	0,27	0,31	
	$U(E)_{BE}$	(m/s)	0,06	0,13	0,32	0,36	0,47	
METAS	v_M	(m/s)	0,500	2,010	4,99	8,01	11,97	
	E	(m/s)	-0,006	0,002	-0,01	-0,06	-0,04	
	U(E)	(m/s)	0,023	0,043	0,10	0,17	0,25	
CETIAT	v_M	(m/s)	0,500	2,000	5,009	7,990	12,000	
	E	(m/s)	0,007	-0,022	-0,041	-0,087	-0,143	
	E_{BE}	(m/s)	0,008	-0,017	-0,029	-0,068	-0,11	
	U(E)	(m/s)	0,012	0,020	0,039	0,053	0,078	
	$U(E)_{BE}$	(m/s)	0,012	0,020	0,040	0,055	0,082	
DTI	v_M	(m/s)	0,500	2,000	5,011	8,003	11,991	
	E	(m/s)	0,024	0,025	0,053	0,082	0,076	
	U(E)	(m/s)	0,051	0,051	0,055	0,061	0,083	
LEI 2	v_M	(m/s)		2,175	5,216	8,196	12,096	
	E	(m/s)		0,060	0,044	0,069	0,133	
	U(E)	(m/s)		0,029	0,045	0,054	0,066	

Tab. B.1 Testo – calibration data; v_M is velocity indicated by the MUT, E is error of the MUT not including corrections for the blockage effect, E_{BE} is error of the MUT including corrections for the blockage effect if applied, $U(E)$ is expanded uncertainty of the error E not including any blockage effect contribution, $U(E)_{BE}$ is an expanded uncertainty of the error E or E_{BE} including the blockage effect contribution if applied.

lab	v_{NOM}	(m/s)	0.5	2	5	8	12	20
DWG	v_M	(m/s)	0,477		5,003	7,999	12,002	20,02
	E	(m/s)	-0,047		-0,183	-0,205	-0,252	-0,48
	U(E)	(m/s)	0,050		0,050	0,050	0,050	0,10
WE 800	v_M	(m/s)	0,534	1,924	4,911	7,940	11,820	19,77
	E	(m/s)	0,004	-0,112	-0,165	-0,157	-0,192	-0,33
	U(E)	(m/s)	0,010	0,020	0,040	0,060	0,080	0,14
CHMI	v_M	(m/s)	0,528	1,993	5,040	8,047	12,035	19,938
	E	(m/s)	-0,013	-0,108	-0,145	-0,145	-0,172	-0,344
	U(E)	(m/s)	0,010	0,019	0,021	0,031	0,046	0,076
	$U(E)_{BE}$	(m/s)	0,010	0,019	0,021	0,031	0,046	0,076
CMI	v_M	(m/s)	0,531	1,995	5,029	8,004	11,993	20,02
	E	(m/s)	-0,032	-0,115	-0,142	-0,112	-0,107	-0,30
	U(E)	(m/s)	0,012	0,016	0,026	0,040	0,060	0,10
	$U(E)_{BE}$	(m/s)	0,012	0,016	0,027	0,041	0,061	0,10
LEI 1	v_M	(m/s)		2,130	5,270	8,420	12,590	20,41
	E	(m/s)		-0,188	-0,031	0,123	0,312	0,38
	U(E)	(m/s)		0,030	0,044	0,057	0,063	0,10
PTB	v_M	(m/s)	0,489	2,009	4,996	7,990	12,007	20,01
	E	(m/s)	-0,043	-0,156	-0,223	-0,236	-0,252	-0,45
	E_{BE}	(m/s)	-0,043	-0,156	-0,216	-0,239	-0,27	-0,49
	U(E)	(m/s)	0,007	0,017	0,040	0,063	0,094	0,15
	$U(E)_{BE}$	(m/s)	0,008	0,020	0,047	0,076	0,11	0,18
UME	v_M	(m/s)	0,490	2,070	5,050	7,970	12,01	20,00
	E	(m/s)	0,01	0,02	0,08	0,19	0,35	0,68
	E_{BE}	(m/s)	-0,01	-0,03	-0,05	-0,01	0,06	0,21
	U(E)	(m/s)	0,010	0,019	0,047	0,073	0,11	0,18
	$U(E)_{BE}$	(m/s)	0,011	0,020	0,047	0,074	0,11	0,18
E+E	v_M	(m/s)	0,427	1,822	4,749	7,761	11,723	19,54
	E	(m/s)	-0,054	-0,135	-0,216	-0,196	-0,182	-0,28
	U(E)	(m/s)	0,008	0,014	0,028	0,042	0,060	0,10
	$U(E)_{BE}$	(m/s)	0,009	0,015	0,030	0,046	0,068	0,110
WE 255	v_M	(m/s)	0,474	1,926	4,914	7,990	11,992	19,98
	E	(m/s)	-0,037	-0,142	-0,222	-0,199	-0,211	-0,33
	U(E)	(m/s)	0,010	0,010	0,030	0,040	0,060	0,10
TCUT	v_M	(m/s)	0,513	2,00	5,02	8,00	12,01	20,06
	E	(m/s)	0,014	-0,11	-0,15	-0,14	-0,20	-0,38
	E_{BE}	(m/s)	0,02	-0,07	-0,05	0,02	0,04	0,02
	U(E)	(m/s)	0,065	0,11	0,29	0,27	0,30	0,40
	$U(E)_{BE}$	(m/s)	0,07	0,12	0,31	0,32	0,39	0,57
METAS	v_M	(m/s)	0,530	1,980	4,98	7,99	12,05	20,00
	E	(m/s)	-0,001	-0,088	-0,14	-0,12	-0,11	-0,10
	U(E)	(m/s)	0,031	0,047	0,11	0,17	0,26	0,41
CETIAT	v_M	(m/s)	0,503	1,992	4,991	8,008	11,990	20,00
	E	(m/s)	-0,020	-0,106	-0,142	-0,132	-0,121	-0,33
	E_{BE}	(m/s)	-0,019	-0,101	-0,129	-0,113	-0,09	-0,28
	U(E)	(m/s)	0,022	0,023	0,037	0,058	0,074	0,12
	$U(E)_{BE}$	(m/s)	0,022	0,023	0,038	0,060	0,08	0,13
DTI	v_M	(m/s)	0,511	2,010	5,006	8,011	12,044	20,02
	E	(m/s)	0,004	-0,057	-0,016	0,055	0,070	0,03
	U(E)	(m/s)	0,060	0,055	0,055	0,061	0,076	0,12
LEI 2	v_M	(m/s)	0,534	1,850	5,310	8,300	12,250	20,62
	E	(m/s)	-0,079	-0,123	0,007	0,078	0,240	0,39
	U(E)	(m/s)	0,015	0,035	0,043	0,054	0,066	0,10

Tab. B.2 Schiltknecht Macro – calibration data; v_M is velocity indicated by the MUT, E is error of the MUT not including corrections for the blockage effect, E_{BE} is error of the MUT including corrections for the blockage effect if applied, $U(E)$ is expanded uncertainty of the error E not including any blockage effect contribution, $U(E)_{BE}$ is an expanded uncertainty of the error E or E_{BE} including the blockage effect contribution if applied.

lab	v_{NOM}	(m/s)	0.5	2	5	8	12	20
DWG	v_M	(m/s)	0,514	1,925	4,965	8,028	12,023	20,03
	E	(m/s)	-0,040	-0,042	-0,035	-0,030	-0,013	0,04
	U(E)	(m/s)	0,050	0,050	0,050	0,050	0,050	0,10
WE 800	v_M	(m/s)	0,463	1,965	5,027	8,002	12,017	20,05
	E	(m/s)	-0,010	-0,038	-0,014	-0,038	-0,020	0,04
	U(E)	(m/s)	0,010	0,020	0,040	0,060	0,090	0,14
CHMI	v_M	(m/s)	0,506	2,025	5,034	8,001	12,016	20,029
	E	(m/s)	-0,044	-0,034	0,000	0,019	0,066	0,209
	U(E)	(m/s)	0,008	0,015	0,020	0,030	0,045	0,074
	$U(E)_{BE}$	(m/s)	0,008	0,018	0,029	0,044	0,067	0,11
CMI	v_M	(m/s)	0,492	1,972	4,985	7,993	12,042	20,00
	E	(m/s)	-0,053	-0,047	-0,027	-0,025	0,003	0,07
	U(E)	(m/s)	0,012	0,016	0,025	0,040	0,060	0,10
	$U(E)_{BE}$	(m/s)	0,012	0,021	0,051	0,081	0,12	0,20
LEI 1	v_M	(m/s)	0,541	2,254	5,330	8,393	12,541	20,19
	E	(m/s)	-0,058	-0,047	0,062	0,145	0,264	0,35
	U(E)	(m/s)	0,015	0,029	0,046	0,087	0,082	0,17
PTB	v_M	(m/s)						
	E	(m/s)						
	U(E)	(m/s)						
UME	v_M	(m/s)	0,504	1,998	5,013	7,950	12,03	20,10
	E	(m/s)	-0,010	0,062	0,219	0,337	0,53	1,07
	E_{BE}	(m/s)	-0,03	-0,03	0,00	-0,01	0,00	0,19
	U(E)	(m/s)	0,010	0,018	0,044	0,070	0,11	0,18
	$U(E)_{BE}$	(m/s)	0,011	0,019	0,046	0,073	0,11	0,18
E+E	v_M	(m/s)	0,421	1,905	4,917	7,903	11,855	19,80
	E	(m/s)	-0,057	-0,042	-0,019	-0,009	0,022	0,10
	U(E)	(m/s)	0,007	0,014	0,028	0,042	0,060	0,10
	$U(E)_{BE}$	(m/s)	0,007	0,014	0,028	0,043	0,063	0,10
WE 255	v_M	(m/s)						
	E	(m/s)						
	U(E)	(m/s)						
TCUT	v_M	(m/s)						
	E	(m/s)						
	U(E)	(m/s)						
METAS	v_M	(m/s)	0,488	2,007	5,02	8,02	11,98	19,77
	E	(m/s)	-0,049	-0,018	0,02	0,05	0,13	0,31
	U(E)	(m/s)	0,025	0,048	0,10	0,17	0,24	0,41
CETIAT	v_M	(m/s)	0,500	1,997	5,010	8,001	12,004	19,98
	E	(m/s)	-0,041	-0,024	0,021	0,064	0,110	0,24
	E_{BE}	(m/s)	-0,040	-0,019	0,033	0,083	0,14	0,28
	U(E)	(m/s)	0,014	0,020	0,034	0,049	0,069	0,11
	$U(E)_{BE}$	(m/s)	0,014	0,020	0,035	0,052	0,07	0,12
DTI	v_M	(m/s)	0,503	2,006	5,000	7,985	12,043	20,04
	E	(m/s)	-0,055	-0,031	0,041	0,083	0,173	0,27
	U(E)	(m/s)	0,050	0,050	0,051	0,061	0,069	0,12
LEI 2	v_M	(m/s)	0,497	2,213	5,321	8,256	12,41	19,92
	E	(m/s)	-0,050	-0,019	0,124	0,227	0,42	0,59
	U(E)	(m/s)	0,026	0,036	0,053	0,066	0,11	0,16

Tab. B.3 RM Young – calibration data; v_M is velocity indicated by the MUT, E is error of the MUT not including corrections for the blockage effect, E_{BE} is error of the MUT including corrections for the blockage effect if applied, $U(E)$ is expanded uncertainty of the error E not including any blockage effect contribution, $U(E)_{BE}$ is an expanded uncertainty of the error E or E_{BE} including the blockage effect contribution if applied.

lab	v_{NOM}	(m/s)	1	2	5	8	12	20
DWG	v_M	(m/s)	1,076	2,126	5,118	8,148	12,080	20,07
	E	(m/s)	0,078	0,146	0,083	0,089	0,060	0,10
	U(E)	(m/s)	0,050	0,050	0,050	0,050	0,050	0,10
WE 800	v_M	(m/s)	1,115	2,160	5,071	8,17	12,10	20,33
	E	(m/s)	0,056	0,118	0,025	0,07	0,11	0,23
	U(E)	(m/s)	0,020	0,020	0,070	0,10	0,18	0,20
CHMI	v_M	(m/s)	1,021	2,028	4,979	8,029	11,929	19,936
	E	(m/s)	0,096	0,077	-0,051	-0,091	-0,023	0,200
	U(E)	(m/s)	0,012	0,013	0,020	0,031	0,045	0,074
	$U(E)_{BE}$	(m/s)	0,013	0,017	0,034	0,054	0,076	0,13
CMI	v_M	(m/s)	1,023	1,996	5,031	8,061	12,023	20,02
	E	(m/s)	0,062	0,077	0,041	0,069	0,118	0,17
	U(E)	(m/s)	0,013	0,016	0,025	0,040	0,059	0,10
	$U(E)_{BE}$	(m/s)	0,014	0,023	0,059	0,093	0,14	0,23
LEI 1	v_M	(m/s)		2,433	5,214	8,243	12,341	19,88
	E	(m/s)		0,054	0,052	0,071	0,109	0,00
	U(E)	(m/s)		0,027	0,043	0,054	0,064	0,10
PTB	v_M	(m/s)	1,010	2,017	4,997	8,018	11,949	19,90
	E	(m/s)	0,046	0,104	0,171	0,233	0,290	0,60
	E_{BE}	(m/s)	0,051	0,095	0,127	0,165	0,190	0,45
	U(E)	(m/s)	0,009	0,016	0,025	0,046	0,091	0,14
	$U(E)_{BE}$	(m/s)	0,043	0,084	0,21	0,34	0,51	0,84
UME	v_M	(m/s)	0,962	1,927	4,844	7,771	11,42	19,34
	E	(m/s)	0,032	0,099	0,227	0,246	0,25	0,64
	E_{BE}	(m/s)	-0,01	0,02	0,03	-0,07	-0,22	-0,16
	U(E)	(m/s)	0,010	0,017	0,043	0,069	0,10	0,17
	$U(E)_{BE}$	(m/s)	0,011	0,018	0,045	0,072	0,11	0,18
E+E	v_M	(m/s)	0,99	1,98	4,85	7,76	11,61	19,30
	E	(m/s)	0,02	0,06	-0,01	-0,03	-0,04	-0,09
	U(E)	(m/s)	0,21	0,21	0,22	0,22	0,22	0,24
	$U(E)_{BE}$	(m/s)	0,22	0,22	0,24	0,27	0,33	0,46
WE 255	v_M	(m/s)						
	E	(m/s)						
	U(E)	(m/s)						
TCUT	v_M	(m/s)						
	E	(m/s)						
	U(E)	(m/s)						
METAS	v_M	(m/s)	1,032	2,046	4,89	7,94	12,08	19,86
	E	(m/s)	0,103	0,108	0,06	0,04	0,09	0,05
	U(E)	(m/s)	0,033	0,066	0,21	0,28	0,38	0,70
CETIAT	v_M	(m/s)	0,511	1,995	4,991	8,031	11,986	19,93
	E	(m/s)	-0,061	0,076	0,027	0,196	0,271	0,43
	E_{BE}	(m/s)	-0,060	0,080	0,039	0,214	0,30	0,47
	U(E)	(m/s)	0,013	0,020	0,042	0,062	0,085	0,12
	$U(E)_{BE}$	(m/s)	0,013	0,020	0,043	0,064	0,09	0,13
DTI	v_M	(m/s)	1,013	2,004	5,021	8,03	11,91	19,97
	E	(m/s)	0,105	0,200	0,262	0,38	0,53	0,81
	U(E)	(m/s)	0,061	0,061	0,077	0,13	0,32	0,36
LEI 2	v_M	(m/s)		2,482	5,487	8,471	12,599	20,88
	E	(m/s)		0,227	0,379	0,526	0,825	1,25
	U(E)	(m/s)		0,027	0,043	0,054	0,064	0,09

Tab. B.4 Vaisala – calibration data; v_M is velocity indicated by the MUT, E is error of the MUT not including corrections for the blockage effect, E_{BE} is error of the MUT including corrections for the blockage effect if applied, $U(E)$ is expanded uncertainty of the error E not including any blockage effect contribution, $U(E)_{BE}$ is an expanded uncertainty of the error E or E_{BE} including the blockage effect contribution if applied.

lab	v_{NOM}	(m/s)	0.5	2	5	8	12	20
DWG	v_M	(m/s)	0,610	1,996	5,026	8,073	12,051	20,06
	E	(m/s)	0,016	0,029	0,015	0,028	0,043	0,11
	U(E)	(m/s)	0,050	0,050	0,050	0,050	0,050	0,10
WE 800	v_M	(m/s)	0,511	1,997	4,946	7,981	11,95	19,89
	E	(m/s)	0,039	-0,043	-0,093	-0,094	-0,07	-0,12
	U(E)	(m/s)	0,010	0,020	0,050	0,080	0,11	0,20
CHMI	v_M	(m/s)	0,509	2,037	4,991	8,012	11,971	20,105
	E	(m/s)	0,015	-0,016	-0,024	-0,025	0,016	0,185
	U(E)	(m/s)	0,008	0,013	0,020	0,030	0,045	0,075
	$U(E)_{BE}$	(m/s)	0,009	0,023	0,050	0,078	0,11	0,19
CMI	v_M	(m/s)	0,519	1,979	4,988	8,026	12,038	20,05
	E	(m/s)	-0,003	-0,009	-0,038	-0,041	-0,019	0,06
	U(E)	(m/s)	0,012	0,016	0,025	0,040	0,060	0,10
	$U(E)_{BE}$	(m/s)	0,012	0,034	0,083	0,13	0,20	0,33
LEI 1	v_M	(m/s)	0,539	2,104	5,205	8,080	12,225	19,62
	E	(m/s)	-0,060	-0,102	-0,054	-0,053	0,011	-0,05
	U(E)	(m/s)	0,016	0,030	0,045	0,074	0,069	0,10
PTB	v_M	(m/s)	0,508	2,018	5,010	8,00	11,99	20,06
	E	(m/s)	-0,023	0,023	0,033	0,05	0,09	0,23
	E_{BE}	(m/s)	-0,024	-0,147	-0,202	-0,23	-0,28	-0,44
	U(E)	(m/s)	0,010	0,031	0,090	0,12	0,18	0,29
	$U(E)_{BE}$	(m/s)	0,026	0,097	0,25	0,39	0,58	0,96
UME	v_M	(m/s)	0,480	1,775	4,381	7,315	10,982	18,14
	E	(m/s)	0,052	0,179	0,364	0,544	0,936	1,82
	E_{BE}	(m/s)	0,02	0,07	0,08	0,06	0,22	0,67
	U(E)	(m/s)	0,010	0,015	0,037	0,062	0,092	0,15
	$U(E)_{BE}$	(m/s)	0,011	0,017	0,040	0,067	0,099	0,16
E+E	v_M	(m/s)	0,45	1,82	4,66	7,57	11,34	18,96
	E	(m/s)	-0,02	-0,06	-0,08	-0,01	0,02	0,11
	U(E)	(m/s)	0,14	0,14	0,14	0,15	0,16	0,17
	$U(E)_{BE}$	(m/s)	0,14	0,16	0,26	0,37	0,53	0,86
WE 255	v_M	(m/s)						
	E	(m/s)						
	U(E)	(m/s)						
TCUT	v_M	(m/s)						
	E	(m/s)						
	U(E)	(m/s)						
METAS	v_M	(m/s)	0,505	1,982	4,99	7,96	11,93	19,75
	E	(m/s)	0,003	-0,017	-0,07	-0,11	-0,26	-0,07
	U(E)	(m/s)	0,029	0,054	0,14	0,22	0,29	0,48
CETIAT	v_M	(m/s)	0,501	1,995	4,989	7,988	12,011	20,07
	E	(m/s)	0,000	0,018	0,025	0,067	0,118	0,35
	E_{BE}	(m/s)	0,001	0,023	0,037	0,086	0,15	0,40
	U(E)	(m/s)	0,013	0,021	0,039	0,055	0,079	0,12
	$U(E)_{BE}$	(m/s)	0,013	0,021	0,040	0,057	0,08	0,13
DTI	v_M	(m/s)	0,499	2,018	4,996	7,95	12,03	20,09
	E	(m/s)	0,033	0,074	0,182	0,28	0,41	0,71
	U(E)	(m/s)	0,051	0,057	0,073	0,12	0,17	0,28
LEI 2	v_M	(m/s)						
	E	(m/s)						
	U(E)	(m/s)						

Tab. B.5 Thies – calibration data; v_M is velocity indicated by the MUT, E is error of the MUT not including corrections for the blockage effect, E_{BE} is error of the MUT including corrections for the blockage effect if applied, $U(E)$ is expanded uncertainty of the error E not including any blockage effect contribution, $U(E)_{BE}$ is an expanded uncertainty of the error E or E_{BE} including the blockage effect contribution if applied.

lab	v_{NOM}	(m/s)	0.5	2	5	8	12	20
DWG	v_M	(m/s)	0,492	2,001	5,006	7,990	12,003	20,02
	E	(m/s)	0,099	0,047	0,063	-0,038	-0,173	0,09
	U(E)	(m/s)	0,050	0,050	0,050	0,050	0,050	0,10
WE 800	v_M	(m/s)	0,540	2,120	5,334	8,203	12,217	20,74
	E	(m/s)	0,080	0,088	0,254	0,156	0,087	0,70
	U(E)	(m/s)	0,010	0,020	0,040	0,060	0,090	0,14
CHMI	v_M	(m/s)	0,561	2,098	5,160	8,158	12,046	20,042
	E	(m/s)	0,052	0,061	0,093	0,021	-0,093	0,140
	U(E)	(m/s)	0,008	0,013	0,034	0,038	0,052	0,074
CMI	v_M	(m/s)	0,510	2,045	5,023	8,016	12,042	20,06
	E	(m/s)	0,042	0,034	0,078	0,037	-0,118	0,18
	U(E)	(m/s)	0,011	0,016	0,025	0,040	0,061	0,10
LEI 1	v_M	(m/s)						
	E	(m/s)						
	U(E)	(m/s)						
PTB	v_M	(m/s)	0,500	2,001	4,990	8,003	12,005	19,98
	E	(m/s)	0,041	0,081	0,209	0,157	0,112	0,41
	U(E)	(m/s)	0,007	0,015	0,035	0,059	0,088	0,14
UME	v_M	(m/s)	0,500	2,000	4,994	8,002	12,00	20,02
	E	(m/s)	0,049	0,095	0,150	0,187	0,10	0,46
	E_{BE}	(m/s)	0,046	0,081	0,113	0,127	0,01	0,31
	U(E)	(m/s)	0,010	0,018	0,045	0,072	0,11	0,18
	$U(E)_{BE}$	(m/s)	0,011	0,019	0,046	0,073	0,11	0,18
E+E	v_M	(m/s)	0,530	2,017	5,104	8,206	11,919	20,19
	E	(m/s)	0,044	0,044	0,099	0,184	-0,073	0,22
	U(E)	(m/s)	0,008	0,014	0,028	0,042	0,061	0,10
	$U(E)_{BE}$	(m/s)	0,008	0,014	0,028	0,043	0,062	0,10
WE 255	v_M	(m/s)	0,570	2,152	5,237	8,273	12,253	20,46
	E	(m/s)	0,057	0,080	0,123	0,084	-0,034	0,14
	U(E)	(m/s)	0,010	0,010	0,030	0,040	0,060	0,10
TCUT	v_M	(m/s)	0,490	2,02	5,02	8,02	12,10	19,97
	E	(m/s)	0,040	0,07	0,09	0,19	-0,01	0,10
	U(E)	(m/s)	0,062	0,11	0,29	0,27	0,31	0,40
METAS	v_M	(m/s)	0,510	2,000	4,980	7,99	12,01	19,97
	E	(m/s)	0,055	0,118	0,243	0,30	0,28	0,99
	U(E)	(m/s)	0,023	0,041	0,099	0,17	0,25	0,41
CETIAT	v_M	(m/s)	0,500	2,000	5,000	7,991	11,993	20,02
	E	(m/s)	0,044	0,026	0,087	0,039	-0,044	0,22
	E_{BE}	(m/s)	0,044	0,026	0,087	0,039	-0,04	0,22
	U(E)	(m/s)	0,012	0,020	0,035	0,054	0,078	0,12
	$U(E)_{BE}$	(m/s)	0,012	0,020	0,037	0,056	0,08	0,13
DTI	v_M	(m/s)	0,540	2,110	5,210	8,227	12,119	20,24
	E	(m/s)	0,046	0,104	0,194	0,200	0,072	0,25
	U(E)	(m/s)	0,051	0,051	0,055	0,068	0,076	0,15
LEI 2	v_M	(m/s)	0,500	2,360	5,190	8,210	12,120	20,00
	E	(m/s)	0,027	0,116	0,154	0,086	0,062	0,35
	U(E)	(m/s)	0,014	0,028	0,042	0,054	0,063	0,10

Tab. B.6 Airflow – calibration data; v_M is velocity indicated by the MUT, E is error of the MUT not including corrections for the blockage effect, E_{BE} is error of the MUT including corrections for the blockage effect if applied, $U(E)$ is expanded uncertainty of the error E not including any blockage effect contribution, $U(E)_{BE}$ is an expanded uncertainty of the error E or E_{BE} including the blockage effect contribution if applied.

lab	v_{NOM}	(m/s)	0.5	2	5	8	12	20
DWG	v_M	(m/s)	0,435	1,946	4,960	7,768	11,505	19,11
	E	(m/s)	-0,051	-0,007	0,012	-0,105	-0,212	-0,48
	U(E)	(m/s)	0,050	0,050	0,050	0,050	0,050	0,10
WE 800	v_M	(m/s)						
	E	(m/s)						
	U(E)	(m/s)						
CHMI	v_M	(m/s)	0,472	2,027	5,058	8,053	12,030	19,99
	E	(m/s)	-0,048	-0,013	-0,018	-0,091	-0,115	-0,32
	U(E)	(m/s)	0,011	0,013	0,020	0,031	0,045	0,08
CMI	v_M	(m/s)	0,519	2,012	5,047	8,033	12,032	20,00
	E	(m/s)	-0,029	-0,006	0,039	0,025	-0,012	-0,29
	U(E)	(m/s)	0,012	0,016	0,025	0,040	0,060	0,10
LEI 1	v_M	(m/s)						
	E	(m/s)						
	U(E)	(m/s)						
PTB	v_M	(m/s)	0,452	1,914	4,945	7,956	12,124	20,26
	E	(m/s)	-0,041	-0,067	-0,065	-0,033	0,127	0,34
	U(E)	(m/s)	0,008	0,015	0,029	0,043	0,064	0,11
UME	v_M	(m/s)						
	E	(m/s)						
	U(E)	(m/s)						
E+E	v_M	(m/s)	0,471	1,915	4,934	7,960	12,115	20,36
	E	(m/s)	-0,014	-0,058	-0,061	-0,052	0,132	0,42
	U(E)	(m/s)	0,010	0,015	0,028	0,042	0,061	0,10
	$U(E)_{BE}$	(m/s)	0,010	0,015	0,030	0,045	0,065	0,10
WE 255	v_M	(m/s)	0,478	2,000	5,048	8,136	12,317	20,65
	E	(m/s)	-0,026	-0,068	-0,076	-0,050	0,094	0,30
	U(E)	(m/s)	0,010	0,010	0,030	0,040	0,060	0,10
TCUT	v_M	(m/s)						
	E	(m/s)						
	U(E)	(m/s)						
METAS	v_M	(m/s)						
	E	(m/s)						
	U(E)	(m/s)						
CETIAT	v_M	(m/s)						
	E	(m/s)						
	U(E)	(m/s)						
DTI	v_M	(m/s)	0,520	2,042	5,165	8,323	12,489	20,86
	E	(m/s)	0,016	0,030	0,162	0,310	0,505	0,79
	U(E)	(m/s)	0,051	0,051	0,051	0,055	0,076	0,12
LEI 2	v_M	(m/s)	0,450	1,930	5,300	8,478	12,370	20,68
	E	(m/s)	-0,065	0,005	0,131	0,223	0,392	0,57
	U(E)	(m/s)	0,014	0,028	0,043	0,055	0,064	0,10

Tab. B.7 Schiltknecht Mini – calibration data; v_M is velocity indicated by the MUT, E is error of the MUT not including corrections for the blockage effect, E_{BE} is error of the MUT including corrections for the blockage effect if applied, $U(E)$ is expanded uncertainty of the error E not including any blockage effect contribution, $U(E)_{BE}$ is an expanded uncertainty of the error E or E_{BE} including the blockage effect contribution if applied.